PUBLICATIONS OF WATER AND ENVIRONMENT RESEARCH INSTITUTE

11

Bertel Vehviläinen

Snow cover models in operational watershed forecasting

Yhteenveto: Lumimallit vesistöjen ennustemalleissa

NATIONAL BOARD OF WATERS AND THE ENVIRONMENT, FINLAND
Helsinki 1992

PUBLICATIONS OF WATER AND ENVIRONMENT RESEARCH INSTITUTE

11

Bertel Vehviläinen

Snow cover models in operational watershed forecasting

Yhteenveto: Lumimallit vesistöjen ennustemalleissa

NATIONAL BOARD OF WATERS AND THE ENVIRONMENT, FINLAND
Helsinki 1992

ISBN 951-47-5712-2
ISSN 0783-9472

Helsinki 1992. Valtion painatuskeskus

CONTENTS

SNOW COVER MODELS IN OPERATIONAL WATERSHED FORECASTING

Bertel Vehviläinen

VEHVILÄINEN, B. 1992. Snow cover models in operational watershed forecasting. Publications of the Water and Environment Research Institute. National Board of Waters and the Environment, Finland. No. 11.

Snow model is an important part of the operational watershed models used in Finland. Correct simulation of the accumulation and melting of snow enables good watershed forecasting in winter and spring. The presence of snow storage in the watershed gives an advantage in forecasting when compared to a snow free situation. The development of snow models based on temperature index and energy balance for watershed scale use is dealt with. The experiences of operational watershed forecasting obtained with temperature index snow models are discussed. Particular attention is paid to the possibility of using snow models for real-time simulation of areal water equivalent. The best results were obtained with a modified temperature index model with areal snow cover distribution. This model gave reliable results in real-time simulation of areal water equivalent in basin scale.

Keywords: Snow models, watershed models, snow accumulation, snowmelt, flood forecasting, degree-day factor, energy balance, snow density

1 INTRODUCTION

1.1 Snow and snow model research

When does snow start to melt? The most common answer to this question is: when the temperature rises over 0°C. The physically correct answer is: when the energy balance on the snow surface (or in any layer of snowpack) becomes positive.

In brief, these two answers are the two main topics of this study in connection with snow simulation for both the accumulation and the snowmelt period in large watersheds. Snowmelt simulation based on the energy balance is the physically correct method to simulate snowmelt. The physics of snowmelt at point and for small experimental areas have been presented, e.g. by Anderson (1976), Price and Dunne (1976), Obled and Rosse (1977), Morris and Godfrey (1978), Fitzgibbon and Dunne (1980), Male and Gray (1981), Harstveit (1984), Kuchment et al. (1986). The calibration of these models usually requires complex meteorological measurements together with observations of the thermal properties of the snowpack, and thus they are often impossible to use on the scale of a large basin. Therefore the temperature-index approach is the most commonly used method to simulate snowmelt on the scale of large basins, and it also gives good results for large watersheds. Some energy balance terms are often included in the simple temperature-index model, in order to improve model performance. Temperature-index related models have been presented by Light (1941), U.S. Corps of Engineers (USCE 1956), Martinec (1960), Kuzmin (1961), Kuusisto

(1978,1980), Braun (1985), WMO (1986), Sand (1990).

The earliest snow research concerning the occurrence and amount of snowfall or snow depth in Finland was done mainly by Korhonen, in the beginning of the 1900s (Korhonen 1914a, Korhonen 1914b, Korhonen 1915, Korhonen 1917). Korhonen also carried out some research concerning snow density, the water equivalent of snow (Korhonen 1923, Korhonen 1926 a,b) and snowmelt and its effect on spring floods (Korhonen 1918, 1926a).

The long experience of snow line measurements in Finland has produced many thorough studies on the regularities and variability of the areal snow cover in Finland (Korhonen 1927, Korhonen 1936, Siren 1936, Kaitera 1939, Lavila 1949, Taivainen 1952, Yli-Vakkuri 1961, Valmari 1971, Päivänen 1973). Hooli (1973) and Ollila (1974,1984) studied the effect of elevation on the areal snow cover in Lapland and in eastern Finland. Seppänen (1961a,b, 1963, 1964, 1965, 1967) investigated the microvariability of the snow cover. Mustonen (1965b,c) studied the effect of meteorological and terrain factors on the water equivalent of snow. The macroscale variability of snow depth was investigated by Huovila (1971) and Solantie (1975, 1978). Kuusisto (1984) presented results for the average development of the coefficient of variation of the water equivalent during snowmelt in different terrain types and in large basins.

Perälä (1971) and Seuna (1971) discussed the representativity and accuracy of snow observations, and Seppänen (1969a,1969b) discussed problems related to the selection of snow observation sites.

Extensive studies concerning snowmelt in different terrain types based on snow course measurements has been published by Kaitera (1939). The depletion of snow cover in forests was studied by Yli-Vakkuri (1961) and in open areas by Ylinen (1968) and Valmari (1969). Snowmelt studies based on snow pillow observations has been done by Lemmelä (1970, 1972) and Kuusisto (1973, 1978). Rapeli (1971) studied the consumption of energy in snowmelt. The application of degree-day factors in snowmelt simulation and estimation was presented by Solantie (1977), Kuusisto (1980), Hiitiö (1982), Vehviläinen and Kuusisto (1984). Lemmelä (1971) studied the liquid water capacities of melting snow. Kuusisto (1981) investigated the maximum decrease of the water equivalent of snow in different parts of Finland.

All these studies, based mostly on snow course observations, give valuable information for the development of snowmelt models for large basins.

Bergström and Brandt (1984), Kuittinen et al. (1985) and Kuittinen (1988) presented results obtained when using aircraft gamma-ray spectrometry and satellite images to evaluate areal water equivalent in Lappland. The effect of snow and snowmelt on floods had been studied by Korhonen (1918, 1926a) and Kaitera (1939, 1949). Long-term snowmelt and rainfall flood forecasting models based on regression models have been developed by Gürer (1973, 1974, 1975) and Kaila (1977). Rainfall and snowmelt flood forecasting models based on conceptual hydrological models have been presented by Kuusisto (1977a, 1977b), Karvonen (1980), Vakkilainen and Karvonen (1982), Vehviläinen (1982, 1987) and Virta (1987). Results obtained by using the conceptual watershed model developed in this study for areal snow cover and discharge/water level simulation and forecasting have been presented by Vehviläinen (1990).

Ground frost is one process which may affect snowmelt runoff. Physically based ground frost models have been developed earlier by Belchikov and Koren (1979), Motovilov (1979), Jansson and Halldin (1980), Engelmark (1986) and Karvonen (1988).

1.2 Focus of this study

The initial starting point for this work is to improve the watershed forecasting models used operationally in Finland (by National Board of Waters and the Environment) by developing snowmelt simulation and snow accumulation simulation. The snow cover development work is thus done with close reference to the rainfall-runoff, river routing and lake models included in the complete watershed models. Still, in nearly all cases, snow cover models are first developed, calibrated and verified against snow cover observations and tested with the watershed model against total water balance in the watershed over 5—10 years. This is true especially with the more physically based snow cover models.

The purpose of this study is first, to develop a temperature-index snowmelt model valid for the Finnish conditions and to determine the important processes which need to be included in temperature-index model. The second goal is to develop a physically based snowpack model with a snowmelt energy balance model, which can be used for large basins with standard meteorological and hydrological data commonly available. The third aim is to find out whether addition of some energy balance terms to temperature-index models would yield better performance of the model. Because

snowmelt models are tested on the scale of a large basin, the snowmelt model verification is made both against snow observations and against total water balance, i.e. against discharge/inflow. Thus, for total water balance simulation, a full hydrological model for example the type of the HBV-model developed by Bergström (Bergström 1976, Arner 1991) is needed.

Snow models are normally used in practice during snowmelt, in flood forecasting models (WMO 1986). It is, however also possible to use them during accumulation period. Thus the possibilities to simulate the areal snow water equivalent in real time throughout the entire winter for large basins with snow models is also studied.

Ground frost is one process which may affect snowmelt runoff. Possibilities for the improvement of snowmelt-runoff simulation by including a ground-frost model in a hydrological model were thus studied. A simple ground-frost depth model, which is usable with standard meteorological data, is presented, as one way to connect it to the snowmelt-runoff model.

Finally, some of the experience gathered by using snowmelt-runoff models in real-time forecasting is discussed: what were the main difficulties encountered and how could they be overcome ?

Some preliminary results of these studies concerning operational forecasting (Vehviläinen 1986a, 1986b, 1989), soil frost (Vehviläinen and Motovilov 1989), the variability of degree-day values (Vehviläinen and Kuusisto 1984) and the simulation of snowpack properties (Vehviläinen 1991) were presented earlier in international journals and publication series. Further, the snow models developed in this work were used in climate change simulations (Vehviläinen and Lohvansuu 1991) in order to evaluate the effect of climate change on snow cover and discharges in Finland.

2 RESEARCH BASINS

The two main research basins used for developing snow cover models are Tujuoja and Loimijoki. Tujuoja is a small experimental basin in Ostrobothnia, inside the Kalajoki basin (Fig.2) 64°N, 25°E. The drainage area of Tujuoja is 20.6 km^2, of which 82 % is forest (canopy density 30 %), 12 % field, 4 % bog and 2 % urban area. There are no lakes in the Tujuoja basin, and the mean slope is 2.3 % (Mustonen 1965a). The volume of growing stock in the forested area has increased from 48 m^3ha^{-1} in 1965 to 56 m^3ha^{-1} in 1975 (Mustonen 1965a; Seuna 1990, personal communication). More detailed information of Tujuoja is shown on the map in Fig. 1 and in Tables 1 and 2.

The other research basin is Loimijoki, a larger basin of 1980 km^2 located in southern Finland (Fig. 2), 61°N, 23°E. The Loimijoki basin is also flat (altitude range 50—100 m) with 55 % open areas (mainly cultivated land and marshlands) and 45 % forest. The study area has practically no lakes, the lake percentage being only 0.5 %.

In addition to the results for these main research basins, results obtained with the snowmelt temperature index method are also presented for nineteen large watersheds (Fig. 2). These areas are presented in Table 3, along with some information on the areas.

3 OBSERVATIONS

In this study all observations are standard meteorological and hydrological data available from registers kept at the Finnish Meteorological Institute and the National Board of Waters and the Environment. It was thus possible to use periods several years long (5 — 10 years) for the calibration and verification of different models. At all basins, the minimum group of observed variables used for the temperature index model for snowmelt were:

Precipitation
Measured at the height of 1.5 metre with a Wild-precipitation gauge (Ahti 1974).

Temperature
Measured at the height of 2 metre, the daily mean value being calculated from eight values taken every three hours (Loimijoki) or from four daily observations (Tujuoja) (Meteorological yearbook of Finland 1974).

Potential evaporation
Class A pan measurements.

Water level
Measured by a water stage recorder or manual observation at water level station.

Discharge
Calculated by means of discharge rating curves from water level observations or got from water-power stations.

Fig. 1. Map from the Tujuoja research basin, with land-use information (Mustonen 1965a).

Table 1. Land use information for Tujuoja basin, 20.6 km^2 (Mustonen 1965a).

Land use	Percentage of the area
Cultivated land	12
Building plot	1
Roads	1
Forest on firm land	28
Spruce hardwood peat-moor	40
Pine peat-moor	14
Open bog	4
Pond, lake	0
	100

Table 2. The distribution of soil types in the Tujuoja basin.

Soil type	Percentage
Graded soils (of which 14 % is coarse sand)	24
Moraines (of which 10 % is coarse sand)	17
Peat soils (of which 28 % is 30—49 cm deep)	59
	100

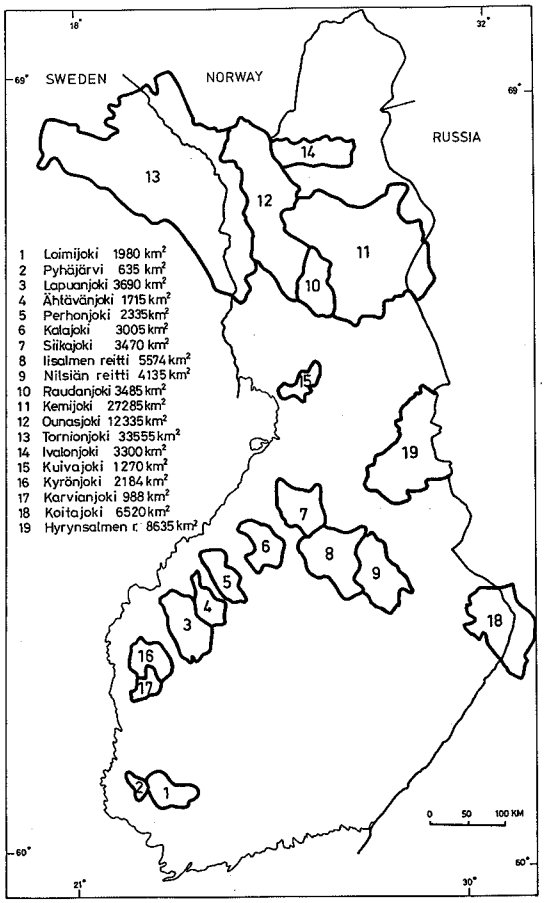

Fig. 2. The watersheds models used in this study.

Table 3. The area, lake percentage and number of sub-basins in the model for a large watershed, results of which are presented in the study (see also Fig. 2).

Watershed	Area km²	Lake percentage	Number of sub-basins
Säkylän Pyhäjärvi	635	25.0	3
Karvianjoki	988	3.1	5
Kyrönjoki	2 184	0.4	9
Lapuanjoki	3 690	3.0	4
Ähtävänjoki	1 715	11.0	3
Perhonjoki	2 335	2.5	5
Kalajoki	3 005	1.8	6
Siikajoki	3 470	1.6	5
Iisalmen reitti	5 574	7.6	6
Nilsiän reitti	4 135	10.4	9
Koitajoki	6 520	9.7	8
Hyrynsalmen reitti	8 635	7.5	9
Kuivajoki	1 270	2.7	3
Kemijoki	27 285	2.4	4
Raudanjoki	3 485	5.0	1
Ounasjoki	12 335	2.3	3
Tornionjoki	33 555	4.5	6
Ivalonjoki	3 300	0.3	1
Mean	7 008	5.6	5
Number of values	18	18	18
Standard deviation	—	5.9	—

Table 4. The number of precipitation (P), temperature (T), Class A pan (C), water level (W), discharge (D) stations and snow courses and snow stakes in parentheses (S) used at each research basin. Also presented are the length of the calibration (CA) and verification (V) periods, in years.

Basin	P	T	C	W	D	S**	CA	V
Säkylän Pyhäjärvi	4	1	1	4	3	3(1)	5	0
Loimijoki	8	2	1	2	2	5(1)	5	6
Ylä-Karvianjoki	7	2	1	4	3	2	10	0
Kyrönjoki Pitkämö	11	2	1	1	4	2	10	0
Lapuanjoki	9	3	1	12	10	6	5	0
Ähtävänjoki	5	2	1	3	3	3	7	0
Perhonjoki	7	3	1	3	3	3	7	0
Kalajoki	8	1	1	10	9	3	5	0
Tujuoja	1	1	1	1	1	1	5	13
Siikajoki	7	3	1	6	5	4	5	0
Iisalmen reitti	16	4	1	4	3	8	7	0
Nilsiän reitti	11	4	2	8	8	5	7	0
Koitajoki	6	1	2	6	3	3	10	0
Hyrynsalmen reitti	19	3	3	10	10	11	10	0
Kuivajoki	7	2	2	1	1	2	6	0
Kemijoki	18	6	2	2	5	11(2)	5	0
Ounasjoki	14	6	2	3	3	6	5	0
Raudanjoki	6	3	1	1	1	3	5	0
Tornionjoki*	14	13	2	5	5	5	9	0
Ivalonjoki	7	2	1	2	2	3	6	0
Mean	9	3	1	4	4	5	7	

* For Tornionjoki near the Finnish-Swedish border: Muonionjoki and Tornionjoki between Pajala and Pello

** Including snow courses in or near the basin

Snow water equivalent

The areal values of snow water equivalentwere read from snow maps of the monthly hydrological reports published by the Hydrological Office of the National Board of Waters and the Environment. These snow maps for every second week are based on snow course measurements made at about 160 lines throughout Finland.

The number of precipitation, temperature, Class A pan, water level and discharge stations and snow courses used at each basin is presented in Table 4.

For the main research basins, Tujuoja and Loimijoki more data were available for testing the models of snowmelt energy balance, snowpack and frozen ground. These additional observations were:

Wind velocity

Measured at the height of 10 metre by a rotating cup anemometer (Loimijoki, Jokioinen) or by a Wild vane (Tujuoja, Haapajärvi) (Meteorological yearbook of Finland 1974).

Relative humidity
Measured at the 2 metre level by a psychrometer (Jokioinen at the Loimijoki basin) or by a hair hygrometer (Haapajärvi at the Tujuoja basin) (Meteorological yearbook of Finland 1974). In both cases, four daily measurements were made, at 02, 08, 14 and 20 hrs.

Cloudiness
Amount of cloud cover at 02, 08, 14 and 20 hrs. Reported on a scale of 0 — 8, the number indicating how many oktas are covered by cloud (Meteorological yearbook of Finland 1974).

Short-wave radiation
At Jokioinen (Loimijoki), the measurements were made with a Moll-Gorczynski pyranometer, and they contain direct solar radiation together with radiation scattered and reflected from the sky (Meteorological yearbook of Finland 1982). At Tujuoja, the short-wave radiation measurements were made with a Bellani type pyranometer on the evaporation principle (Mustonen and Seuna 1969). This pyranometer was calibrated against the Moll-Gorczynski pyranometer at Jokioinen.

Snow depth
At Tujuoja, snow depth was measured from a snow course with 50 measurement points. At Loimijoki, areal snow depth was calculated from the measurements made at five snow lines and one snow stake station.

Snow density
Snow density was calculated at Tujuoja from one snow course and at Loimijoki the areal value was calculated from measurements made at five snow courses and one snow stake station.

Soil frost depth
At Tujuoja, frost depth is the mean for ten measurement points. Up till the year of 1980, frost depth was measured using a steel rod which was 3/4 inches thick and had a groove along one side. When the rod was turned round in the earth, soil stuck to the groove and the frost depth could be determined (Mustonen 1965a). Beginning from the year 1981, the frost depth measurements were made with methylene blue tubes (Hydrologiset havainto- ja mittausmenetelmät 1984). The depth of frost was determined from the change in the colour of methylene blue. When the temperature is below 0°C, methylene blue has a blue colour; above 0°C it is colourless. The difference between the measurements made with these two methods is 1—2 cm (Seuna 1990, personal communication).

With these additional observations, the calibration period was 1976—1981 and the verification period was 1970—1976 for both the Tujuoja and the Loimijoki basins.

4 METHODOLOGY

4.1 Development of snow cover models against the observed snow cover and total water balance

Snow cover models are developed with the aid of snow cover observations. They are then tested against the total water balance of the watershed, i.e. against discharge/water level observations. A complete watershed model is needed to test the snow cover models against the total water balance of the watershed. The different parts of the watershed model used are presented in the following paragraphs.

Snowmelt-runoff model. The basic rainfall-runoff model used in this study is a modification of the Swedish HBV model (Bergström 1976), which is widely used in Scandinavia, where it has over 50 applications (WMO 1986). This model contains a description of the following processes: areal precipitation (form and correction), snow accumulation and snowmelt, infiltration and storage of water in soil moisture zone and formation of runoff through subsurface and groundwater storage (Fig. 3).

In the precipitation model, precipitation is divided into the solid and liquid parts according to the daily mean temperature. The change occurs linearly within a given temperature range near zero. The solid and liquid precipitation is then multiplied by a correction factor, which is mainly due to the effect of wind on the catch of precipitation gauges. In the original HBV model, the snow water equivalent was simulated with a temperature index model. In the main part of this study, different versions of temperature-index models and energy balance models are tested. The different snow cover models are presented in Chapters 6,7, and 8.

The soil moisture content in the aeration zone is calculated by the water balance equation for the soil moisture zone

$$\frac{dMVS(t)}{dt} = YIELD(t) - Es(t) - INF(t) \quad (1)$$

$$Es(t) = HP(t)\frac{MVS(t)}{LP} \quad (2)$$

$$INF(t) = YIELD(t)\left(\frac{MVS(t)}{MVAK}\right)^{EX} \quad (3)$$

YIELD (mm d^{-1}) is the sum of snowmelt and rain at the watershed. Es (mm d^{-1}) is the evaporation intensity; INF (mm d^{-1}) is the intensity of water inflow into the upper storage. HP (mm d^{-1}) is the potential evaporation and LP (mm) is the soil moisture content after which evaporation achieves its maximum. MVAK (mm) is the maximum soil

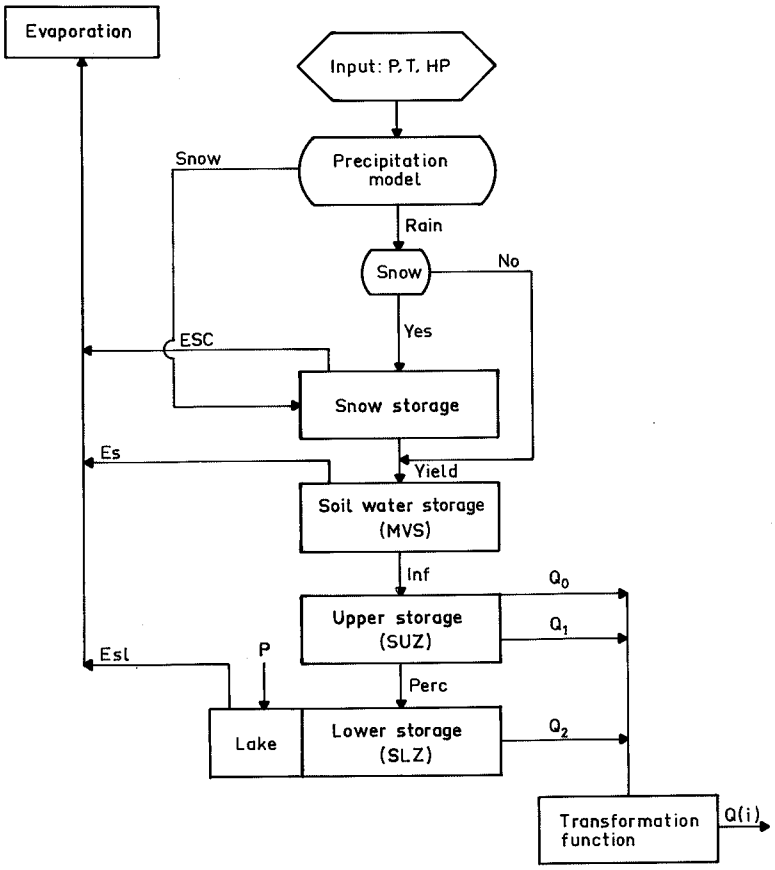

Fig. 3. General structure of the snowmelt-runoff model used for this study.

moisture, the physical value of which is close to the soil moisture content under field capacity.

A transformation model is needed to simulate the damping and time delay caused when rain and melt water goes through snow and soil layers or as surface runoff into rivers. The transformation model presented below simulates surface, sub-surface and ground water flow.

The upper storage SUZ (Fig. 3). The water balance equation for the upper storage SUZ (mm) is calculated according to

$$\frac{dSUZ}{dt} = INF(t) - Q_0(t) - Q_1(t) - PERC \quad (4)$$

$$Q_1(t) = K_1\, SUZ(t) \quad (5)$$

$$Q_0(t) = K_0\, UZ(t) \quad (6)$$

$$UZ(t) = SUZ(t) - LUZ,\ SUZ(t) > LUZ \quad (7)$$
$$UZ(t) = 0,\ SUZ(t) < LUZ$$

PERC (mm d^{-1}) is the intensity of water inflow into the lower storage; K_1 (d^{-1}) and K_0 (d^{-1}) are parameters. LUZ (mm) is the threshold value of upper storage for outflow Q_0 (mm d^{-1}).

The lower storage SLZ (Fig. 3). The water balance equation for the lower storage SLZ (mm) is as follows:

$$\frac{dSLZ(t)}{dt} = PERC - Q_2(t) \quad (8)$$

$$Q_2(t) = K_2\, SLZ(t) \quad (9)$$

For the timing of runoff after release from lower and upper storages, the Eq. 10 is used:

$$Q(i) = KR\,(Q_0+Q_1+Q_2)+(1-KR)\,Q(i-1) \quad (10)$$

Water balance model for lakes. For lakes and reservoirs, the normal water balance equation is

used as follows:

$$\Delta V = (QI - QO) + (P - Esl) + CORR \quad (11)$$

where
ΔV = the change of storage in the lake
QI = inflow to the lake
QO = outflow from the lake
P = precipitation
Esl = lake evaporation
CORR = correction of storage change due to lake ice on the lake bottom

Flood routing models. In cases without formidable flood areas along the river, the Muskingum flood routing model (e.g. Linsley et al. 1975) is used to route the flood in long river reaches:

$$QO(i) = C0\ QI(i) + C1\ QI(i-1) + C2\ QO(i-1) \quad (12)$$

where
QO(i) = the outflow discharge from the river reach
QI(i) = the inflow to the river reach
C0, C1, C2 = parameters which are functions of K and x.
K = storage constant; the ratio of storage to discharge, which is approximately equal to the time needed to travel through the reach.
x = the relative importance of inflow and outflow determining storage. For a reservoir, x = 0 as inflow has no effect and x = 0.5 when inflow and outflow are equally effective.

When there is a comprehensive flood area along the river, the flood routing model presented by Quick and Pipes (1975) has been used. The routing is divided into two stages. Flow translation is calculated first without a change in storage by the equation

$$QOT(i) = QI(i-1) + XZ \quad (13)$$

$$XZ = (1 - TT)\ dQ \quad (14)$$

where
QOT(i) = translated downstream flow at the time step
i QI(i) = inflow at the time step i
dQ = QI(i) — QI(i − 1)
T = RTK L/v
L = length of the reach (m)
v = flow velocity in the reach (m s^{-1})
RTK = the inverse of the kinematic wave speed constant (0.67)
TT = T/dt, travel time along the reach as fraction of the time step of the calculation (dt = 1 d)

The effect of storage change on the river reach is then calculated by the storage equation

$$dQO = 1/(1 - 2KT)\ dQI \quad (15)$$

$$dQI = QI(i+1) - QI(i)$$
$$dQO = QO(i+1) - QO(i)$$

$$KT = L \frac{dA}{dQ} \frac{STK}{dt} \quad (16)$$

where
A = cross-sectional area
STK = storage constant modification factor

The value of KT describes wedge storage in a river with an inclined water surface during flood wave. Therefore it is assumed to be half of the value calculated for a reservoir with a level surface. This correction is made by the constant STK, which is given the value 0.5.

The routing period should equal the true travel time of the flood wave so that for a channel reach, the flow increment will produce a change only in wedge storage.

Should the water levels at many points of the river be needed with high precision, one can use a dynamic physical river routing model based on Saint-Venant equations, which are solved by the double sweep method with Preissman discretization (see e.g. Forsius 1984). The Saint-Venant equations are for conservation of mass

$$b \frac{\delta y}{\delta t} = \frac{\delta Q}{\delta x} + q, \quad (17)$$

and for conservation of momentum

$$\frac{\delta Q}{\delta t} + \frac{\delta}{\delta x} \frac{(BQ^2)}{A} + gA \frac{\delta y}{\delta x} + gAS_f = 0, \quad (18)$$

where
y = water surface elevation above the datum
b = storage width
t = time
Q = discharge
x = longitudinal space co-ordinate in a horizontal plane
q = lateral inflow
A = cross-sectional area
g = acceleration due to gravity
S_f = friction slope
B = coefficient of non-uniform velocity distribution

This model is used in the Kemijoki watershed model, in the real-time forecasting version (Fig. 2).

Model subdivision and distribution of meteorological data. In the case of large basins, subdivision of the model is necessary. Subdivision is achieved by dividing the area according to vegetation, land use, elevation, area, etc. to more or less homogenous sub-basins. For these sub-basins, the areal value of precipitation and temperature are calculated by the Thiessen method (see e.g. Linsley et al. 1975) in the case of precipitation and by the Thiessen method or by elevation correction with temperature.

For areal values of air moisture, potential evaporation, cloudiness, radiation and wind, the observations of the nearest station had to be used, because these observation stations are so sparse that no areal calculation method could be used. Fortunately, these variables are more conservative in area than precipitation.

4.2 Optimization procedures for snow models

Model performance criteria. In this study, the objective function in calibration and verification of different snow and watershed models was the sum of squares of differences between observed and simulated values F^2:

$$F^2 = \Sigma(X_{t,obs} - X_{t,sim})^2 \quad (19)$$

The optimization results are presented in the form of a criterion called the efficiency of a model R^2 (Nash and Sutcliffe 1970):

$$R^2 = (F_0^2 - F^2)/F_0^2 \quad (20)$$

$$F_0^2 = \Sigma(X_{t,obs} - X_{mean,obs})^2 \quad (21)$$

F^2 or R^2 is a criterion of the agreement between computed and observed values in model simulation. The fit is better with a smaller F^2 or a higher R^2. R^2 and F^2 are essentially the same criterion. They will yield the same optimum parameter values. The advantage of the R^2 criterion is its character of relative measure, facilitating better comparisons between models when applied to the same basin and the same period of time. The values of F_0^2 vary from period to period and from basin to basin; therefore the R^2 values are not directly comparable between different time periods or basins. If the variance F_0^2 is low, small errors cause low R^2 values, while with high F_0^2 values the situation is the opposite. Still, if the variance and the accuracy of observations are comparable — as they often are with snow observations — the model efficiency fairly well reflects the general performance of a model also between different periods and basins.

The R^2 value is generally a good indication of the overall fit of the model as long as the comparison is restricted to identical periods of time and to one catchment. The best fit according to visual inspection and the R^2 value mostly coincide. With small differences in R^2 values, the results according to visual inspection do not differ and the models can be considered equally good. The R^2 value varies from minus infinity to +1; +1 means complete agreement between the observed and simulated values.

The R^2 or F^2 values emphasize large errors. Peak discharges with larger errors get more emphasis in calculation of the R^2 or F^2 values than low flow parts of the hydrograph. The correct timing of snow melt and peak discharge is also emphasized with this performance criteria, so that large errors can be avoided.

The F^2 and R^2 values are calculated for the areal water equivalent of snow, discharge, snow depth, snow density, short-wave radiation and frost depth, depending of the type of snow cover model developed. With simple temperature index models, performance criteria are calculated only for discharge and water equivalent, because simple models do not simulate other observed characteristics of snow cover.

Finally, with numerical optimization criteria, a visual inspection of snow cover and watershed models was used to check the performance of these models. Long sequences of positive or negative residuals of snow water equivalent or discharge ($= \Sigma(X_{t,obs} - X_{t,sim})$) can be detected in this way. It is also seen, if the errors in snow cover or watershed models are similar at a certain time of the year. These inspections provide suggestions on how the models may be inadequate and what kind of modification of the snow cover model is needed to correct these regularly occurring errors.

Optimization algorithms. Two complementary methods have been used for the optimization of different snow models during the calibration period. The main optimization method has been Rosenbrock's method (Rosenbrock 1960). In cases when Rosenbrock's method has not converged, which may happen at the beginning of the optimization of a new model structure with poorly known initial parameters, a parameter grid method has been used.

In the parameter grid method, which is a basic trial and error method, the best combination of parameter values is sought within a given range of parameters with a given increment. The increment may be quite large when better initial values for Rosenbrock's method are being sought. After the initial optimization, Rosenbrock's method has worked well. Finally with an entirely new model structure, a grid method has been used to check that the optimum values of parameters are not at a local minimum of verification criteria (F^2).

Different model versions are usually quite near to each others. The initial values of parameters are thus near the optimum, and Rosenbrock's method is used mainly to search for optimum values for one or two new parameters. With physically based snow and frost depth models, Rosenbrock's method is used to refine the initially known physical parameter values.

Calibration was done over the whole calibration period, which was usually 5—10 years for the 19 operational watershed models (presented in Fig. 2). For the two research basins, Tujuoja and Loimijoki, the calibration period was five years.

The R^2 values against discharge and areal water equivalent for the watershed models used in operational real-time forecasting are presented for all calibrated sub-basins in App. 1.

App. 1 includes some exceptionally low R^2 values for discharge/outflow (Karvianjärvi, Venetjärvi, Iso-Lamujärvi). The main reason for this is inadequate data. Calibration was done against outflow from a regulated lake for which water level observations were available only once a week. The residuals (Eq. 19) between observed and simulated outflows were calculated only on those days: the calculated water level has been forced to the observed level, and the error has been added to the calculated outflow. This led to a large F^2 value and a low R^2 value, because of the accumulated error. In all cases when the R^2 value against discharge is below 0.7, the calibration has been made against outflow calculated with the same method as above. Thus the residuals included the errors in water level measurements and the effect of wind, which diminish the R^2 value, especially if the storage of the lake is large compared to inflow into the lake. Naturally the performance values (R^2) of snow cover model are as high as normally (0.85—0.94) in those sub-basins. The inadequate water level and outflow observations do not deteriorate the snow cover model calibration against snow observations.

Optimization procedure for temperature index snow models. The optimization was made first against the areal snow water equivalent for simple temperature index snow models. After this snow model calibration, a limit for performance criteria (R^2) against areal water equivalent of snow was set, which could not be broken later. This limit was very near to the highest R^2 value obtained in the snow model calibration against snow observations as this guaranteed the best possible snow cover model to be used with the whole watershed model.

The next step was to calibrate the runoff model (snow model parameters not included) against total water balance, i.e. against discharge or runoff. The final calibration of the watershed model (all parameters included) was done against total water balance (discharge). During this stage, the model performance (R^2) limit against observed areal snow water equivalent takes care of it, that snow simulation is not deteriorated when model simulation against discharge is improved by changing snow parameters. This emphasizing of the total water balance in calibration may strengthen the interdependency between the snow model parameters and the runoff model. The snow model structure, and especially the parameters giving the best results, is not necessary the best with an other runoff model structure.

Optimization procedure for physical snow cover models. With physically based models, the R^2 and F^2 values are calculated separately for all observed quantities simulated in the snow cover model: snow density, depth, water equivalent, frost depth, short-wave radiation.

The model calibration proceeds now by calibrating different sub-models against relevant observations. The short-wave radiation model is calibrated against short-wave radiation measurements. The physically based snow cover model is calibrated against snow density, depth and water equivalent, in this order. After the calibration of parameters relevant in density simulation is completed, a limit for performance criteria (R^2) against density observations is set. This limit is not allowed to be broken in further calibrations. This has to be done, because the snow cover model is next calibrated against snow depth partly by using the same parameters as those used in density calibration. After this calibration, a limit for the R^2 value against snow depth observations is also set. The next step is to calibrate the snow model against the water equivalent of snow, using the R^2 value limits for density and depth. Again, a limit for the R^2 value against the water equivalent is set. Next, the runoff model (snow model parameters not included) is calibrated against observed discharge in order to fit the runoff model to the developed snow model. Finally, all parameters active during the snowmelt period are calibrated against discharge, because

during the short snowmelt period in spring, only data from one or two snow line measurements are available, and the information included in discharge observations is used to calibrate the snow cover model in this period. Naturally, the performance criteria limits for snow density, depth and water equivalent are valid during this final calibration, in order to retain the quality of the snow model against snow cover observations.

It is necessary to carry out runoff model calibration after snow model calibration, because there is a clear interdependency between the parameter values of a calibrated snow cover model and of a runoff model. However, the structure of a snow cover model, if calibrated against snow observations, is not specific for a runoff model structure.

4.3 Verification criteria in snow model development

The final check of the performance of a snow model is based on a watershed model run in a verification period different from the calibration period during which the parameter values were optimized. This verification is done after the optimization in the calibration period is finished. The verification period for the Tujuoja basin was 13 years with temperature index models and six years with energy balance models. For the Loimijoki basin, the verification period in both cases was six years. For the operational watershed models, the results are based only on the calibration period (App. 1).

For research watersheds, the verification criteria (R^2 or F^2) are calculated against observed discharge, areal water equivalent, snow density and snow depth when a physically based snow cover model is developed and against discharge and water equivalent when temperature index models are developed.

In this study, the decision concerning the best snow cover model is based mainly on the value of R^2 (or F^2) calculated against snow and discharge observations. This means that a model with a higher R^2 value in the verification period is always considered better than a model with a lower R^2 value even when less parameters have been calibrated. This choice had to be made, because with physically oriented snow cover models, the number of parameters increases considerably, but most of the values of these physical parameters are known more or less accurately. Thus we cannot choose the best snow cover model from the statistical point of view with verification criteria where the model performance, the R^2 value and the number of parameters are combined. The same is also true for sensitivity analysis when using physically based snow cover models. The sensitivity of many physically based parameters is often very low, and will thus lead to the rejection of a physically based snow cover model. In many cases, the difference according to R^2 criteria is very small and often negligible. In these cases, the conclusion is that these models are equally good for snow cover and snowmelt runoff simulation.

5 PRECIPITATION MODEL

The precipitation model is the first submodel in the snowmelt-runoff simulation part of the watershed model (Fig. 3). The precipitation model calculates the form of precipitation and the correction to be made for measured precipitation, to keep water balance correct for the entire watershed. The precipitation model presented here is used with both temperature index and energy balance snow simulation models.

Precipitation form. The form of precipitation is an essential factor in snow cover simulation. In Finnish conditions — long winters with temperatures well below zero — the problems encountered in simulation of the form of precipitation appear at the beginning and end of the snow cover period. During most of the winter itself such difficulties do not occur very often. Slight errors will not affect the performance of the snow cover model or, in particular the whole watershed model because the snowpack can retain a large amount of liquid water in the beginning of the snowmelt period. In most cases, the precipitation in the snowpack will refreeze during mid-winter. When the snow cover is thin or does not exist at all, errors in form simulation are critical to the performance of the snow cover model and to the simulation of runoff.

The mean daily temperature is used to calculate the form of precipitation. According to the results published by Hankimo (1976), the temperature at which 50 per cent of rain is solid and liquid is +0.9°C for the whole winter period; the temperatures corresponding to 25 and 75 per cent probabilities for snow were +1.3°C and 0.0°C and the temperatures for the probabilities of 10 and 90 per cent being +2.5°C and −1.2°C. The same

results are presented in Fig. 4. Similar results have also been presented in the Snow Hydrology report of the USCE (1956), according to which about 90 per cent of the cases of simulating the form of precipitation with the temperature range method would be correct.

App. 2 gives the temperature ranges between which the change of precipitation from solid to liquid is simulated linearly with the precipitation model used in this study. In the App. 2, the mean for this range is −3.0 ... +1.5 °C. The difference between the temperature range values is slightly less than that of Hankimo. The range has shifted 1.0 °C in the colder direction. The reason for this difference may rest in the fact that calibration is made against the overall performance of the watershed model and that the periods at the beginning and end of snow cover had the greatest effect on the calibration results. During mid-winter, the watershed model and the snow cover model are not very sensitive to the parameter values of the temperature range, owing to the retention capacity of the snowpack.

Precipitation correction. The precipitation input, which is used in all watershed models, is uncorrected. These values have to be corrected before they can be used in watershed models to keep the water balance correct. Most of the errors in precipitation measurements tend to diminish the measured precipitation value, especially during snowfall.

With point precipitation measurements, the errors are roughly the following (WMO 1982, WMO/ IHD 1973):

Error in liquid precipitation due to wind	2 ... 10 %
in solid precipitation due to wind	10 ... 50 %
Wetting error	2 ... 10 %
Evaporation error	0 ... 4 %
Splashing error	1 ... 2 %

Further, the error due to unsuitable position is strongly linked with the wind error and depends on the degree of sheltering of the rain gauge. This error varies from 2—14 % for liquid and 5—80 % for solid precipitation (NHP 1986). The affecting factors with these two interconnected errors are wind velocity, wind direction compared to sheltering structures and vegetation, and the form of precipitation.

Watershed models are used to calculate areal precipitation values. The accuracy of these values depends on the density of the precipitation station network (Fig. 5). The error in the areal estimate

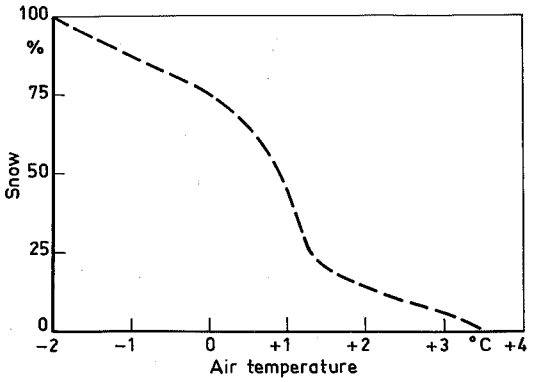

Fig. 4. The percentage of solid precipitation as a function of air temperature according to Hankimo(1976).

decreases as the gauging density increases and as the area with the same gauging density increases (Guschina et al. 1967). The values of the precipitation network density and the number of stations for the main watersheds used in this study are presented in App. 3.

In watershed models, precipitation is not corrected according to different error sources. Instead, the correction is made with one correction factor for solid precipitation and one for liquid precipitation. In model calibrations, these correction factors also include the possible effects of interception and elevation. Elevation differences in sub-basins are usually less than 100 metres and therefore in most cases elevation is not corrected separately. Further, the errors in discharge and water level measurements and in the sub-basin area can affect the calibrated correction factors. The initial correction values were 1.30 for solid precipitation and 1.06 for liquid precipitation. The correction factors obtained from calibration of different sub-basin models are presented in App. 3. From all calibrations, the mean value for the correction of liquid precipitation is 1.08, with a standard deviation (S.D.) of 0.05, that for the correction of solid 1.23 with S.D. of 0.10. The tendency of increasing correction factors for northern basins may result from an effect of elevation, as in those areas, precipitation gauges are situated mostly in valleys.

The solid precipitation correction factors obtained are near the values reported in previous studies. Based on 57 precipitation stations and 63 small watersheds with snow lines, Mustonen (1965c) has obtained winter precipitation correction values ranging from 1.00 to 1.50, with a mean of 1.19 and a S.D. 0.14. On the basis of comparisons of snow line measurements and uncorrec-

ted precipitation in 12 small watersheds, for solid precipitation, Gürer (1975) obtained a correction factor ranging between 1.19 and 1.44, with a mean of 1.31 and a S.D. of 0.14.

Precipitation correction with wind. Wind is the most important factor affecting precipitation correction. Thus it is reasonable to test, whether the addition of wind velocity to the correction function improves calibration and, particularly, the verification results. For the model of the Tujuoja basin, the following wind correction was tested:

$$PL_{corr} = PL_{obs} (CPL + CPLU\ U) \quad (22)$$

$$PS_{corr} = PS_{obs} (CPS + CPSU\ U) \quad (23)$$

where

PL = liquid precipitation
PS = solid precipitation
CPL = correction constant for liquid precipitation
CPS = correction constant for solid precipitation
CPLU = wind correction constant for liquid precipitation
CPSU = wind correction constant for solid precipitation
U = wind velocity (m s^{-1})

The values obtained in calibration for the parameters of the above precipitation function were

CPL = 1.04 CPLU = 0.012 (s m^{-1})
CPS = 1.12 CPSU = 0.045 (s m^{-1})

With 10 mm of precipitation, this means that the correction due to wind having a velocity of 3 m s^{-1} is 13.5 % or 1.35 mm for solid precipitation and due to wind having a velocity of 10 m s^{-1} the correction is 45 % or 4.5 mm. For liquid precipitation, the effect is 3.6 % or 0.36 mm in the first case, and 12 % or 1.2 mm in the second case. These values are reasonable when compared to the values presented by Allerup and Madsen (1980). According to them, the correction values (%) for the aerodynamic effect on liquid precipitation is 3 % with a rain intensity of 5.5 mm h^{-1} and with a wind velocity of 3 m s^{-1}. When the wind velocity is 10 m s^{-1} and the rain intensity same, the correction is 10 %. The aerodynamic correction factor with snowfall is also well in the range presented before in this text (10—50 %).

For the Tujuoja basin, the calibration and verification results with the basic watershed model and with the modified wind correction, as R^2 values are as follows:

Model	Calibration 1976—1981	Verification 1970—1976
Basic model	0.856	0.725
With wind correction	0.818	0.726

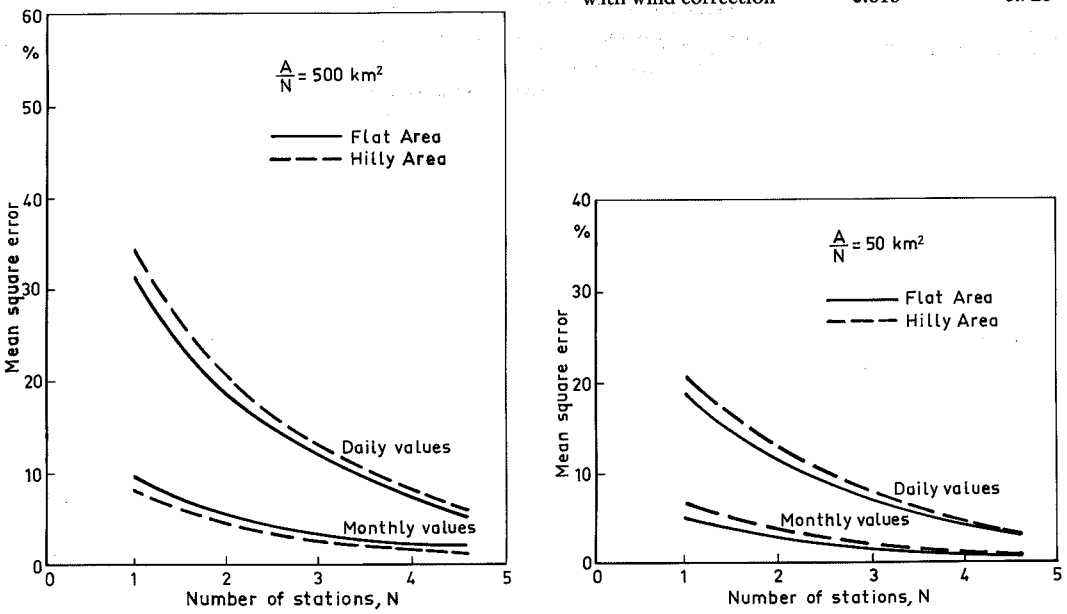

Fig. 5. Percentage mean-square error (% of mean total) of the areal precipitation estimate for large areas (2 000—40 000 km^2) in Russia (NHP 1986 with reference to Gushchina et al. 1967). A/N = precipitation gauge density. A = area (km^2).

The results showed that inclusion of wind does not improve the performance of the model during the verification period. This is because the average wind effect is taken into account in the precipitation correction factors in the basic model (App. 6). Precipitation correction increases the accumulated snow storage during winter, and the effect of correct precipitation is evaluated in spring with snowmelt flood. Thus the better daily correction of precipitation does not improve the performance of the watershed model.

6 TEMPERATURE INDEX SNOW MODELS

The starting point in the snow cover model development is the temperature index snow model used in operational watershed simulation and forecasting. This basic temperature index model is developed both in a simpler and more physically orientated direction in order to find the best snow model for large watersheds.

6.1 The operational snow model

As stated in the introduction, the energy balance approach is the physically correct method to simulate snowmelt. However, the most used method is the temperature index approach, of which there are many different versions. The energy balance approach is dealt later in this study. In the temperature index models, the physically correct snowmelt energy balance simulation, presented in Chapter 7, is substituted by a function where snowmelt depends only on air temperature.

This chapter presents the temperature index snow model originally used in operational watershed models, with some modifications.

Surface snowmelt and retention capacity of snow cover. In the simplest temperature index model, at least the following two processes have been modelled:

1. Surface snowmelt M (mm d^{-1}) as a function of the daily mean air temperature T (°C):

$$M = KM\,(T - TM)\ ,\ T > TM \qquad (24)$$
$$M = 0\ ,\ T \leq TM$$

where
KM = the degree-day constant (mm $°C^{-1} d^{-1}$)
TM = the threshold air temperature for snowmelt (°C)

2. The water retention capacity of snowpack WH (mm) and simulation of water storage WS (mm) in snowpack:

$$WH = CAP\,W \qquad (25)$$

$$\frac{d\,WS}{dt} = M + PL,\ WS < WH \qquad (26)$$

$$\frac{d\,WS}{dt} = \frac{(WS - WH)}{dt} + M + PL,\ WS > WH$$

$$YIELD = \frac{d\,WS}{dt} \qquad (27)$$

where
W = the water equivalent of snow (mm)
PL = liquid precipitation (mm d^{-1})
YIELD = water from snowpack (mm d^{-1})

The melt function is usually calculated with a one-day time-step, as revealed by the other name of the temperature index method — i.e. the degree-day method. Bengtsson (1986) compared the energy balance and degree-day methods and concluded that, when studying the correlation between the snow surface energy balance and the air temperature, the degree-day method is not valid for a time period shorter than one day.

Simulation of the water retention capacity is also essential because at the beginning of snowmelt the capacity can reach 20—30 % of the snow water equivalent (Kuzmin 1961). This retention storage can lead to a significant delay in snowmelt-induced runoff.

Refreezing. One possible way to improve the performance of temperature index model is to take into account the refreezing in snowpack during cold periods. This can be calculated in the same way as snowmelt; however due to the insulating effect of the snowpack, refreezing is not linearly dependent on temperature but on the square root of temperature as shown by Bengtsson (1982):

$$F = FM\,(T - TF)^e\ ,\ T < TF \qquad (28)$$
$$F = 0\ ,\ T \geq TF$$

where
F = refreezing of melted water in snowpack (mm d^{-1})
FM = parameter (mm $°C^{-e} d^{-1}$)
TF = the temperature threshold value for

refreezing (°C)
e = exponent (about 0.5)

The purpose of the threshold value in calculating melt and refreezing is to take into account the possible difference in temperature at the observation station and at the area of snow simulation. It can also take into account the possible differences between the true snowmelt and the temperature index simulation. For example, the cold content of snowpack can lead to a threshold value slightly above zero. On the other hand, during clear weather, the short-wave radiation can be so intense that snowmelt starts at a daily air temperature that is below zero. This kind of overlapping of the processes taken into account is typical for the temperature index method, and it does not necessarily lead to poor model performance. On the contrary, in this way it may be possible to choose the most important factors into the model and to omit less important dependencies during calibration of a model.

Variable degree-day factor and retention capacity. During the snowmelt period, the physical properties of snow change considerably. Snow becomes more granulated, its density increases and, most important, the albedo of the snow surface drops from about 0.8 to about 0.5 (USCE 1956, Kuusisto 1984) owing to the increase of density, water in snow and debris accumulated on melting snow. Finally the shallow snowpack allows solar radiation to penetrate into the ground, which increases the energy available for snowmelt. Further, patches of bare ground increase the melt rate particularly when the sky is clear and solar radiation is intense, because the melting is promoted by advective transport of sensible heat from the warm soil patches. All these processes contribute to increasing the snowmelt rate during the melting period. This has been noted by Hiitiö (1982) in studies concerning the value of the degree-day factor at the beginning and at the end of the snowmelt period in three research basins in Finland. A sudden increase in the intensity of melting in the aapa-mire following flooding of the mire has been earlier reported by the Tulvakomitean mietintö (1939) and by Nisula (1988). Flooded water caused a sudden decrease of snow albedo and increase of snowmelt. The approximation for the combined effect of these processes is to increase the degree-day factor as a function of cumulative snowmelt (Bergström 1975):

$$KM = KMIN\,(1 + KC\,SM) \qquad (29)$$
$$KM = KMAX,\ KM > KMAX$$

where
KMIN = the value of KM at the beginning of snowmelt (mm $°C^{-1}\,d^{-1}$)
KMAX = the value of KM at the end of snowmelt (mm $°C^{-1}\,d^{-1}$)
KC = parameter (mm^{-1})
SM = cumulative snowmelt (mm)

Another possibility, used by Anderson (1973), is to calculate the variable degree-day function according to the time of the year:

$$KM = (KMAX + KMIN)/2 + SIN(2N\pi/366)\,(KMAX - KMIN) \qquad (30)$$

where
N = the day number, beginning with 21st March
KMAX = the maximum melt factor, which occurs on 21st June
KMIN = the minimum melt factor, which occurs on 21st December

The development of the liquid water retention capacity is opposite that for the degree-day factor. The increase in grain size and the drains developing in the snowpack during snowmelt diminish the water retention capacity. Lemmelä (1970) verified this phenomenon by measurements. For this process an approach similar to that for the degree-day factor can be tested:

$$CAP = CMAX\,(1 - CC\,SM) \qquad (31)$$
$$CAP = CMIN\ ,\ CAP < CMIN$$

where
CMAX = the retention capacity at the beginning of melt (per cent of the water equivalent of snow))
CMIN = the retention capacity at the end of snowmelt (per cent of the water equivalent of snow)
CC = parameter (mm^{-1})
SM = cumulative snowmelt (mm)

Depression storage. During the calibration of snowmelt-runoff models for different sub-basins, the initial value of the retention capacity tends to reach 20—30 per cent of the water equivalent before good model performance could have been obtained, in the beginning of snowmelt. One possible reason for this is that in the beginning of snowmelt, a good deal of water storage is generated on flat areas, behind snowdrifts on marshlands and fields, before proper runoff from the area starts. Kuusisto (1984) came to a similar conclusion in

spring runoff studies on two small experimental basins at Finland. According to Kuusisto, the average maximum temporary depression storage in spring in these two basins was 52 mm and 62 mm. Nisula (1988) found a clear storage effect of a large aapa-mire in northern Finland during snowmelt. In the beginning of snowmelt, a large flood lake arose on the aapa-mire. Later, the water of the flood lake was released, suddenly causing a high runoff peak.

In order to keep the retention capacity of snow at reasonable limits, it was divided into two parts: the original water retention capacity of snow, with an upper limit of about 20 per cent, and a depression storage, with a maximum value SVM of 10—50 mm and with outflow dependent on the value of storage SV (mm):

$$dSV/dt = YIELD - SO \quad (32)$$

$$SO = SC\ SV \quad , SV \leq SVM \quad (33)$$

$$SO = SC\ SV + \frac{(SV-SVM)}{dt} \quad , SV > SVM$$

In about half of the models, the maximum value of depression storage (SVM) has been calculated as a function of the snow water equivalent:

$$SVM = CS\ W \quad (34)$$

where
W = the water equivalent of snow
CS = parameter (usually in the range of 0.1—0.8)

Depletion of snow covered area. After snowmelt has proceeded for some time, the first spots of bare ground appear, and the snow covered area diminishes with snowmelt. This process diminishes the water yield from a sub-basin, because the contributing area of snowmelt diminishes. It is important at the end of snowmelt, especially with snowmelt delayed by alternating cold and warm periods. If snowmelt proceeds quickly, in one short period, diminishing of the contributing area is not a very important process, because the lag time from snowmelt to runoff can cover it. The use of a snow cover depletion curve also reduces the need to subdivide the watershed (WMO 1986) when areal differences can be taken into account within a basin in this way.

In the snowmelt-runoff model, the depletion has been simulated with the following functions:

$$SA = 1 - \left(\frac{SM-SL}{WMAX-SL}\right)^{exs} \quad , \text{if } SM > SL \quad (35)$$

where

$$SL = WMAX\ LS \quad (36)$$

SA = the snow covered area (0 − 1)
SM = cumulative snowmelt (mm)
WMAX = the maximum water equivalent before melt (mm)
LS = parameter (0.5 − 0.9)
exs = parameter

or with a similar function

$$SA = (W / SL)^{exs2} \text{, if } W < SL \quad (37)$$

where
W = the water equivalent of snow (mm)

$$SL = WMAX\ LS2 \quad (38)$$

where
LS2 = parameter (0.5 − 0.9)

The depletion curve is type A in Fig. 6 if the exponent exs < 1 or exs2 > 1. The depletion curve B applies with exs > 1 or exs2 < 1.

Soil frost. The effect of soil frost is not simulated with the temperature index model or with the rainfall-runoff model (HBV-structure). A simple soil frost simulation model to be used in the HBV-model structure, is developed in Chapter 9.

6.1.1 Simplification of operational snow models

The structure of the basic temperature index model is presented in Fig. 7. It includes a variable degree-day parameter, a variable maximum retention capacity and simulations of refreezing, depression storage and areal depletion of the snow cover. This model version was then compared to versions

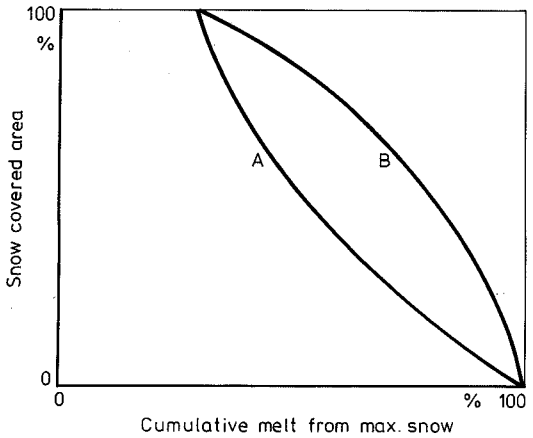

Fig. 6. Areal depletion of the snow cover as a function of cumulative snowmelt. The two basic cases A and B.

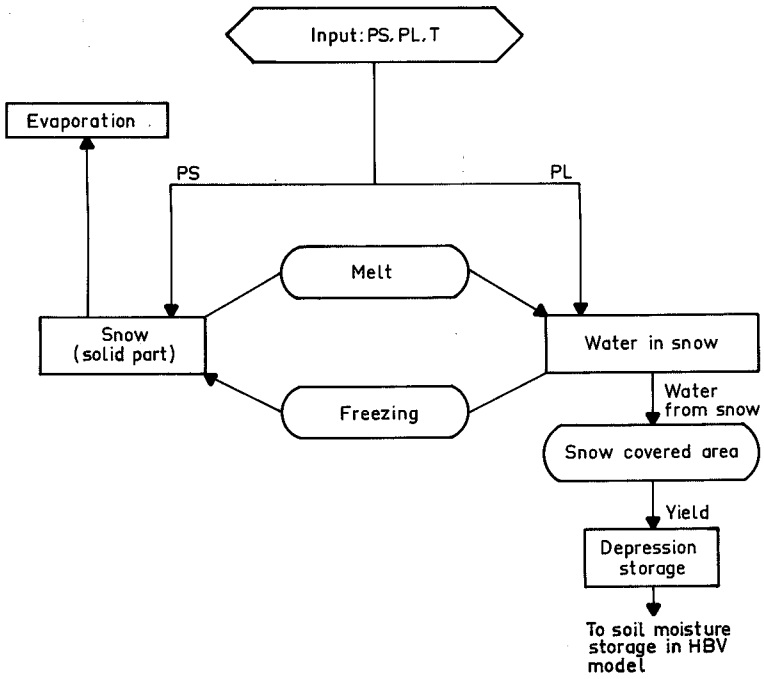

Fig. 7. The basic temperature index snowmelt model.

where one or more simulated process has been omitted.

This study investigating the effects of simplification of the basic temperature index snow model is done exceptionally with calibration and verification only against discharge/runoff observations but not against snow observations.

In the comparison the main emphasis has been on the results from the verification period. Because, the verification period constitutes the true check of the model performance. Two verification periods were used for the Tujuoja basin because only the verification period of 1970—1976 was usable for comparison against the energy balance models.

As could be expected, the results of the comparison are not at all clear if the objective is to find the best single model. At the Tujuoja basin, the two best model structures were the basic model (R^2=0.730 against discharge) and the model without depression storage and areal depletion simulation (R^2=0.734).

At the Loimijoki basin, all model versions performed nearly as well. The best results were obtained with the basic model, a model without simulation of refreezing and a model with a constant degree-day function. The very simple model without any modifications also gave good results in the verification period. The differences in model performance at the Loimijoki basin were generally less than at the Tujuoja basin: the choice between modifications was thus not as important at the Loimijoki basin. However, the basic model with all modifications gave the second best results in both basins during the verification period; this can be taken as proof that it is an acceptable way to simulate snowmelt.

6.1.2 Results obtained with parameter calibration of operational snow models

Degree-day constant. App. 4 presents the parameter values obtained with calibration of all watershed models in Fig. 2. For all the sub-basins, the mean initial value for the degree-day parameter (KMIN) is 1.4 $mm°C^{-1}d^{-1}$ and the mean value at the end of the melt period (KMAX) is 4.7 $mm°C^{-1}d^{-1}$. According to the results of Hiitiö (1982), the degree-day parameter increased during the melt season from 2.5 $mm°C^{-1}d^{-1}$ to 3.0 $mm°C^{-1}d^{-1}$, averaged over all terrain types. The results reported by Hiitiö are based on direct measurement of the snow cover once every five days. A mean value of 0.043 was obtained for the parameter KC in Eq. 29, which means that the

maximum value of the degree-day parameter is reached after 77 mm of snowmelt. The standard deviation for KMIN was 0.52 mm°C^{-1}d^{-1} that for KMAX being 1.9 mm°C^{-1}d^{-1}.

In all but one case, the variable (and increasing) degree-day parameter gave better results than a constant value. The exception was Pello sub-basin at Tornionjoki. The App. 4 also shows that the maximum value of the degree-day parameter is greater in southern watersheds — the mean for them being 5.1 mm°C^{-1}d^{-1} — than in the north (at Kemijoki, Ounasjoki, Raudanjoki, Tornionjoki, Ivalonjoki), where the mean value was 3.2 mm°C^{-1}d^{-1}. Otherwise the sub-basins used in northern rivers are much larger than at southern basins, which may cause the tendency for smaller maximum degree-day values, the results of averaging over a large area. The temperature stations are usually in valleys. The temperature values may thus be too high for areas with a higher elevation, this may be compensated by diminishing the degree-day values. The threshold temperature value for snowmelt (TM) was, on the average, 0.31 °C and the standard deviation was 0.49 °C. The threshold temperature parameter was able to take into account the difference in temperature between the station and the main area of the sub-basin, caused by elevation. The temperature lapse rate for elevation 0.6 °C/100m was used (WMO 1986). The results reveal that most of the threshold values are within the range of −0.6 and +0.6 °C except for the values for sub-basins of Tornionjoki and some other sub-basins (Ylä-Karvianjoki, Nilsiän reitti and Hyrynsalmen reitti). One reason for the greater threshold values at Tornionjoki and other basins is that they take the temperature lapse rate into account. The temperature stations are situated in river valleys, and the elevation difference between most of the temperature stations and a large part of the area of each sub-basin is near or over 100 m (Tornionjoki).

In autumn, the increasing degree-day factor is not necessarily a valid assumption, but then the values of cumulative melt are quite low and the degree-day is near the initial value. According to the results (App. 14 and 15), the model satisfactorily simulates the autumn snowmelt as well.

Retention capacity. The mean value of parameter CC in Eq. 31 was 0.018. This means that after 7 mm of snowmelt the retention capacity had reached the minimum. In this case the decreasing retention capacity is not a valid process, because the minimum value of retention capacity is reached in the very beginning of the snowmelt period, whereafter the retention capacity remains constant. In 29 cases, 38 % of all cases, when parameter CC was less than 0.01, the mean values for CMAX, CMIN and CC were: 0.16, 0.05 and 0.005. In those cases the minimum value is reached after 21 mm of snowmelt.

In many cases, the decreasing retention capacity hypothesis is probably rejected owing to the inclusion of depression storage in the model. Both storages have a similar effect on runoff, and they may overlap each other in calibration. From the viewpoint of large watersheds, the larger temporary storage dominates the retention storage effect, and this causes rejection of retention storage.

Depression storage. Two different methods have been used to define the maximum value of depression storage. The maximum value of depression storage (SVM) is constant, or it is a function of water equivalent of snow (Eq. 34), because according to Kuusisto (1984), the depression storage was greater in those springs, when the water equivalent of snow was large. In the first case, the maximum depression storage for 20 sub-basins had a mean of 24 mm with a standard deviation of 11 mm. The outflow constant for storage (SC) was 0.16 d^{-1}. With the other version, the maximum storage was 54 per cent of the water equivalent on the average with a standard deviation of 27 per cent; the mean for the outflow constant SC was 0.19 d^{-1}, with a standard deviation of 0.22 d^{-1}. In the latter case, the depression storage was clearly greater in the beginning of snowmelt. For example, with a water equivalent of 150 mm, depression storage is 81 mm on the average.

The only difference between retention capacity and depression storage in the later case is that depression storage has an outflow before it is filled up. Thus depression storage could be taken as an additional retention storage of snow, but the combined value of these two storages could be 70—100 per cent by weight, which is an overly high value, even though in some cases such large values have been reported for retention storage in the literature (Erbel 1969); most of the reported values, however, are 20—30 per cent by weight (Braun 1985). Depression storage can be also considered as an additional delay function for snowmelt runoff, compared to rainfall runoff in summer.

Refreezing. For 21 sub-basins, the refreezing Eq. 28 with an exponent of 1.0 was used. The mean degree-day constant thus obtained from optimization was 3.0 mm°C^{-1}d^{-1}, and the threshold temperature for refreezing was −1.14 °C; see App. 5. For 55 sub-basins, the exponent was also optimized; the mean value then was 0.12 (S.D. 0.21) with a degree-day constant for refreezing of 1.3 mm°C^{-1}d^{-1} (S.D. 1.4 mm°C^{-1}d^{-1}) and a

threshold value of −1.9 °C (S.D. 1.2 °C). Westerberg (1982) used values of 0.5 for the exponent and 2 mm°C^{-1}d^{-1} for the degree-day constant, in accordance with Bengtsson (1982). The refreezing process is important if warm and cold periods follow each other during the snowmelt period.

Depletion of the snow covered area. Eq. 35 was used to simulate the snow covered area of five sub-basins. The mean values for parameters LS and exs were 0.58 and 0.77 (App. 6), which means that the snow covered area starts to diminish after 58 per cent of the snow has melted, and that the depletion curve takes the shape of curve A in Fig. 6: bare ground appears after cumulative snowmelt limit is overridden at an increasing rate and later at a decreasing rate as the snow cover ablates.

With depletion Eq. 37, the number of calibrated sub-basins was 55. In this case, the mean values of parameters LS2 and exs2 were 0.67 and 1.3; see App. 6. The snow covered area now starts to diminish after 33 per cent of the snow has melted on the average. The depletion curve again takes a shape rather like that of A in Fig. 6, as in the previous case.

Kuusisto (1984) obtained results from eight small experimental basins where the value of LS ranged from 0.0 to 0.4 — bare ground appears after 0—40 per cent of the snow has melted — and the depletion curve took the shape of curve B in all cases: bare ground appears at a continually increasing rate as the snow cover ablates.

At the end of the snowmelt period, the snow covered area has a lower limit of 10 per cent with Eq. 35; with Eq. 37; the mean for this parameter, AMIN was 13 per cent. This parameter is needed to prevent the area contributing snowmelt from diminishing to near zero at the end of melting period.

Evaporation from snow. A constant value of evaporation from snow (ESC) was calibrated for all sub-basins. Its mean value was 0.09 mm d^{-1} (App. 5), which means 2.7 mm evaporation per month and about 15 mm for the snow cover period. According to Kaitera (1939), snow evaporation in southern Finland ranged from −0.7 mm d^{-1} to 1.9 mm d^{-1} in March and April during the springs of 1937 and 1938. The results reported by Kaitera and Teräsvirta (1972) showed that condensation prevails from December (3 mm) to February (1.5 mm), with evaporation in the snowmelt period prevailing in spring, accounting for 5.7—13.5 mm monthly. According to Bengtsson (1980), the total amount of evaporation during the whole snow covered season amounts to only 10—20 mm. Kuusisto (1984) arrived at values of 32 mm for open areas and 48 mm for forests during the period from January to April. Lemmelä (1990) presented the value of 0.22 mm d^{-1} for mean daily snow evaporation in snowmelt season or 4 mm per season. The values obtained for sub-basins are reasonable when compared against these results.

Ground melt. The mean value for snowmelt due to heat from the ground (GM) is 0.047 mm d^{-1}, or 1.4 mm per month (App. 5). Kuusisto (1984) arrived at larger values, from 5 mm to 20 mm per month.

The results from calibrations of snow evaporation and ground melt of course are unreliable, because their effect on the hydrological cycle is slight and can be hidden by measurements errors in precipitation (input) and discharge (calibration criteria). Still the results give some information concerning reasonable values for these parameters in the frame of a watershed model and water balance. As can be seen, these values are also reasonable when compared the to results obtained by using other methods. This kind of comparison provides information on the overall performance of a model.

The effects of various parameters are also overlapping, being dependent on each other; this means that model performance could have given the same results with a different combination of parameters. Still, this interdependency does not spoil the performance of the model, as can be seen from the results. Further, all parameters have some limited range of variation taken into account during the calibration of the models.

6.2 Snowmelt in open areas and in forests

Both the accumulation of snow and snowmelt in open areas differ from those in forested areas. During the accumulation period, forests have two main effects, which influence the accumulation of snow in different directions. The shielding effect of the forest prevents wind from transferring and redistributing snow. This increases the water equivalent of snow in the forest as compared to a large open area, where snow is transferred and accumulated at the edges of the forest and near other obstacles which prevent further transport of snow. This shielding effect is at its peak in sparse spruce and pine forests and in deciduous forests, where the interception effect of snow is small. The greatest amount of snow was found in small forest openings (Seppänen 1961b, Brechtel 1984). The interception effect is emphasized in dense forests,

especially spruce forests where the lowest water equivalent values of snow were found (Seppänen 1961a,b, Mustonen 1965b and Brechtel 1984). The amount of snow in large open areas is then larger than in dense forests but less than in sparse forests or in small forest openings and at marshlands sparsely covered with forest (Kaitera 1939).

During snowmelt, the main effect of forest is to shield the snow cover from direct solar radiation and from the effect of wind, i.e. turbulent exchange of sensible heat. On the other hand, the forest crown emits long-wave radiation after it is warmed up by solar radiation, so that the effect of solar radiation does not altogether disappear owing to covering by the forest crown. However, the overall effect of the forest on snowmelt is that melting proceeds more slowly the denser the forest is (Kaitera 1939, Kuzmin 1961 and Kuusisto 1984). The degree-day factor in the forest is thus clearly smaller than in open areas. Vehviläinen and Kuusisto (1984) obtained the following results for a small experimental basin in southern Finland by calibration of a temperature index model over data for 42 years:

	Forest	Field	Bog
Degree-day factor KM (mm $d^{-1}°C^{-1}$)	1.73	4.08	4.69
Threshold temperature TM (°C)	0.1	0.1	0.1

The calibration was done against measurements made every fifth day during the snowmelt period. The snow course was 4 km long, consisting of 91 observation points (50 in coniferous forests, 24 in open fields and 17 in open bogs). The same results are presented as a frequency distribution in Fig. 8.

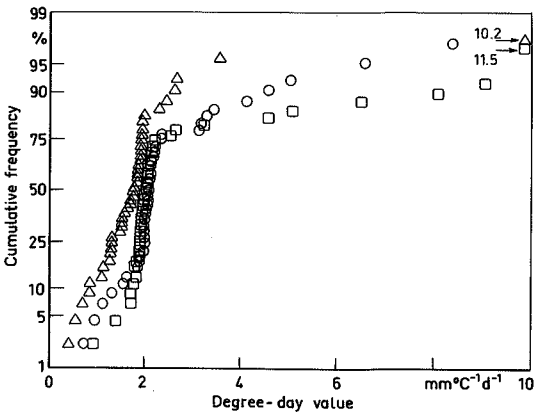

Fig. 8. The frequency distribution of degree-day value KM at the snow course in Vihti. The terrain types are forest (triangle), open field (circle) and open bog (square); Vehviläinen and Kuusisto (1984).

The results reveal that in the forest, the average snowmelt rate is 42 per cent of that in open field and 36 per cent of that in open bog.

According to Bergström (1990), the degree-day varies from 1.5 to 4.0 mm $d^{-1}°C^{-1}$ in the HBV-model applications used in Sweden. The value of 2.0 mm $d^{-1}°C^{-1}$ for forests and 3.5 mm $d^{-1}°C^{-1}$ for open areas is used as the first approximation.

Hiitiö (1982) calculated the degree-day factor for different terrain types from water equivalent observations made at three small research basins every fifth day. According to her, the degree-day factors were:

	Spruce forest	Deciduous forest	Open area
Degree-day factor KM	2.24	2.80	3.09
Threshold temperature TM	0.0	0.0	0.0

The range of change in degree-day values for open and forested areas during the melting season was also presented by Hiitiö (1982):

Degree-day factor KM	Open area	Deciduous forest	Spruce forest
At the beginning of the melt season	2.9	2.4	2.1
At the end of the melt season	3.3	3.1	2.4

In Russia Gurevich (1950) also calculated degree-day factors for different terrain types, and obtained the following results:

	Degree-day factor
Dense spruce forests	1.4—2.0
Spruce forests and dense deciduous forests	1.7—2.2
Sparse spruce forests	2.5
Open areas	3.9—5.2

The approach of different melt rates for open and forested areas has also been tested at the Tujuoja and Loimijoki basins. At Tujuoja the percentage of open areas is 14 at Loimijoki 55 per cent. At Tujuoja a temperature index model version with constant separate degree-day factors for open and forested areas was tested with the following parameter results from calibration:

Tujuoja	Forest	Open area
Degree-day factor KM (mm° C^{-1})	4.55	6.41
Threshold temperature TM (°C)	1.9	0.7

The threshold temperature was 1.2 °C higher in forests than in open areas, and the degree-day factor of forested areas was 70 per cent of that of open areas. The model performance with this

model version compared to the basic model of Table 5 for the Tujuoja basin were (performance criteria R^2, Eq. 20)

Tujuoja	Calibration 1976–1981	Verification 1970–1976	1963–1976
Basic model	0.856	0.730	0.717
Forest/open melt	0.837	0.630	0.652

The results indicate that this model version did not work well at the Tujuoja basin, which has a rather low percentage of open areas.

At the Loimijoki basin, the model version tested had separate and variable degree-day factors for both open and forested areas, with the following parameter values:

Loimijoki	Forest	Open area
Initial degree-day factor KMIN (mm° $C^{-1}d^{-1}$)	3.0	4.9
Final degree-day factor KMAX (mm° $C^{-1}d^{-1}$)	3.9	9.0
Parameter KC	0.015	0.021
Threshold temperature TM (°C)	0.9	0.9

The threshold value of air temperature for snowmelt was the same for open and forested areas. The initial value of the degree-day factor in the forest was 61 per cent of that in the open area. The degree-day factor at the end of the snowmelt period in the forest was only 43 per cent that in the open area and the final value was reached after 20 mm of melt in the forest and after 40 mm of melt in the open area (Eq. 29). In this case, the model performance results against discharge (Q) and water equivalent (W) were as follows (performance criteria R^2):

Loimijoki	Calibration 1976–1980		Verification 1970–1976	
	Q	W	Q	W
Basic model (Table 5)	0.858	—	0.768	0.667
Forest/open melt	0.856	0.853	0.780	0.837

The model version with a different snowmelt rate for the forest and open area gave better results than a model with the same degree-day factor for the whole area. In particular, the performance criteria against water equivalent was much higher,

Table 5. Comparison of different temperature index models at the Tujuoja and Loimijoki basins, based on the R^2 values. The basic model includes simulation of the variable degree-day parameter and the maximum retention capacity of snow, refreezing, depression storage and areal depletion of the snow covered area. The other versions are simplifications of this basic model, where:
1 = the degree-day parameter is constant, 2 = the maximum retention capacity of snow is constant, 3 = no refreezing of melted water, 4 = no depression storage, 5 = no simulation of areal depletion of the snow cover.

	Calibration	Verification	
	1976—1981	1970—1976	1963—1976
Model version	R^2	R^2	R^2
TUJUOJA:			
Basic model	0.856	0.730	0.717
Basic model+1+4	0.841	0.627	0.645
Basic model+2+4	0.831	0.681	0.678
Basic model+1+2+4	0.820	0.643	0.627
Basic model+1+2+3+4	0.798	0.599	0.621
Basic model+1+2+3+4+5	0.798	0.586	0.613
Basic model+1+2+4+5	0.797	0.563	0.598
Basic model+4+5	0.805	0.734	0.725
Basic model+3+4	0.835	0.663	0.669
Basic model+4	0.813	0.717	0.709
LOIMIJOKI:			
Basic model	0.858	0.768	
Basic model+1	0.860	0.769	
Basic model+2	0.857	0.753	
Basic model+1+2	0.858	0.750	
Basic model+1+2+3	0.844	0.743	
Basic model+1+2+3+5	0.776	0.751	
Basic model+1+2+3+4+5	0.766	0.763	
Basic model+5	0.795	0.754	
Basic model+3	0.841	0.769	
Basic model+4	0.850	0.759	

0.837 compared to 0.667, with the basic model. Measured in per cent, the Loimijoki basin has about four times more open areas than the Tujuoja basin. The Loimijoki basin is also much larger, so that the average differences between open and forested areas may be more stable from year to year. Exceptional snow distributions would not affect the results as much as on a small basin.

Due to the good results obtained for open/forest snowmelt modelling in the Loimijoki basin, this approach was taken into use in new operational watershed models. The calibration results from operational watershed models with a separate degree-day model for open and forested areas are presented in App. 7. The mean initial degree-day values were 1.7 $mm°C^{-1}d^{-1}$ for open areas and 1.4 $mm°C^{-1}d^{-1}$ for forests, and the final values were 7.8 $mm°C^{-1}d^{-1}$ for open areas and 4.7 mm $°C^{-1}d^{-1}$ for forests. On the average, the final degree-day value is reached after 109 mm of cumulative melt in open areas and after 83 mm of melt in forests. The values of snow cover model performance R^2 (Eq. 20) against observed areal water equivalent of snow are also high, ranging from 0.82 to 0.95 (App. 1) for all sub-basins where the open/forest degree-day model has been used.

Experiences of this version of the degree-day snowmelt model for operational flood forecasting have been good. Field observations have shown that the simulation of snow melt and snow cover separately in open and forested areas has been correct. Open areas are free of snow approximately two weeks earlier than forested areas. The obtained degree-day values are clearly higher than those obtained by Hiitiö (1982), partly because of the higher snowmelt threshold value TM. The degree-day values presented by Kuusisto (1980) were quite near those obtained in this study.

The seasonal degree-day function (Eq. 30) was also tested at the Loimijoki basin. The model parameters obtained separately for open and forested area from calibration of Eq. 30 for Loimijoki basin were

	Forest	Open area
KMIN ($mm°C^{-1}d^{-1}$)	4.7	5.5
KMAX ($mm°C^{-1}d^{-1}$)	4.7	9.8
TM (°C)	0.8	0.5

The development of the degree-day factor according to Eq. 30 is presented in Fig. 9. The results indicate that the degree-day factor remains constant in the forest throughout the whole year, and only the degree-day value for open areas varies as assumed in Anderson's original model. The explanation for this phenomenon may be that short-wave radiation, with which the seasonal

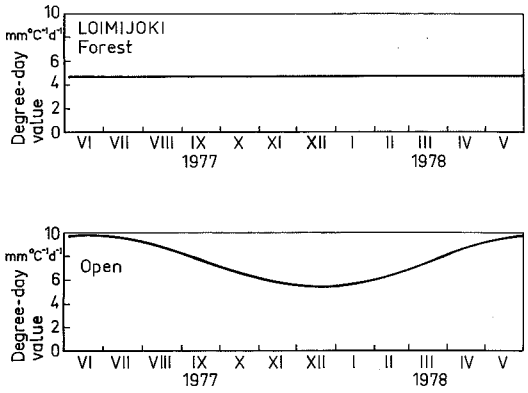

Fig 9. The variation in the degree-day value according to Eq. 30 over one year in forested and open areas in the Loimijoki basin.

degree-day function is correlated in this case, is less important in the forest than in open areas. Thus the degree-day value in the forest does not follow the seasonal variation presented by the Eq. 30, but is more or less independent of it. The model performance obtained from the verification period was 0.748 against discharge and 0.817 against water equivalent. Thus the results were not as good as those obtained by the model version, where variation in the degree-day factor was based on Eq. 29.

6.3 Distributed snow cover models

In Chapter 6.2, the snow cover was simulated by a model which calculated snowmelt differently in open and forested areas, with good results for the Loimijoki basin. This kind of model is a first step to a distributed snow cover model. Killingtveit and Aam (1978) used a statistically distributed snow cover model, which resembles the areal depletion curve presented in Chapter 6.1, with the HBV-model. According to the results of Kuusisto (1984), in most cases both normal and gamma distributions can adequately describe the variability of snow depth in small river basins.

Kuchment et al. (1986) used a 2-parameter gamma-distribution of the water equivalent of snow in simulating snowmelt runoff. The coefficient of variation C_v of the water equivalent of snow was calculated using the following empirical formulae:

$$C_v = ((CV1 + CV2\ W)/W)^2 \text{ if } W < CV5 \qquad (39)$$

$$C_v = CV3\ W + CV4 \qquad \text{if } W > CV5 \qquad (40)$$

where
W = the water equivalent of snow (cm)
CV1, CV2, CV3, CV4, CV5 = parameters
(2.5, 0.23,—0.0038, 0.32 and 8 for the Sosna river)

This method has been used for the Sosna river (drainage area 16 300 km^2) for flat and only partly forested area in the region of the northern Don river, but it may also be applicable to Finnish conditions, with flat but more forested areas. According to the Eqs. 39 and 40 the coefficient of variation of snow cover is large, about 2.5 in the beginning of the accumulation of snow cover, and it then diminishes with an increasing snow water equivalent to about 0.32 during the maximum snow water equivalent, if the maximum water equivalent is over 8 cm.

According to Kuusisto (1984), the coefficient of variation of the maximum snow water equivalent is about 0.28 for large watersheds with an area of 1 700 km^2 to 60 000 km^2. In general, there was a decreasing tendency in the coefficient of variation from southern to northern Finland: typical values were 0.30—0.40 in the south and 0.20—0.25 in the north.

A model which simulates the areal distribution of the water equivalent of snow during accumulation and ablation according to a gamma distribution was programmed. It calculates gamma distributed snow water equivalent values for five classes, which correspond to 10, 20, 40, 20 and 10 per cent of the basin area. The gamma distribution is retained by dividing new snow for each class according to the discrete density values of gamma distribution of each class. After temporary snowmelt, new snow is added to the five classes so that the gamma distribution is caught up again; thereafter new snow is distributed normally according to the discrete density values.

In the first model version tested in the Loimijoki basin, the coefficient of variation was calculated according to the Eqs. 39 and 40, in the second attempt with Eq. 39 and in the third version with Eq. 40. For the fourth version, the coefficient of variation was calculated according to both Eqs. 39 and 40 but the soil moisture storage, upper storage and lower storage (Fig. 3) were also simulated separately for the five classes.

The results, expressed as model efficiency, are presented in Table 6.

The model performance during the calibration period was as good as with snow simulated differently for open and forested areas in section 6.2 against discharge and somewhat worse against the water equivalent of snow. These results reflect the overall picture that distributed snow models tend to give better results. One has still to remember that all snow models discussed in this paper are distributed during snowmelt at least for snow free and snow covered areas. The test when the snow cover was simulated without any snow distribution at the Loimijoki basin gave an R^2 value as low as 0.755 against discharge during the verification period (Table 5).

Table 6. The model efficiency (R^2) against observed discharge (Q) and mean areal water equicalent (W) in the Loimijoki basin during the verification and calibration periods.

Model	Model efficiency R^2			
	Calibration period		Verification period	
	Q	W	Q	W
First version	0.816	0.905	0.779	0.798
Second	0.809	0.905	0.777	0.808
Third	0.818	0.904	0.778	0.831
Fourth	0.816	0.905	0.780	0.798

Figs 10 and 11 present examples from simulation of the water equivalent of snow in five classes with the fourth (Fig. 11) and third (Fig. 10) model versions at the Loimijoki basin during the winter of 1971—1972 in the verification period. In the first model version, both Eqs. 39 and 40 were used to calculate the distributed snow cover. Thus the variation in the water equivalent values in different classes is at greatest in the beginning of the snow cover period and then diminishes as the maximum snow cover is approached. The development of the coefficient of variation according to Eq. 40 is also described in Fig. 11. The values of the parameters in Eqs. 39 and 40 are presented in Table 7. In the third model version (Fig. 10), with the best model performance against the observed water equivalent, the coefficient of variation was practically constant, being 0.36 over the whole snow period, and the differences between snow in five classes were proportionally the same all the time.

According to Table 7, the coefficient of variation for the maximum snow cover is about

Table 7. The values of the parameters CV1, CV2, CV3, CV4 and CV5 in Eqs. 39, 40 for different model versions.

Model	CV1	CV2	CV3	CV4	CV5
First version	2.5	0.23	$-.12 \cdot 10^{-5}$	0.35	5.6
Second version	2.5	0.24	—	—	—
Third version	—	—	$-.10 \cdot 10^{-3}$	0.36	—
Fourth version	2.5	0.23	$-.11 \cdot 10^{-5}$	0.35	5.6

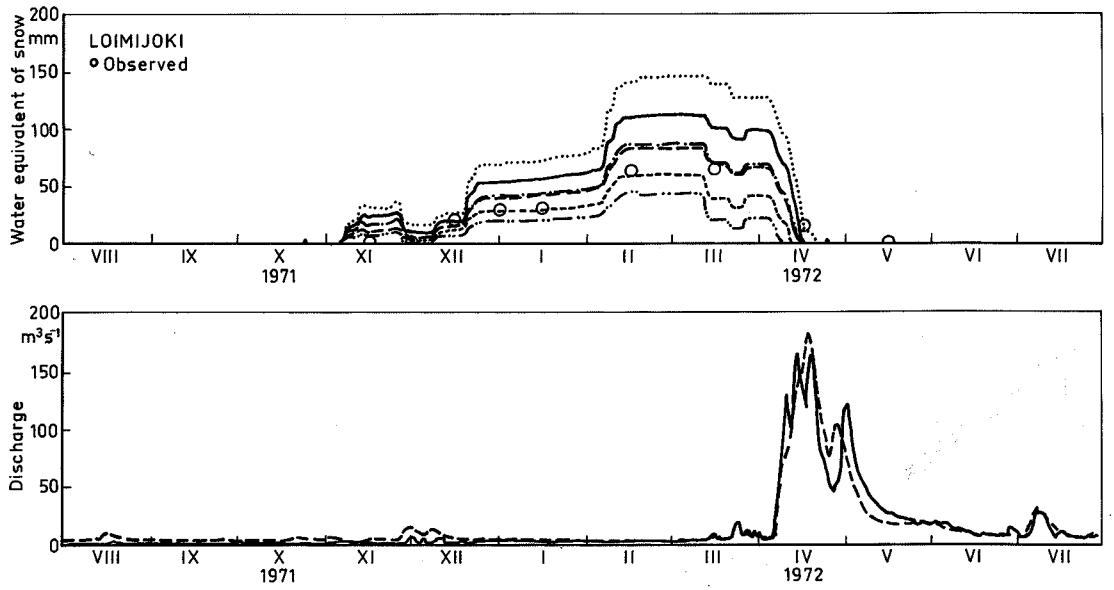

Fig. 10. Loimijoki basin: The values of water equivalent in the five classes (0.1 - · · -, 0.2 - - - , 0.4 — — , 0.2 —— , 0.1 ...) of gamma-distribution in the winter of 1971—1972. The coefficient of variation is 0.35 (third model version, Tables 6, 7). The observed areal values of water equivalent are marked by (o) and the simulated areal value by (— · —). Observed (——) and simulated (- - -) discharges are presented in the lower picture.

0.35, which is in the middle of the range presented by Kuusisto (1984) for coefficient of variation of maximum water equivalent of snow for large river basins in southern Finland: 0.30—0.40. Further refining of this distributed model may include the use of different distributions for different terrain types.

6.4 The effect of liquid precipitation

Rainfall affects snowmelt directly by heating snowpack. Sometimes it may also cool it, if the temperature of liquid precipitation is below zero. This direct effect is not very important in snowmelt. Melt due to heat-storage in liquid precipitation (PM) is calculated by

$$PM = PKM\,(T_s - T_p) \qquad (41)$$

where

PM = melt (mm d^{-1})
PKM = 0.0125 (mm $°C^{-1}$ mm^{-1}), constant based on specific heat of water 4.19 J $°C^{-1}$ g^{-1} and the latent heat of fusion of ice 334 J g^{-1}.
P = precipitation (mm d^{-1})
T_s = the temperature of snow (°C)
T_p = the temperature of precipitation (°C)

For example, with 10 mm of precipitation at an air temperature of 10 °C, the melt due to the heat in precipitation is only 1.3 mm, while snowmelt calculated by the degree-day factor of 3 mm $°C^{-1}$ d^{-1} is 30 mm. The heat in precipitation accounts for only 4 per cent of the melt in this case.

The other effects of rainfall on snow during snowmelt are more important. Rainwater accelerates the ripening process of the snowcover by reducing the thermal and capillary retention capacity of snow. Before snow can melt, the temperature of snow has to rise to 0°C; liquid precipitation can cause this rise very quickly. Every millimetre of frozen water releases 33 J of energy per square centimetre, and the specific heat of snow is 2.1 J $°C^{-1}$ g^{-1}. For example, the cold content of a 100 cm deep snowpack with a density of 0.25 g cm^{-3} at a temperature of −10 °C is fulfilled by liquid precipitation of 16 mm, i.e. the temperature increases from −10 °C to 0°C, after which all energy is used for snowmelt.

Liquid precipitation during snowmelt accelerates the metamorphosis of the snowpack. The snowpack becomes denser, more coarse in structure and vertical drains are developed in the snowpack. This leads to the reduction of the liquid water retention

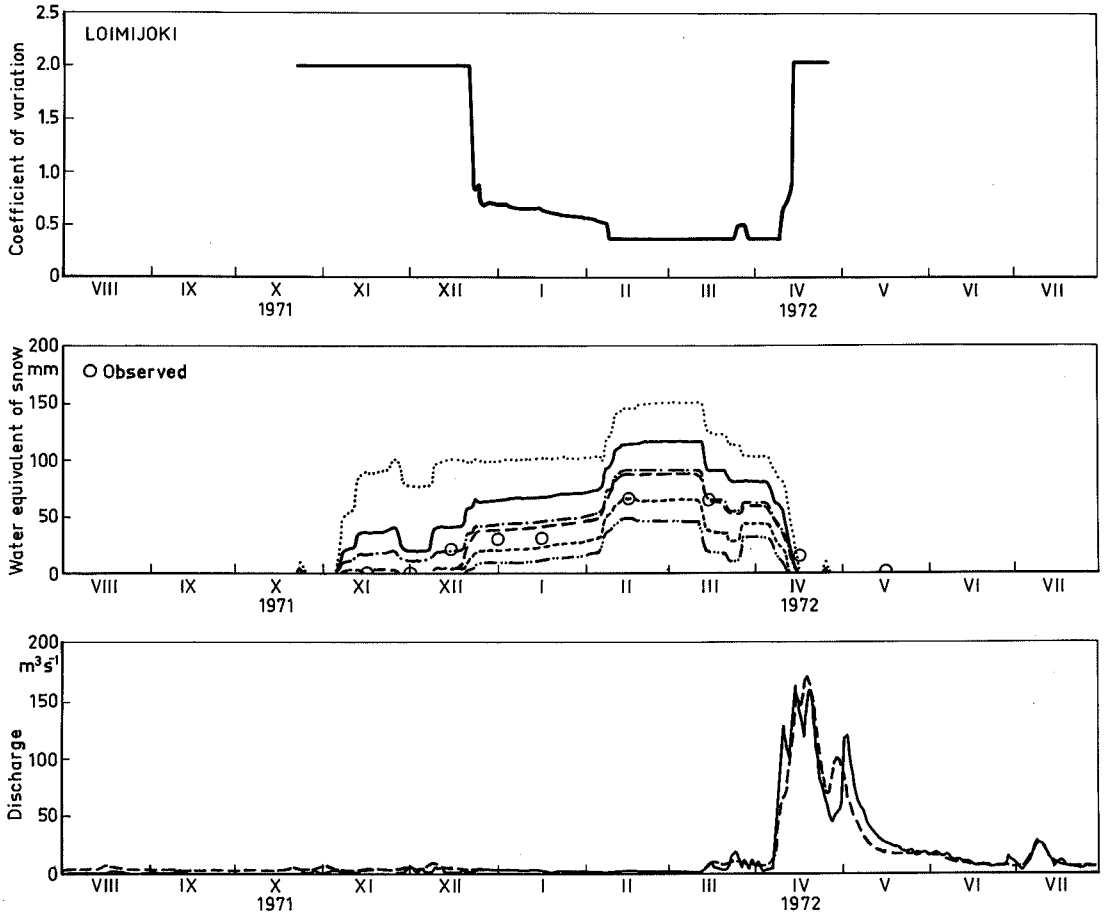

Fig. 11. Loimijoki basin: The values of water equivalent in the five classes of the gamma distribution (0.1 – · · –, 0.2 – – –, 0.4 — — , 0.2 ——, 0.1 ...) and the development of the coefficient of variation calculated by Eq. 39 over the winter of 1971—1972 (fourth model version, Tables 6, 7). The observed mean areal values are marked by (o) and the simulated areal value by (– . –). Observed (——) and simulated (– – –) discharges are presented in the lowest picture.

capacity, which accelerates the water yield from the snowpack. The reduced retention capacity has been taken into account in the basic snowmelt model of Table 5. Measurements of the reduction of liquid water retention capacity during snowmelt has been done by Lemmelä (1979).

In flat country, as at Tujuoja and Loimojoki, during rainfall the conditions for snowmelt are similar over a large area, and melt starts at approximately the same time. This emphasizes the effect of rainfall on melt-runoff.

With the discussion above as the background, it is feasible to suppose that the effect of liquid rain on snowmelt may be more than just the heating effect expressed in Eq. 41 by the theoretical value of PKM.

App. 8 presents the values for parameter PKM obtained from calibration of the snowmelt model for different sub-basins. Snowmelt has been calculated in those cases with degree-day Eq. 29 with a variable degree-day factor and with precipitation melt of Eq. 41. The mean value for parameter PKM is 0.092 mm $°C^{-1}$ mm^{-1} d^{-1}, which is seven times the value calculated from the direct heating effect. The variation in PKM is rather large, and according to the calibration results, liquid precipitation has no effect on snowmelt in twelve sub-basins. This indicates of observation errors and the fact that the increase in melt or snowpack yield caused by liquid precipitation is not a very important process. If we take into account only cases when the value of PKM is effective, i.e. greater than 0.001 in 35 cases, the mean value is 0.15 mm $°C^{-1}$ mm^{-1} d^{-1}. Now the

increase in snowmelt with liquid precipitation of 10 mm is 7.5 mm when the mean temperature is 5 °C. This means a 50 % increase in snowmelt with a degree-day factor of 3 mm $°C^{-1}$ d^{-1}.

For Loimijoki, the model performance according to R^2-criteria (Eq. 20) has also been tested with and without precipitation melt Eq. 41 in snowmelt simulation:

Loimijoki	Calibration 1976–1981	Verification 1970–1976
Basic model (Table 5)	0.858	0.768
-with precipitation-melt	0.864	0.771

At Loimojoki the snowmelt model with precipitation-melt gave slightly better results than the basic model of Table 5. At Tujuoja the results for the basic model and for the version with precipitation-melt were about the same, because the value of parameter PKM was near zero (App. 8). Thus, although the effects of liquid precipitation may be important especially at the beginning of snowmelt, the inclusion of precipitation-melt in the snowmelt model does not greatly affect the model performance over the whole snowmelt period.

Another possibility of handling the effects of rain during snowmelt is to separate the calculation of snowmelt between clear-sky and rainfall situations. For example

$$\text{Clear-sky: } KM = KMIN\,(1 + KC\,SM), \quad P < PLIM \qquad (42)$$
$$KM = KMAX,\ KM > KMAX$$
$$\text{Rainfall: } KM = PKM2,\ P > PLIM$$
$$M = (KM + PKM\,PL)\,(T - TM),$$

where

KM = the degree-day factor (mm $°C^{-1}d^{-1}$)
KMIN = the initial degree-day factor
KMAX = the maximum degree-day factor
SM = cumulative snowmelt (mm)
KC = parameter (mm^{-1})
P = total precipitation (mm d^{-1})
PL = liquid precipitation (mm d^{-1})
PLIM = threshold precipitation (mm d^{-1})
PKM2 = the degree-day factor during rainfall (mm $°C^{-1}$ d^{-1})
PKM = snowmelt due to heat in precipitation (mm mm^{-1} $°C^{-1}$)
T = the air temperature (°C)
TM = the threshold air temperature for snowmelt (°C)

With this model version, in which at clear-sky situation separate degree-days are used for open and forested areas, the parameters from optimization at Loimijoki were

	Whole area	Open areas	Forested areas
TM	—	0.66	0.69
KMIN	—	3.7	2.7
KMAX	—	10.0	6.6
KC	—	0.033	0.0079
PKM2	3.9	—	—
PKM	0.018	—	—
PLIM	4.5	—	—

According to these results the melt rate is lower during rainfall due to the absence of solar radiation with overcast sky. During rainfall the degree-day factor is 3.9 m $°C^{-1}$ d^{-1}, but in open and forested areas, the degree-day factor increases from 3.7 to 10.0 and from 2.7 to 6.6 after 52 mm and 182 mm of snowmelt. The degree-day factor of the forest is quite near the value of the degree-day factor of the rainfall situation. In both cases, the solar radiation is decreased strongly by cloudiness and the forest crown. The model performance according to R^2 criteria was also slightly lower than with the basic model of Table 5:

Loimijoki	Calibration 1976–1981	Verification 1970–1976
Basic model (Table 5)	0.858	0.768
Rain/clear-sky melt	0.848	0.752

6.5 Temperature index models combined with energy balance terms

The energy balance of the snowpack, which determines the amount of snowmelt, is written as

$$RTOT = RSN + RLN + RLAT + RSEN + RP + RG - CO, \qquad (43)$$

where

RSN = short-wave radiation balance
RLN = long-wave radiation balance
RLAT = latent heat exchange
RSEN = sensible heat exchange
RP = heat content of liquid precipitation
RG = heat exchange at the soil surface
CO = heat deficit of the snowpack (cold content)

These different energy balance components are functions of standard meteorological data:

$RSN = f(RS, AL)$
$RLN = f(T, T_s, e_a)$
$RLAT = f(e_a, U)$

RSEN = f(T, U)
RP = f(T, T_s, PL)

where
AL = the albedo of the snowpack
RS = the incoming short-wave radiation ($J\ cm^{-2}\ d^{-1}$)
e_a = vapour pressure (mb)
T = the air temperature (°C)
T_s = the snow surface temperature (°C)
U = wind velocity ($m\ s^{-1}$)

Only shortwave radiation and latent heat are not direct functions of the air temperature. Inclusion of these terms into the temperature index snowmelt model could thus improve the results. With the basic degree-day model of Table 5 the following energy balance components are tested for short-wave radiation:

$$RSN = RKM\ (RS - TR) \quad (44)$$

$$RSN2 = 1/LH\ (RS - TR2)\ (1 - AL) \quad (45)$$

$$AL = 0.9\ (W/WMAX)^{eal}, \text{ if } AL < 0.3\ AL = 0.3 \quad (46)$$

where
TR, TR2 = threshold radiation ($J\ cm^{-2}\ d^{-1}$)
RKM = parameter ($mm\ J^{-1}\ cm^{-2}$)
LH = parameter ($J\ mm^{-1}\ cm^{-2}$)
W = water equivalent of snow
WMAX = maximum water equivalent of snow

For net short-wave radiation, Lang (1984) proposed the use of Eq. (45), where LH signifies the latent heat of fusion (33 $J\ mm^{-1}\ cm^{-2}$). For simulation of the albedo, the approximate Eq. 46 has been used. Eq. 44 is a simpler version of the short-wave component without albedo.

The following equations are used for sensible and latent heat exchange (Kuzmin 1961):

$$RSEN = UKM\ (T - TM)\ U \quad (47)$$

$$RLAT = EKM\ (e_a - e_s)\ U \quad (48)$$

where
UKM = parameter ($mm\ m^{-1}\ s\ °C^{-1}\ d^{-1}$)
EKM = parameter ($mm\ m^{-1}\ s\ mb^{-1}\ d^{-1}$)
e_a = air vapour pressure (mb)
e_s = saturation vapour pressure at the melting snow surface (mb)
U = wind velocity ($m\ s^{-1}$)
T = temperature (°C)
TM = threshold temperature for snowmelt (°C)

The measurement height for wind U was mostly 2 metres at open sites in Kuzmin's studies. Other researchers have used measurement heights from 0.6 to 3 metres (Kuzmin 1961, Male and Gray 1981). The wind speed ratio at the level of 10 metres and 2 metres — used in this study — computed theoretically from the logarithmic wind speed formula $u_{10}/u_2 = \ln(z_{10}/z_0)/\ln(z_2/z_0)$ (Kuzmin 1961) is 1.19. The parameter z_0 is the roughness height of the snow surface, 0.05 cm. The parameters UKM and EKM should be divided by this value to get two-metre values, if the logarithmic distribution is valid. In a forested watershed, the distribution of wind is not logarithmic. Wind velocity is greatly reduced within tree stands. Reifsnyder and Lull (1965) suggest a general range of 20 to 60 per cent reduction. Reifsnyder's (1965) study showed a 50 to 60 per cent maximum attenuation under lapse conditions and a 60 to 70 per cent reduction under inversion conditions. Eq. 41 is used for precipitation heat.

Table 8 presents the results according to model performance from calibrations and verifications of different model versions. At Tujuoja, the basic model with terms for short-wave radiation, sensible heat and latent heat gave slightly improved results in overall model performance. The improved combinations according to R^2 criteria were

Basic + RSN	0.733
Basic + RSN + RLAT	0.736
Basic + RSN + RSEN	0.737

At Loimijoki, only the model version where the latent heat exchange component was connected to the basic temperature index model from Table 5 (Chapter 6.1.1) gave slightly better results.

The parameter values used in different model versions are presented in App. 8 and 9.

Of the two equations tested for short-wave simulation, i.e. Eqs. 44 and 45 the simpler version 44 gave better results.

The inclusion of energy balance terms in the temperature index model did not significantly improve the overall model performance. All the additional components are not without effect in melt simulation, as can be seen from the following example where the amount of melt due to different melt components in the temperature index model is calculated with the input data from Table 9. Table 9 presents weather data for Jokioinen in April, with 5, 25 and 50 per cent probabilities for occurrence (Heino and Hellsten 1983), short-wave radiation being an exception. For shortwave radiation, the 50 per cent value is the daily mean for April in 1971—1980, while the five per cent

Table 8. Results from testing the basic temperature index model of Table 5 with different energy balance components. Model performance criteria R^2 (Eq. 20). Calibration and verification were made against runoff and discharge.

	Model performance criteria R^2			
	Tujuoja		Loimijoki	
	Calibration	Verification	Calibration	Verification
Model	1976—81	1970—76	1976—81	1970—76
Basic model	0.856	0.730	0.858	0.768
Basic+RSN2	0.847	0.716	0.851	0.764
Basic+RSN	0.847	0.733	0.851	0.767
Basic+RLAT	0.841	0.698	0.844	0.774
Basic+RSEN	0.840	0.730	0.865	0.753
Basic+RSN2+RLAT	0.846	0.628	—	—
Basic+RSN+RLAT	0.847	0.736	0.829	0.736
Basic+RSN+RSEN	0.847	0.737	0.844	0.734
Basic+RSEN+RLAT	0.841	0.724	0.841	0.761
Basic+RSN+RSEN+RLAT	0.848	0.724	0.839	0.718
Ba+RSN+RSEN+RLAT+RP	0.849	0.712	0.826	0.732
Basic+RSEN+RLAT+RP	0.841	0.731	0.818	0.730
Basic+RSN+RP	—	—	0.844	0.670

value for short-wave radiation is the mean daily maximum from the same period in April (Meteorological yearbook of Finland 1982).

The amount of melt from each component of energy balance is calculated with the main input from the probability category and other possible input values as means. The results are presented in Table 10. For the degree-day component, only the mean temperature value was used as input in every case. The parameter values used are means from App. 9—12. The degree-day value is considered to be the mean maximum value of degree-day from the same appendices.

This example in Table 10 shows that in the extreme case, the component of latent heat

Table 9. Five, 25 and 50 per cent probabilities for the occurrence of daily temperature (T), wind (U), vapour pressure (ea) and short-wave radiation (RS) in April at Jokioinen.

Variable	Probability of occurence (per cent)		
	5	25	50
T (°C)	7.6	4.1	1.8
U ($m\ s^{-1}$)	7.8	5.3	3.7
e_a (mb)	8.2	6.5	5.5
RS ($J\ cm^{-2}\ d^{-1}$)	2200	1750	1300

Table 10. Snowmelt in millimeters and in per cent from total snowmelt due to different components, when the main input variables are chosen from Table 9 (except temperature, which is mean value).

Snowmelt component	Probability of main input variables		
	5	25	50
Loimijoki			
Degree-day component	3.1 mm (15%)	3.1 mm (28%)	3.1 mm (42%)
RSN	6.4 mm (30%)	5.1 mm (47%)	3.8 mm (52%)
RSEN	0.8 mm (4%)	0.6 mm (6%)	0.4 mm (6%)
RLAT	10.8 mm (51%)	2.0 mm (19%)	0.0 mm (0%)
Total	21.1 mm (100%)	10.8 mm (100%)	7.3 mm (100%)
Tujuoja			
Degree-day component	3.8 mm (51%)	3.8 mm (71%)	3.8 mm (81%)
RSN	0.9 mm (12%)	0.8 mm (15%)	0.6 mm (13%)
RSEN	0.7 mm (10%)	0.4 mm (7%)	0.3 mm (6%)
RLAT	2.0 mm (27%)	0.4 mm (7%)	0.0 mm (0%)
Total	7.4 mm (100%)	5.4 mm (100%)	4.7 mm (100%)

becomes more and more important; this is especially so at Loimijoki, but also at Tujuoja. This is reasonable, because latent heat is simulated with an equation that does not include the air temperature. The solar radiation term dominates the mean weather conditions more at Loimijoki. At Tujuoja the degree-day component is the most important in all cases.

The difference in the percentage of open areas at Loimijoki and Tujuoja is also seen in the results. Loimijoki has 55 per cent of open area, compared to 18 per cent at Tujuoja. In open areas the effect of solar radiation, sensible heat and latent heat exchange are more important than in forest areas, where the long-wave radiation balance dominates the snowmelt and where the degree-day snowmelt model gives a good approximation of snowmelt.

6.6 The use of daily minimum and maximum temperatures

Day and night snowmelt calculated from daily temperature variation. Popov (ref. Kuzmin 1961, WMO 1974) presented a temperature index model, which is related to the energy balance approach. In this model incoming short-wave radiation RS ($J\,cm^{-2}\,d^{-1}$), effective long-wave radiation RL ($J\,cm^{-2}\,d^{-1}$) and vapour pressure e_a (mb) are expressed as a function of the daily maximum T_{max}, minimum T_{min} and mean T_{mean} (°C) temperature:

$$RS = 238\ J\,cm^{-2}\,d^{-1}\,°C^{-1}(T_{max} - T_{mean}) - 50\ J\,cm^{-2}\,d^{-1} \quad (49)$$

$$RL = 92\ J\,cm^{-2}\,d^{-1}\,°C^{-1}(T_{mean} - T_{min}) \quad (50)$$

$$e_a = 0.35\ mb\,°C^{-1}\,T_{air} + 4.11\ mb \quad (51)$$

Using these equations as an energy balance approach, snowmelt (mm) is calculated separately for day and night with the formulae

$$M_{day} = 6.2\,(1 - AL)\,(T_{max} - T_{mean}) + 0.65\,(T_{mean} - 0.5) - 1.4\,(T_{mean} - T_{min}) \quad (52)$$

$$M_{night} = 0.65\,U\,(T_{mean} - 0.5) - 1.4\,(T_{mean} - T_{min}) \quad (53)$$

Albedo (AL) is calculated using Eq. 46 and U ($m\,s^{-1}$) is wind velocity. According to Popov, this model gives the best results for snowmelt calculations in northern regions with abundant snow.

For the Tujuoja basin, this model gave a model efficiency R^2 of 0.25 against runoff, which means that it was not at all suitable. With a modification in the advective part and with optimization, a model efficiency of 0.82 (calibration against runoff) was obtained using the formulae

$$M_{day} = 0.67\,(1 - AL)\,(T_{max} - T_{mean}) + 1.89\,(1 + 0.05\,U)\,(T_{mean} - 1.3) - 0.25\,(T_{mean} - T_{min}) \quad (54)$$

$$M_{night} = 1.89\,(1 + 0.05\,U)\,(T_{mean} - 1.3) - 0.25\,(T_{mean} - T_{min}) \quad (55)$$

This model is quite near the degree-day model and the effects of the short-wave radiation term and the sensible heat term (wind) have been reduced considerably compared to the original model.

The best model efficiency, $R^2 = 0.83$ in calibration against runoff, was obtained with the model:

$$M_{day} = 2.2\,(1 + 0.04\,U)\,(T_{mean} - 2.7) \quad (56)$$

$$M_{night} = 2.2\,(1 + 0.04)\,(T_{mean} - 2.7) \quad (57)$$

This is just a normal degree-day model with wind as an extra term. It seems that Popov's model is not valid for forested conditions at the Tujuoja basin.

Diurnal temperature difference in the snowmelt model. According to Eq. 49, presented by Popov, short-wave radiation should be a function of the difference between the daily maximum and mean temperature (°C). This temperature difference term can then be used as an additional short-wave term in the basic degree-day model (Table 5) as follows:

$$RST = KST\,(T_{max} - T_{mean}), \quad \text{if } T_{mean} > TM_{mean} \quad (58)$$

where

KST = parameter ($mm\,°C^{-1}\,d^{-1}$)

TM_{mean} = threshold daily mean temperature for snowmelt (°C)

Another way to take the solar radiation into account is to use the difference between the daily maximum and minimum temperatures. A large difference correlates with clear sky conditions with abundant solar radiation in the daytime:

$$RST2 = KST2\,(T_{max} - T_{min})\text{, if } T_{max} > TM_{max} \quad (59)$$

KST2 = parameter (mm $°C^{-1}\,d^{-1}$)

Kuusisto (1984) obtained results according to which a large diurnal temperature difference would decrease the rate of snowmelt, i.e. the difference between the maximum and minimum temperatures is correlated with long-wave radiation. This is tested by the following refreezing equation, which is added to the basic temperature index model:

$$RLT = KLT\,(T_{max} - T_{min}),\text{ if } T_{min} < TM_{min} \quad (60)$$

KLT = parameter (mm $°C^{-1}\,d^{-1}$)

These three melt terms were tested with the basic temperature index model and the results presented in Table 11. The results indicate that the inclusion of temperature difference terms did not improve model performance according to R^2-criteria against runoff.

The parameter values obtained from optimization are presented in App. 13.

At Tujuoja, the RST and RST2-term accounts for about 30 per cent of total melt in an average situation in April. At the Loimijoki basin, RST2 was about 10 per cent of the average melt and RLT, which is now a freezing component, was 19 per cent of the average melt. The average condition was the mean values of the mean, maximum and minimum temperatures at Loimijoki in April: $T_{mean} = 2.1$ °C, $T_{max} = 6.4$ °C, $T_{min} = -1.9$ °C. At Loimijoki basin, the RST2-term in the basic temperature index model offsets the effect of increasing degree-day value.

Modified daily mean temperature. Solantie (1977) suggested that the following modified mean temperature could be used in the temperature index model:

$$T = (T_{max} + T_{min})/2\text{, if } T_{min} > 0\ °C \quad (61)$$

$$T = (T_{max} + 0.5\,T_{min})/2\text{, if } T_{min} < 0\ °C \quad (62)$$

In this method, the maximum temperature value is emphasized when minimum temperature is below 0°C. This method allows some melt during days with a mean temperature below zero, which is true in the clear sky situation with abundant solar radiation. In this model, the degree-day factor is constant and not variable as in the other tests.

The results from the Tujuoja and Loimijoki basins according to R^2 criteria were:

	Tujuoja		
	Calibration	Verification	
	1976—81	1970—76	1963—76
Basic model	0.856	0.730	0.717
Modified T_{mean}	0.774	0.603	0.597

	Loimijoki	
	Calibration	Verification
	1976—86	1970—76
Basic model	0.858	0.768
Modified T_{mean}	0.855	0.713

At the Loimijoki basin, the results obtained with the modified mean temperature model were better than at Tujuoja, but in both cases they were not as good as with the basic model of Table 5.

The values of the constant degree-day factor and threshold temperature (Eq. 24) were 2.2 mm $°C^{-1}d^{-1}$ and 0.6 °C at Tujuoja and 4.5 mm $°C^{-1}d^{-1}$ and 1.1 °C at Loimijoki.

The use of degree-hours in snowmelt simulation. Westerberg (1982) presented a method by which the sum of the positive and negative degree-hours during a day can be calculated on the basis of the daily maximum and minimum temperatures. This information takes the diurnal temperature variation into account better than mean temperature alone.

The part of a day (DP) when the temperature is over 0 °C is calculated by

Table 11. Calibration and verification results against runoff/discharge using different snowmelt models with diurnal temperature difference as an input variable.

	Tujuoja			Loimojoki	
	Calibration	Verification		Calibration	Verification
Model	1976—81	1970–76	1963–76	1976–81	1976–81 1970–76
Basic	0.856	0.730	0.717	0.858	0.768
Basic+RST	0.850	0.673	0.704	—	—
Basic+RST2	0.863	0.695	0.703	0.858	0.736
Basic+RLT	—	—	—	0.855	0.753

$$DP = 1 \text{ , if } T_{min} > 0\ ^{\circ}C \quad (63)$$
$$DP = T_{max} / (T_{max} - T_{min}) \text{ , if } T_{min} < 0\ ^{\circ}C$$

The sum of positive degree-hours (H_+) is calculated by

$$H_+ = 0 \text{ , if } T_{max} < 0\ ^{\circ}C \quad (64)$$
$$H_+ = 12\ DP\ T_{max} \text{ , if } T_{max} > 0\ ^{\circ}C \text{ and } T_{min} > 0\ ^{\circ}C$$
$$H_+ = 12\ DP\ (T_{max} + T_{min}) \text{ , if } T_{max} > 0\ ^{\circ}C \text{ and } T_{min} < 0\ ^{\circ}C$$

The sum of negative degree-hours (H_-) is calculated by

$$H_- = 0 \text{ , if } T_{min} > 0\ ^{\circ}C \quad (65)$$
$$H_- = -12\ (1 - DP)\ T_{min} \text{ , if } T_{min} < 0\ ^{\circ}C$$
$$H_- = -12\ (T_{max} - T_{min}) \text{ , if } T_{max} < 0\ ^{\circ}C$$

Snowmelt is now calculated by the degree-hour model

$$M = KMH\ H_+ \quad (66)$$
$$KMH = \text{degree-hour factor (mm } ^{\circ}C^{-1} h^{-1})$$

and the refreezing of liquid water in snow by:

$$F = FMH\ H_-^{0.5} \quad (67)$$
$$FMH = \text{parameter (mm } h^{-0.5})$$

With the melt model presented above together with the decreasing cumulative retention capacity and depression storage as presented in the basic snowmelt model of Table 5, the model performance in the calibration period at the Tujuoja basin was 0.745 against runoff, which is much less than 0.856, the value obtained with the basic degree-day model.

The value of the degree-hour constant (KMH) from optimization was 0.10 mm $h^{-1}\,^{\circ}C^{-1}$, and for refreezing the value of parameter FMH was 0.41.

6.7 Separate melt models for clear-sky and rainy days

During a clear-sky situation, short-wave radiation melt is an important component for total snowmelt, and the increasing degree-day approach fits well with the solar radiation melt simulation with decreasing albedo during the melt period, because the decreasing albedo enhance the melt.

On rainy days long-wave radiation melt, sensible heat and latent heat melt become more important compared to short-wave radiation. The degree-day factor in rainy days may stay rather stable over the whole melt period. Thus the values of the degree-day factor may be different on clear-sky and rainy days.

This kind of model structure was tested at the Loimijoki basin, with the following functions:

Clear-sky melt is calculated with Eqs. 24 and 29, i.e. with a growing degree-day factor as a function of cumulative snowmelt.

Rain-melt is calculated with the constant degree-day factor:

$$M_{rain} = KM_{rain}\ (T - TM) + PKM\ P\ (T_s - T_p) \text{ , if } P > P_{lim} \quad (68)$$
$$P_{lim} = \text{precipitation threshold value for rain-melt (mm)}$$

This model structure was tested with different parameters for open and forest areas in clear-sky situation and without this separation. The results as model performance, indicated by the R^2 value against discharge, were:

	Calibration 1976—81	Verification 1970—76
Open/forest areas	0.848	0.752
No separation of land use	0.845	0.736

The results with separate melt parameters for open and forest areas were better than with common parameters. However the basic model of Table 5, and especially the version with open and forest areas (Chapter 6) were still better.

The parameter values obtained from optimization of these two model versions at the Loimijoki basin were:

Model	TM	KMIN	KC
Separate melt for:			
— Forest	0.69	2.7	0.0079
— Open areas	0.66	3.7	0.033
Forest + Open:	0.87	4.7	0.012

Model	KMAX	KM_{rain}	P_{lim}	PKM
Separate melt for:				
— Forest	6.6	3.9	4.5	0.018
— Open areas	10.0	3.9	4.5	0.018
Forest + Open:	7.0	4.9	4.6	0.015

The parameter values suggest that on rainy days

snowmelt does not exceed clear-sky melt at the end of snowmelt season.

6.8 Results from the best temperature index models

App. 14 and 15 present the simulation of runoff and water equivalent of snow with the best temperature index snowmelt models for the basins of Loimijoki and Tujuoja in the verification period.

The best temperature index model for Loimijoki was the basic operational temperature index model improved with the different melt functions for open and forest areas presented in Chapters 6.1 and 6.2. For the verification period, the R^2 criteria was 0.780 for discharge and 0.837 for the water equivalent of snow. An equally good model was the temperature index model with snow cover gamma distribution; its performance was 0.778 against discharge and 0.831 against snow, presented in Chapter 6. Important is that these two models were the best according to both the results based on verification against water equivalent and discharge measurements. Thus the best snow model also gives the best simulation of discharge. The optimization was done first against the observed water equivalent of snow, but the final optimization was done against discharge, because discharge observations are made daily while snow observations are made twice a month.

The snow melted 5—20 days earlier in open areas than in the forest at the Loimijoki basin (App. 14). According to Kaitera (1939), the difference on the basis of field measurements is approximately 5—10 days.

The results for simulation of runoff and the water equivalent of snow with the best model version at the Tujuoja basin in the verification period of 1970—1976 are presented in App. 15. This model version was the combination of the basic degree-day model presented in Chapter 6.1 with the short-wave radiation and sensible heat terms presented in Chapter 6.5. The performance criteria of this model was 0.737 against runoff and 0.567 against snow water equivalent. The observations of the water equivalent of snow are from a snow line with 50 measurements points. At the Tujuoja basin, the best model according to snow measurements was not the best according to runoff. One reason for the worse results at the Tujuoja basin may be that there was only one precipitation station available, and even that was outside the basin.

7 ENERGY BALANCE SNOW MODEL

Temperature index models are not very stable. The best values for the degree-day factor vary from spring to spring and within spring. An energy balance snowmelt model is applied because it simulates the snowmelt phenomenon physically correctly. It is also assumed that energy balance model should be more stable from spring to spring and does not cause errors due to variable model parameters as temperature index model.

The energy balance of snowpack (RTOT), which determines the amount of snowmelt is given by Eq. 43. The different components will be discussed in the following.

7.1 Short-wave radiation

The short-wave radiation (wavelength less than 3μ m) originates from the sun, but part comes as a diffused component reflected from clouds and terrain. A thick cloud cover can reduce the short-wave radiation to one quarter of the clear-sky value.

A large amount of incoming short-wave radiation is reflected by snow cover. This portion of incoming short-wave radiation, which is mainly a function of snow albedo, depends on the wavelength, the geometry of the radiation and especially on the snow structure. New snow reflects more than 80 per cent, whereas coarse-grained old snow reflects only 30—40 per cent (Slaughter 1969, Kuusisto 1984, Lemmelä 1990).

Incoming short-wave radiation. The incoming short-wave radiation either can be measured or it can be calculated from information on local latitude, date and cloudiness. Measurements of short-wave radiation are made by a Bellani type pyranometer at Tujuoja and by a Moll-Gorczynski at Loimijoki (Chapter 3).

To calculate direct solar radiation above clouds incident upon a horizontal surface (RS_i), the following function is used (Kuchment et al. 1983):

$$RS_i = SLR \sin a - SLR2 \sin a^{0.5} \quad (69)$$

where

SLR = solar constant, about 8.4 J cm^{-2} min^{-1}
a = the angle of the radiation with the horizontal surface
SLR2 = parameter

The solar constant is the average intensity of solar

radiation received on a plane unit area normal to the incident radiation at the outer limit of the earth's atmosphere.

The following function from spherical trigonometry is used to calculate sin a (Eagleson 1970):

$$\sin a = \sin d \sin f + \cos d \cos f \cos h \qquad (70)$$

where
d = declination
f = latitude
h = sun's hour angle

The effect of cloud is taken into account with the following equation:

$$RS = RS_i (1 - CS\ CL) \qquad (71)$$

where
CL = cloudiness (cloudless sky, CL = 0, overcast sky, CL = 1)
CS = parameter

The complex processes of atmospheric absorption, scattering and reflection (cloudless sky situation) are not taken into account. These effects are included in the parameter values of this simpler model.

With Eqs. 69, 70 and 71, the incoming solar radiation model has been calibrated against the measured incoming solar radiation at the Tujuoja and Loimijoki basins. The results of model performance according to R^2 criteria were:

	Calibration 1976—1981	Verification 1970—1976
Tujuoja	0.822	0.750
Loimijoki	0.901	0.903

Especially the results for the Loimijoki basin were good. No change in model performance according to R^2 values between calibration and verification periods occured, which implies a good and stable model and high quality observations.

The parameter values obtained from calibration were

	SLR	SLR2	CS
Tujuoja	6.7 J cm^{-2} min^{-1}	0.00	0.67
Loimijoki	9.6 J cm^{-2} min^{-1}	0.96	0.71

The calibrated values of the solar constant SLR at Tujuoja were smaller and at Loimijoki greater than the value of 8.4 J cm^{-2} min^{-1} proposed by Eagleson (1970). With this incoming solar radiation model, the energy balance snowmelt model is usable without measured short-wave radiation. Fig. 12 is an example of the verification period of simulation of incoming short-wave radiation using this model.

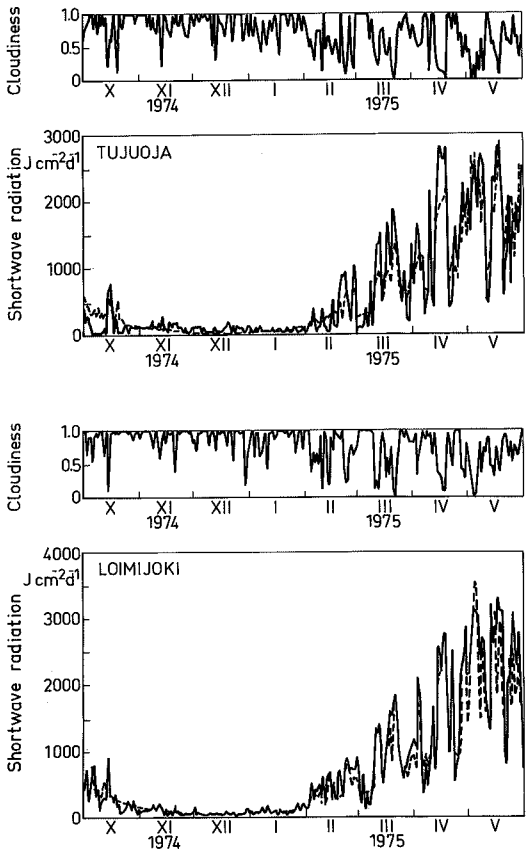

Fig. 12. Simulation of incoming short-wave radiation (---) compared to measured values (——) at the Tujuoja and Loimijoki basins during the winter of 1974—1975.

Incoming solar radiation in forests. In forest, snow cover receives a reduced amount of solar radiation. The reduction factor is called the forest transmission coefficient (CF), which is a function of forest canopy density and forest type. This dependency is presented in Fig. 13.

Canopy density is the percentage of the horizontal projection of the canopy. This coefficient, CF, is calculated by the equation (WMO 1974)

$$CF = 1 - CF1\ (1 - (1 - CD)^2)^{0.5} \qquad (72)$$

where
CF1 = transmission coefficient with 100 per cent canopy density, dependent on forest type (about 0.9)
CD = canopy density

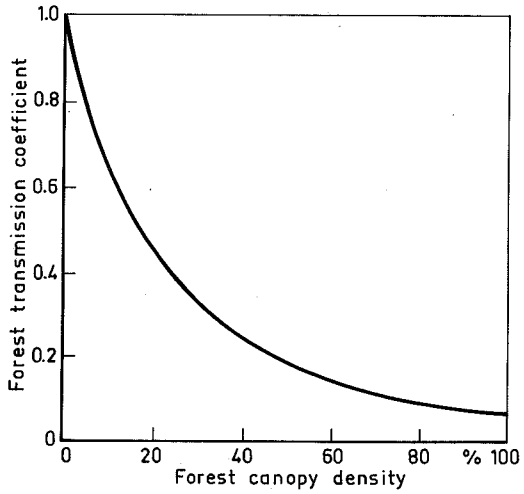

Fig. 13. Transmission of solar radiation by coniferous forest as a function of canopy density (USCE,1956).

The incoming solar radiation through the forest (RSf) is now calculated by the equation

$$RS_f = CF\,RS \tag{73}$$

The values of canopy density calculated for the whole area about 30 per cent for Tujuoja and about 10 per cent for Loimijoki. The values of the transmission coefficient with 100 per cent canopy density (CF1) have been a little lower than 0.9: about 0.85 for Tujuoja and about 0.75 for Loimijoki (the exact value obtained in calibrations is presented later). With these average values, the transmission coefficient according to Eq. 72 is 0.40 for Tujuoja and 0.67 for Loimijoki. These values are quite near the values shown in Fig. 13 according to canopy density CD only.

Snow albedo. The short-wave radiation balance on snow cover can be presented as (Mantis 1951)

$$RS = RSN + RSR + RSB \tag{74}$$

where
RS = incident radiation on snow
RSN = absorbed radiation
RSR = reflected radiation
RSB = transmitted radiation

It is assumed usually that RSB = 0, and the net incoming radiation (RSN) is calculated according to the albedo (AL) of snow cover, which is the ratio of reflected radiation (RSR) to the incident radiation on snow cover (RS):

$$AL = RSR/RS \tag{75}$$

For a forested area, the net short-wave radiation RSN is now

$$RSN = (1 - AL)\,RS_f \tag{76}$$

The albedo can be measured at a point, but daily measurements of the albedo for the Loimijoki basin are not available. In this study empirical functions were used to calculate watershed albedo during snow cover time. Snow albedo is a function of snow structure and therefore also a function of snow density. According to Kuchment et al. (1983), the following simple equation is usable for snow albedo simulation:

$$AL = C_{al} - D_s \tag{77}$$

C_{al} = parameter (about 1.03)
D_s = snow density (g cm^{-3})

The depth of snow cover also has an effect on snow albedo. When the depth is so small that a portion of incoming short-wave radiation is transmitted through the snow cover, the effect of the transmitted radiation (RSB) can be taken into account with the following functions:

$$AL = A1\,(1 - A2) + AL\,A2 \tag{78}$$
$$AL = AL_{min}, \text{ if } AL < AL_{min}$$

where
$A1 = C_{a2} - D_s$
$A2 = H/H_{lim}$
C_{a2} = parameter (about 0.9)
H = the depth of the snow cover (cm)
H_{lim} = the threshold value for snow depth (cm)
AL_{min} = the albedo of the soil surface (0.20—0.35)

Figs. 14 and 15 present examples from Tujuoja and Loimijoki, where snow albedo is simulated with Eqs. 77 and 78. Snow density and snow depth are simulated by a physical snowpack model, which is presented later in Chapter 8.

In many cases, albedo is calculated as a function of the age of snow (USCE 1956). It is also possible to calculate it as a function of the water equivalent (Fig. 16). This method has already been used with the daytime melt simulation (Eq. 52). Eq. 46 can be presented more generally as follows:

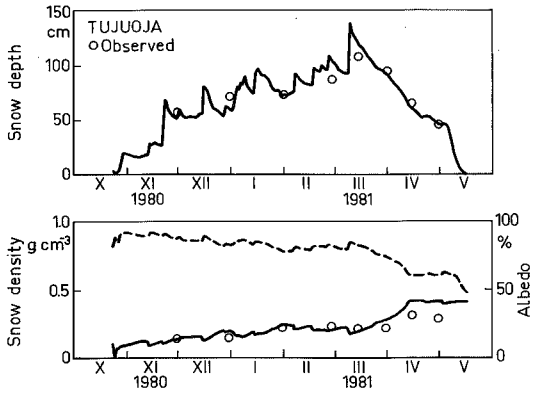

Fig. 14. An example of the simulation of snow depth, albedo (- - -) and density (——) in the Tujuoja basin. The observed values of depth and density are marked by (o).

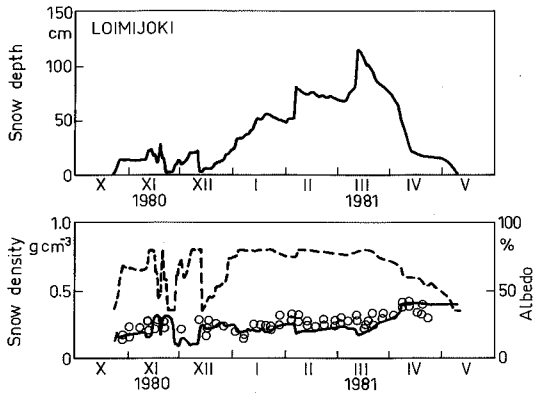

Fig. 15. An example of simulation of snow depth, albedo (- - -) and density (——) in the Loimijoki basin. The observed densities are marked by (o).

$$AL = AL_{max}\,(W/WMAX)^{eal} \qquad (79)$$
$$AL = AL_{min}, \text{ if } AL < AL_{min}$$

where
AL_{max} = snow albedo before melt
AL_{min} = albedo at the end of snowmelt period
eal = exponent (near 1.0)

7.2 Long-wave radiation

The net long-wave energy RLN for snowpack is the difference between downward (RLD) and upward (RLU) long-wave radiation:

$$RLN = RLD - RLU \qquad (80)$$

With snow, the upward long-wave energy is the sum of emitted (RLUE) and reflected (RLUR) energy by snow.

$$RLU = RLUE + RLUR$$

Snow albedo for long-wave radiation is only about 0.03 (Dunkle et al. 1949), and therefore the reflection of long-wave radiation by snow cover is omitted in long-wave radiation calculations by assuming RLUR = 0.

The upward long-wave emission by snow is calculated on the assumption that snow is a near-perfect blackbody in the long-wave portion of the spectrum, with an emissivity between 0.97—1.00 (Kondratyev 1969):

$$RLUE = E_s\,SF\,T_s^4 \qquad (81)$$

where
E_s = the emissivity of the snow surface (0.97—1.00)
SF = the Stefan-Boltzmann constant (3.40×10^{-11} J cm^{-2} min^{-1} K^{-1})
T_s = the snow surface temperature (K). T_s is approximated by air temperature at the 2 m level when snowmelt does not occur

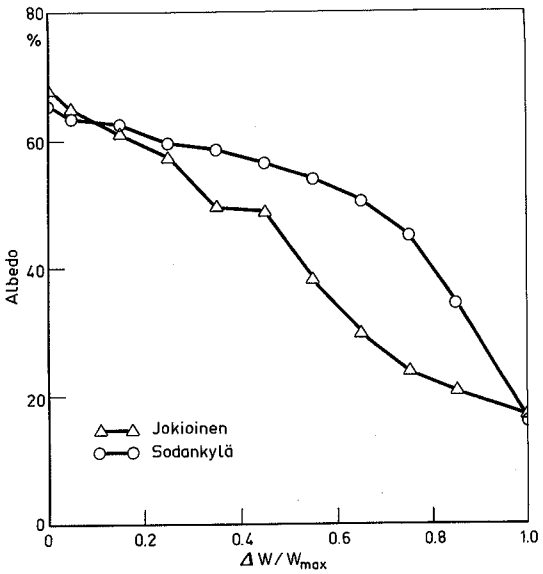

Fig. 16. The average development of snow albedo during the melting period at open sites of two snow stakes in 1971—1980. W_{max} = initial water equivalent, ΔW = decrease of the water equivalent (Kuusisto 1984).

below 0 °C temperatures. This is a valid approximation, because of the long time step used in the model. When snow is melting, Ts=273 K is used.

Most of the downward long-wave radiation comes from the lower 100 m of the atmosphere. Two per cent of it is emitted by ozone, 17 per cent by carbon dioxide and 81 per cent by water vapour in the clear-sky situation (Geiger 1961). Thus variation in downward long-wave radiation is mainly dependent on the variation of humidity and temperature in the 100 m layer of atmosphere above the soil surface. In clear-sky conditions, this downward radiation is calculated by

$$RLD = E_a \, SF \, T_K^4 \tag{82}$$

E_a = atmospheric emissivity (0.75—0.85)

There are many empirical equations expressing the atmospheric emissivity as a function of water vapour pressure and air temperature. One of the most commonly used is as follows (Brunt 1952):

$$E_a = a + b \, e_a^{0.5} \tag{83}$$

Hatfield et al.(1983) found this function as one of the best and most consistently performing atmospheric emissivity formulas. Kuzmin (1961) has suggested the parameter values of a = 0.62 and b = 0.05 on the basis of thorough studies in steppe and forest regions in Russia.

For a cloudy sky, the atmospheric emissivity is also a function of cloud thickness, cloud density, cloud type and cloud altitude. For a partly cloudy sky, the estimation of downward long-wave radiation is difficult, and many empirical functions have been proposed. Kuzmin (1961) used the following function:

$$RLD = E_c \, SF \, T_K^4 \tag{84}$$

$$E_c = (1 + C_L \, (CL + CL_1)) \, E_a \tag{85}$$

where

C_L = parameter, about 0.12

CL = total cloudiness (0—1)

CL_1 = the cloudiness of the lower sky (0—1)

The forest canopy is an efficient absorber and emitter of long-wave radiation. The long-wave absorptivity and emissivity is at least 0.90 (Brooks 1959), perhaps as high as 0.97 (Baumgartner 1967). Thus a forest canopy can be treated as a blackbody at the ambient air temperature during windy periods. In the absence of wind, the temperature of the forest canopy has been observed to be 19 °C above the air temperature in daytime during the growing season (Gates 1965) and 2.5 °C lower at night (Reifsnyder and Lull 1965).

In a forest, the downward long-wave radiation is calculated by the equation (Eagleson 1970)

$$RLD = E_f \, SF \, T_K^4 \tag{86}$$

$$E_f = CD_f \, E_{ff} + (1 - CD_f) \, E_a \tag{87}$$

where

CD_f = forest canopy density for long-wave radiation

E_{ff} = the emissivity of the forest (near unity)

If the effect of clouds is still taken into account in the downward long-wave radiation simulation, Eq. 87 can be presented in the form:

$$E_f = CD_f \, E_{ff} + (1 - CD_f) \, E_c \tag{88}$$

In Eq. 88, the total emissivity is divided in two parts — that of the forest and of sky — as in Eq. 86, but the emissivity of the sky is calculated according to Eq. 85, where the effect of clouds is also included.

7.3 Sensible heat exchange

Sensible heat exchange is the product of turbulent exchange processes of heat in the layer above the snow surface. This turbulent heat flux can be measured directly by eddy correlation techniques (e.g. Male and Gray 1981), which requires sophisticated instrumentation. This method was not used in this study.

A more common method is to evaluate sensible heat exchange on the basis of wind and temperature profiles above the snow surface (Prandtl 1932):

$$RSEN = -C_a \, D_a \, K_h \, dT_{pot}/dz \tag{89}$$

where

C_a = the specific heat of air (kJ kg^{-1} $°C^{-1}$)

D_a = air density (kg m^{-3})

K_h = the eddy diffusivity for convective energy transfer (m^2 s^{-1})

T_{pot} = the potential temperature, i.e. temperature at the surface pressure (°C)

In practice, the eddy diffusivity is calculated from

the wind profile and assuming that the eddy diffusivity for convective heat transfer K_h equals the eddy diffusivity for momentum K_m, which is usually valid during snowmelt (Anderson 1976). The sensible heat exchange is calculated by equation:

$$RSEN = D_a C_a k^2 (K_h/K_m)(U_2 - U_1) (T_{pot2} - T_{pot1})/(\ln z_2/z_1)^2 \quad (90)$$

where

k = von Karman's constant (0.4)
K_m = the eddy diffusivity for momentum ($m^2 s^{-1}$)
U_1 = the wind velocity (m s^{-1}) at the snow surface (usually extrapolated)
U_2 = the wind velocity (m s^{-1}) at the height of measurement device
z_1 = the height (m) of extrapolated wind velocity near the snow surface
z_2 = the height (m) of measurement device

This equation is usable with standard meteorological observations, when it is assumed that $U_1 = 0$, and $T_{pot1} = 0$, and $K_h/K_m = 1$ during snowmelt.

This method of profiles assumes logarithmic wind profiles to exist over snow cover. Therefore it is valid only for open areas. In forested areas, the vegetation prevents the formation of well-defined logarithmic wind profiles above snow cover. Reifsnyder and Lull (1965) suggest a general range of 20 to 60 per cent reduction in wind velocity due to forest. Reifsnyder's (1965) study showed a 50 to 60 per cent maximum attenuation under lapse conditions, 60 to 70 per cent under inversion conditions. The ratio between the wind speeds at the 20 metre and 2 metre levels, computed from the logarithmic wind speed formula $u_{20}/u_2 = \ln(z_{20}/z_0)/\ln(z_2/z_0)$ (Kuzmin 1961), is 1.28. The roughness height of the snow surface $z_o = 0.05$ cm is used. Further, the wind speed used in this study is measured at an open site. Therefore it is reasonable to use simplified equations for sensible heat exchange RSEN in the forested basins of Tujuoja and Loimijoki. These equations are usually in the form:

$$RSEN = CSEN\ U\ (T - T_s) \quad (91)$$

where

CSEN = bulk transfer coefficient for sensible heat exchange (kJ m^{-3} $°C^{-1}$), the value of which varies from 0.001 to 0.015 (Male and Gray 1981)

The values of bulk transfer coefficients are usually averages over relatively long periods, and Eq. 91 should not be applied over time periods of less than 24 hours, at least with the presented coefficient values. In fact Eq. 91 is nearly the same as Eq. 90. when the bulk transfer coefficient CSEN is presented as:

$$CSEN = D_a C_a k^2 (K_h/K_m)/(\ln z_2/z_1)^2 \quad (92)$$

7.4 Latent heat exchange

Turbulent mixing of the air layers is the main process causing heat and moisture transfer above the snow surface. Because the origin of these two exchange processes is the same, they also occur simultaneously. To exist, sensible and latent heat exchange needs the gradient of temperature and moisture, on one hand, and wind on the other hand. Moisture and temperature gradients are developed due to the energy supply of short-wave and long-wave radiation. Wind tends to eliminate gradients simultaneously increasing turbulent heat absorption/intake and moisture evaporation/condensation. In the absence of wind, heat and moisture transfer ceases although gradients exist; there is no turbulent transport process.

The same method of profiles or gradients that is used for sensible heat exchange is also valid for latent heat exchange RLAT (Prandtl 1932):

$$RLAT = - HV\ D_a\ K_e\ de_a/dz \quad (93)$$

where

HV = the heat of vaporization (2830 kJ kg^{-1} from snow, 2500 kJ kg^{-1} from liquid water at the melting snow surface)
K_e = the eddy diffusivity of latent energy transfer (m^2 s^{-1})
e_a = vapour pressure in air (mb)

The eddy diffusivity of momentum K_m is calculated first from the wind profile. With the assumption that K_e/K_m is unity during snowmelt, latent heat exchange can be evaluated on the basis of measurements at two levels, z_1 and $z_2$2:

$$RLAT = D_a\ HV\ (K_e/K_m)\ (U_2 - U_1)(e_{a2} - e_{a1})/(\ln z_1/z_2)^2 \quad (94)$$

The values of the ratio K_e/K_m reported in the literature have a wide range, and the assumption of unity is not at all clear during snowmelt.

The same reasons which led to the use of

simplified equations for sensible heat in forested areas, i.e. the absence of well-defined wind and moisture profiles near the surface, are also valid for latent heat exchange. For the simulation of latent heat exchange in the forested basins of Tujuoja and Loimijoki, an equation similar to that for sensible heat RLAT is used:

$$RLAT = CLAT\ U\ (e_a - e_s) \quad (95)$$

where

CLAT = the bulk transfer coefficient for latent heat exchange (kJ m^{-3} mb^{-1})

e_s = vapour pressure on the snow surface (mb)

e_a = vapour pressure in the air over snow (mb)

The values of CLAT vary from 0.002 to 0.025 kJ m^{-3} mb^{-1} according to Male and Gray (1981).

7.5 Precipitation heat

Precipitation heat is the heat or energy that is delivered to a snowpack when liquid water from precipitation reaches the temperature of the snowpack. If the temperature of the snowpack is below 0°C, the liquid precipitation freezes and delivers the latent heat of fusion to the snowpack. In this case without freezing, the energy supply to the snowpack (RP) is

$$RP = D_w\ C_w\ (T_p - T)\ P/1000 \quad (96)$$

where

D_w = the density of water (kg m^{-3})

C_w = the specific heat of water (kJ kg^{-1} $°C^{-1}$)

T_p = the temperature of rain (°C)

P = the depth of rain (mm d^{-1})

The energy supplied by this process is quite small compared to the main components (RSN, RLN, RSEN, RLAT) of energy balance (Eq. 43).

In case all liquid precipitation is frozen in the snowpack, the energy supplied from liquid precipitation becomes important compared to other energy balance terms. The latent heat of fusion of water is 335 kJ kg^{-1}. This is possible only in the beginning of snowmelt, when the temperature of the snowpack is below 0 °C (for example see Figs. 19 and 22 and Tables 13—20).

The energy supplied by 1 mm of rain at 5 °C air temperature the temperature of the snowpack is −10 °C is about 6 J cm^{-2} Eq. 96; when the water is frozen, the additional energy supply to the snowpack is 34 J cm^{-2}.

With abundant rainfall on the snow, the heat from liquid precipitation is distributed rapidly into the whole snowpack. Rainfall may change the structure of snow very quickly compared to the normal melting process.

7.6 Heat exchange at the soil surface

The main form of heat transfer in the soil is molecular conduction. The heat flux from the ground to the snowpack (RG) is given by the equation:

$$RG = -k_g\ dT_g/dz \quad (97)$$

T_g = the temperature of the ground surface layer (°C)

k_g = the thermal conductivity of the ground surface layer (J cm^{-1} $°C^{-1}$ s^{-1})

z = depth from soil surface (cm)

The value of the thermal conductivity of the soil is strongly dependent on soil moisture. Thermal conductivity increases with increasing soil moisture content. The thermal conductivity of frozen soil is also higher than the thermal conductivity of unfrozen soil, because the thermal conductivity of ice is approximately four times that of water.

In the snowmelt period, the heat exchange depends on the condition of the soil. If the underlying soil is unfrozen, the melting snow receives heat from the soil. When soil frost exists, the heat flux to the ground is positive, and the snow loses energy. In both cases, the heat flux is usually in the limits of −40 ... +40 J cm^{-2} (Kuzmin 1961), which means snowmelt or freezing of 0.1 mm of water. This value is negligible compared to other terms in the energy balance equation.

In southern Finland, Sucksdorff (1982) obtained the value of 31 J cm^{-2} for ground heat flux below the maximum depth of soil frost. Data from the Finnish Meteorological Institute gave values from 8 to 35 J cm^{-2} during the winter of 1979 (Kuusisto 1984); the maximum value occurred in the beginning of the winter and minimum at the end of the winter.

7.7 Internal energy

Before snow starts to melt, the temperature of snow has to rise to 0 °C. This negative energy storage, called the cold content, CO, can be calculated by:

$$CO = H\,(D_i\,C_i + D_w\,C_w + D_v\,C_v)\,T_s \qquad (98)$$

where
CO = cold content (J cm^{-2})
H = snow depth (cm)
D_i, D_w, D_v = the density of ice, water and vapour (g cm^{-3})
C_i, C_w, C_v = the specific heat of ice, water and vapour (J g^{-1} °C^{-1})
T_s = mean snowpack temperature (°C)

The energy content of water vapour is negligible, and for practical calculations Eq. 98 is used in the form

$$CO = C_s\,D_s\,H\,T_s \qquad (99)$$

where
C_s = the specific heat of snow (2 J g^{-1} °C^{-1})
$D_s H$ = the water equivalent of snow as cm equals g cm^{-2}
D_s = the density of snow (g cm^{-3})

The correct simulation of internal energy requires the simulation of heat transfer by conduction and mass transfer into the snowpack. When the energy balance of the snow surface is negative, energy transfer into the snowpack is calculated by conduction by using equation (Leavesley 1973):

$$q = 2\,D_s\,C_i\,(k_1\,dt/D_s\,C_i\,3.14)^{0.5}\,(T_s - T_b) \qquad (100)$$

where
q = heat flux into the snowpack in dt time (J cm^{-2})
k_1 = the effective thermal conductivity of snow computed by Eq. 138 ($k_1 = c\,D_s^2$) J cm^{-1} s^{-1} °C^{-1}
dt = the time step of simulation
T_b = the temperature of bulk of snowpack (°C)

The cold content (CO) is increased or decreased by conducted heat, and this cumulative sum is used to compute the bulk snowpack temperature by equation:

$$T_b = -CO/W\,C_i \qquad (101)$$

W = the water equivalent of snow (mm)

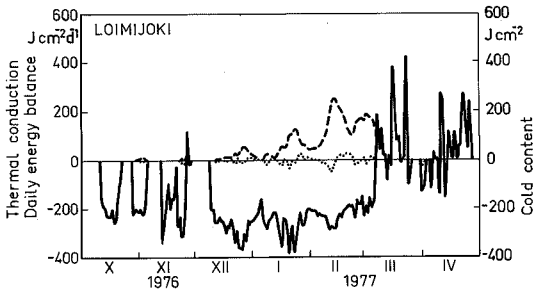

Fig. 17. Simulation of the daily energy balance(——) on snow surface, the cold content of the snowpack (- - -) and thermal conduction (...) into the snowpack in the basin of Loimijoki during the winter of 1976—1977.

When the snow surface energy balance RTOT is positive, it is used to melt snow and heat is conveyed into the snowpack by mass transfer. Melt is first used to satisfy the cold content by refreezing of some or all of the melt. When the cold content is satisfied, the remaining water is used to satisfy the free water retention capacity of the snowpack. Melt in excess of the free water retention capacity is delivered to the soil surface for routing through the transformation model.

In a case where there is liquid water inside the snowpack during a cold period, the negative heat conducted into the snowpack is first used to freeze the water. During this process, the temperature of the snowpack is zero and the cold content is also nil.

An example of simulation of the cold content is presented in Fig. 17. The cold content is usually fulfilled in one or two days in the beginning of snowmelt. Thus cold content is not very important process in snowmelt-runoff simulation.

7.8 Results from energy balance simulations

An energy balance snowmelt model where Eqs. 73, 76 and 79 were used for simulation of the short-wave radiation balance, Eqs. 81 and 86 for long-wave simulation, Eq. 91 for sensible heat simulation, Eq. 95 for latent heat and Eq. 96 for precipitation heat was tested for the Tujuoja and Loimijoki basins.

In this case, heat exchange at the soil surface was omitted and the cold content was taken into account by assuming a constant temperature profile for the snowpack, which was calculated

based on the air temperatures and surface energy balance of the previous days. The latent heat of freezing of liquid precipitation in cold snowpack —temperature below zero before freezing — was also considered as precipitation heat.

The calibration of model parameters is made first against observed areal snow water equivalents, the number of which is only about 30 during the five to six year calibration period. The final calibration is made against observed runoff and discharge values, the number of which is 150—300 during the melting period lasting one to two months in each spring. During this calibration against discharge, the model performance values for snow simulation are not allowed to worsen. The final check of whether a model is approved or not is made during the verification period with independent data of a five to six year period.

In the following paragraphs, the results are discussed in more detail.

Results of short-wave radiation balance simulations. Eq. 79 was used for simulation of the albedo of snowpack. The incoming short-wave radiation RS was measured in this case. The parameter values for the Tujuoja and Loimijoki basins were

	AL_{max}	AL_{min}	eal
Tujuoja	0.62	0.62	1.0
Loimijoki	0.87	0.41	0.046

For the Tujuoja basin the albedo of snowpack is constant in this case. At the Loimijoki basin, the values of the albedo for the water equivalent of 50, 10, 5 and 1 per cent of the maximum water equivalent are 0.87, 0.78, 0.75 and 0.41. Fig. 18 presents the progress of albedo in the Loimijoki basin during the winter of 1970—1971.

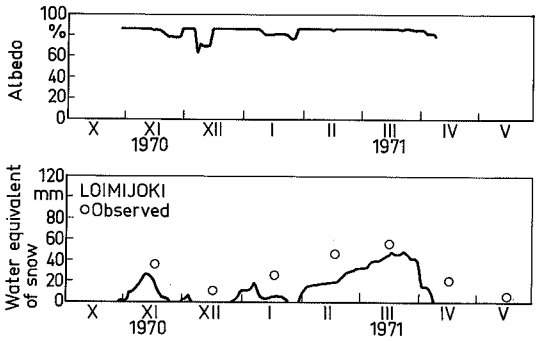

Fig. 18. Simulation of the snow albedo with Eq. 79 in the basin of Loimijoki and the water equivalent of snow during the winter of 1970—1971. The observed water equivalents are marked by (o).

In both basins, the values of albedo simulated by Eq. 79 tend to be somewhat too high compared to the results of Kuusisto (1984) in Fig. 16. Also, they do not change realistically during the snowmelt period, especially in the Tujuoja basin, where the simulated albedo is constant.

The forest transmission coefficient CF is calculated with Eq. 72; the parameters and the values of CF were:

	CF1	CD	CF
Tujuoja	0.91	0.34	0.32
Loimijoki	0.78	0.08	0.69

The net shortwave radiation RSN in per cent of the incoming short-wave radiation on snow surface is after forest and albedo reduction in the beginning and at the end of snowmelt period:

	RS(%)	RS_f(%)	RSN(%)	
			in the beginning	at the end
Tujuoja	100 %	32 %	12 %	12 %
Loimijoki	100 %	69 %	9 %	17 %

Results of long-wave radiation simulation. The upward long-wave radiation is simulated by Eq. 81 and the downward energy flux by Eq. 86 with atmospheric emissivity simulated by Eq. 83. The effect of clouds is not taken into account, because it is assumed that the effect of the forest masks it. Later in Chapter 8.3, a model including the effect of clouds (Eq. 85) was also tested.

In calibration, the parameter values obtained for the equations used were (E_{ff} was taken as 1.0, and it was not calibrated):

	DN	a	b	CD_f	E_{ff}
Tujuoja	0.93	0.73	0.051	0.34	1.0
Loimijoki	0.94	0.75	0.059	0.21	1.0

The values used for the emissivity of snow and for parameters a and b in the atmospheric emissivity function are very near or within the values presented in the literature. The forest canopy density for long-wave radiation at the Loimijoki basin is much higher than in the case of short-wave radiation. This is possible because the effect of the forest is different in these two cases. With short-wave radiation, the forest cover shadows the snow surface, preventing short-wave radiation from reaching the snow cover. With long-wave radiation, the whole biomass of the forest canopy emits long-wave radiation, and the forest increases the downward long-wave radiation.

Fig. 19 presents an example of the progress of long-wave radiation during winter. The net long-wave radiation RLN is negative over the whole

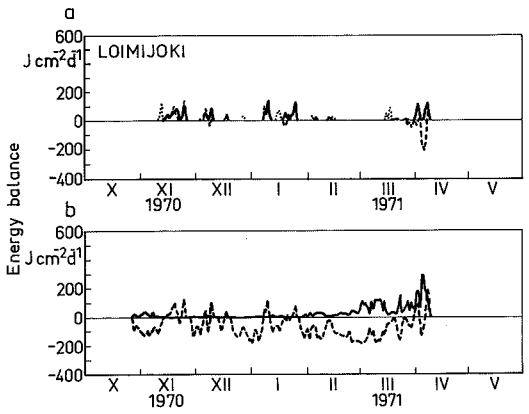

Fig. 19. Simulation of the snowmelt energy balance terms in the basin of Loimijoki during the winter of 1970—1971. Fig. a: Sensible heat (——), latent heat (- - -) and precipitation heat (...), Fig. b: Short-wave radiation (——) long-wave radiation (- - -).

winter, and it can become positive in the last days of the snow cover period, when the air temperature is high and the forest and air mass over the snow effectively emit long-wave radiation.

Results for sensible and latent heat exchange. At the Loimijoki basin, two sets of equations of sensible and latent heat exchange were tested. One includes Eqs. 91 and 95, presented earlier, and the other includes equations presented by Kuzmin (1961):

$$RSEN = (a_S + b_S U)\, c_S\, (T - T_s)\, 3600 \qquad (102)$$

where

$$RLAT = (a_S + b_S U)\, c_S\, c_L\, (e_s - e_a)\, 3600 \qquad (103)$$

U = wind speed (m s^{-1})

e_a = air vapour pressure (mb)

e_s = saturation vapour pressure at the snow surface (mb)

a_S, b_S, c_S, c_L = parameters: 0.18, 0.098, 0.11, 1.75 according to Kuzmin (1961) for open areas

The studies of Kuzmin (1961) were done mostly at the Hydrological Research Center at Valdai, which is situated at the latitude of 57° and is thus a more southerly area than the research areas used in this study. Due to the more continental climate, the temperature and snow conditions of the Valdai area are more or less similar to those of southern Finland during the melting time.

The results from calibration and verification period according to R^2-criteria against water equivalent (W) and discharge (Q) in the Loimijoki basin were:

	R^2 (calibration)		R^2 (verification)	
	Q	W	Q	W
Eqs. 91, 95	0.821	0.947	0.723	0.757
Eqs. 102, 103	0.740	0.910	0.596	0.637

The set of Eqs. 91, 95 gave better results in the calibration and especially in the verification period.

In the Tujuoja basin, only Eqs. 91 and 95 were used in the simulation. The parameter values obtained from calibration were:

	CSEN	CLAT	a_S	b_S	c_S	c_L
Tujuoja	3.9	9.1	—	—	—	—
Loimijoki	6.0	17	0.18	0.10	0.078	1.3

If we express the parameter values CSEN and CLAT in kJ m^{-3} °C^{-1} and kJ m^{-3} mb^{-1} we can compare the values to those reported by Male and Gray (1981) for open areas:

	CSEN	CLAT
Tujuoja	0.00045	0.0011
Loimijoki	0.00068	0.0020
Male and Gray (1981)	0.001...0.015	0.002...0.025

In both basins, parameters CSEN and CLAT are below or at the lower limit of the values reported by Male and Gray (1981). This is reasonable, because the reported values are valid for open areas, and in forested areas such as Tujuoja and Loimijoki, the parameter values should be lower due to the shielding effect of the forest. For the same reason, the parameter values were lower in the Tujuoja basin (forest canopy density about 30 per cent) than in Loimijoki (forest canopy density about 10 per cent). The latitudes of sites where studies have been carried out in Japan, USA, Norway and Canada and referred to by Male and Gray (1981) were usually more southerly than the latitude of the research areas in this study. This may have had some effect on results, but the effect is likely to come out in the contribution of short-wave radiation to snowmelt. The proportion of short-wave radiation may be larger in northern areas in spring, owing to the longer days. Results of this kind have been reported by Sand (1990), and also in Chapter 8.5 of this study.

7.9 The energy balance snow model compared to the best temperature index model

The model performance of the watershed model with energy balance snowmelt model, compared to the best temperature index models, is presented below as R^2 values. The model performance R^2 was calculated against runoff (q) in the Tujuoja basin and against discharge (Q) and snow observations (W) in the Loimijoki basin:

	Tujuoja	
	Calibration	Verification
	q	q
Energy balance	0.821	0.708
Temperature index	0.847	0.737

	Loimijoki			
	Calibration		Verification	
	Q	W	Q	W
Energy balance	0.821	0.947	0.723	0.757
Temperature index	0.856	0.853	0.780	0.837

In both basins the watershed model with the temperature index model performed better in the verification period (Apps. 14—15) than the watershed models with the energy balance model. The larger errors made by energy balance models were concentrated in the beginning of snowmelt especially in the Loimijoki basin (Fig. 22, App.16). Snowmelt according to the energy balance model started too early in the springs of 1973 and 1975 in the verification period. This error did not occur in the calibration period in the Loimijoki basin.

The best temperature index models were described in Chapter 6.

Examples of simulation of the energy balance model and the temperature index model in winter 1974 in the Loimijoki basin is presented in Figs. 20—23. In other years, the energy balance and temperature index models also performed equally, and in most cases the temperature index model performed a bit better.

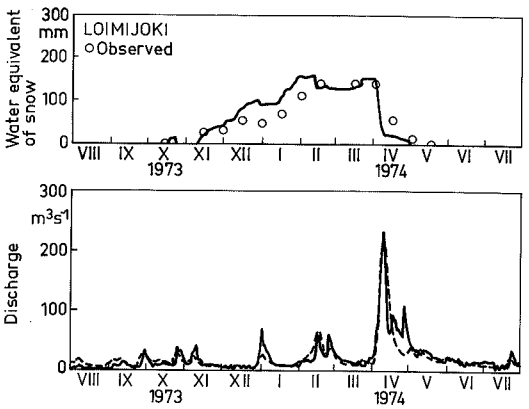

Fig. 21. Simulation of water equivalent and discharge by the watershed model with the temperature index model in the Loimojoki basin during the winter of 1973—1974. Observed water equivalent (o) and observed discharge (—).

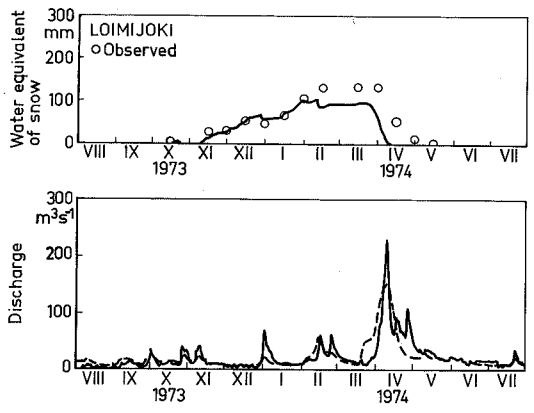

Fig. 20. Loimijoki: Simulation of the water equivalent and discharge by the watershed model, with the snowmelt energy balance model included, during the winter of 1973—1974. Observed water equivalent (o) and observed discharge (—).

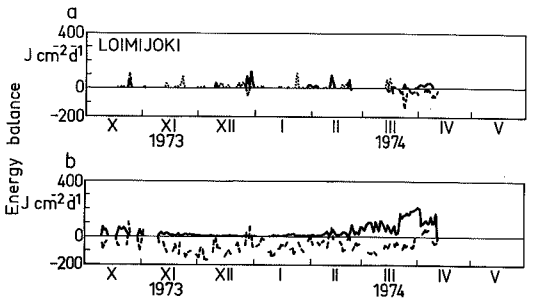

Fig. 22. Loimijoki: Simulation of the energy balance terms of snowmelt during the winter of 1973—1974. Fig. a: sensible heat (—), latent heat (- - -) and precipitation heat (···). Fig. b: short-wave radiation (—) and long-wave radiation (- - -).

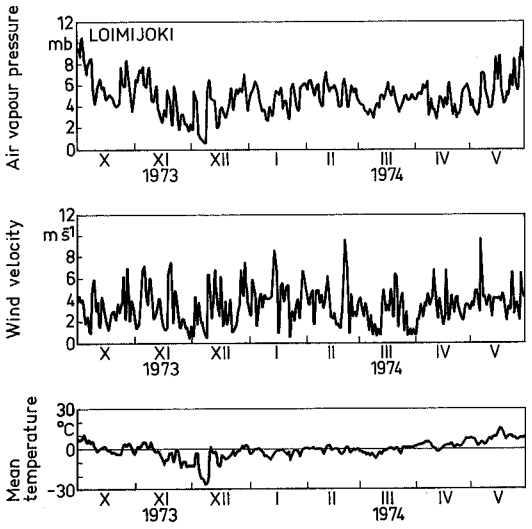

Fig. 23. Observed air vapour pressure, wind velocity and daily mean temperature in the basin of Loimojoki during the winter of 1973—1974.

8 PHYSICALLY BASED SNOW COVER MODEL

The simulation of the albedo of snow by Eqs. 77 and 78 requires information about the density and depth of the snow cover. In model simulation work, one reasonable way to get that information is to simulate it by using a model, as this provides continuous data, which is needed especially, if the snow model is used for real-time simulation for large areas and for forecasting. A physically based snow cover model, of which original version was developed by Motovilov and Vehviläinen (1987), is presented and tested here. This snow cover model simulates the water equivalent, ice concentration, density, depth and liquid water in the snowpack (Fig. 24). The input for the snow cover model is precipitation, evaporation from snow cover, and potential melt/freezing simulated by energy balance model as presented above.

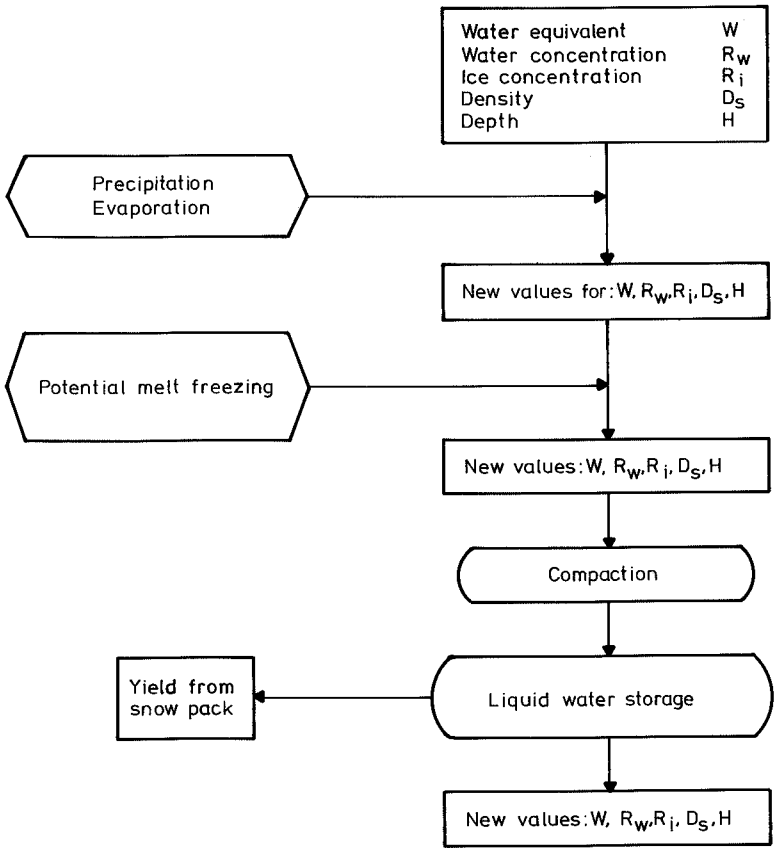

Fig. 24. The structure of the snow cover model.

8.1 Description of the model

In this snow cover model, snow is divided into three phases: air, water and ice. The processes which change the concentrations of different snow phases are precipitation, snow evaporation, melt/freezing and compaction of snow.

The change of snowpack due to precipitation and evaporation. The density of snow in precipitation D_p (g cm^{-3}) is a function of air temperature T ($^{\circ}$C) after Kuchment et al. (1983):

$$D_p = 0.13 + 0.0135\ T + 0.00045\ T^2 \qquad (104)$$

Snow precipitation PS (cm) and evaporation from snow cover ESC (cm) cause changes in the depth, water equivalent, ice concentration, water concentration and density of snow. Any liquid precipitation will change the water equivalent, water concentration and density of snow.

The change in the depth of snow H (cm) due to solid precipitation PS and evaporation from the snow cover ESC is calculated by the equation

$$dH_p = PS\ D_w/D_p - ESC\ D_w/D_s \qquad (105)$$

where
D_w = the density of water (g cm^{-3})
D_s = the density of snowpack (g cm^{-3})

The change in the water equivalent of snow W (cm) is then

$$dW_p = PS + PL - ESC \qquad (106)$$

The change in the ice concentration R_i of snow is

$$dR_i = (PS - ESC)\ D_w/D_i\ 1/(H + dH_p) \qquad (107)$$

where
R_i = the ice concentration of snow in volumetric units (cm^3 cm^{-3})
D_i = the density of ice (g cm^{-3})
H = the depth of snowpack (cm)

The change in the water concentration R_w needs to be calculated, if liquid precipitation PL (cm) occurs, using the following equation:

$$dR_w = PL\ /\ (H + dH_p) \qquad (108)$$

where
R_w = the water concentration of snow in volumetric units (cm^3 cm^{-3})

The average snow density D_s (g cm^{-3}) for snowpack is now

$$D_s = (W + dW_p)/(H + dH_p) \qquad (109)$$

The change in snow cover due to melt. The potential snowmelt M (cm) is calculated by the snow surface energy balance model presented in Chapter 7. The change in snow depth due to melt is calculated by the equation

$$dH_m = M\ D_w/D_i\ 1/R_i \qquad (110)$$

The change in the water concentration is now

$$dR_w = M/(H - dH_m) \qquad (111)$$

and the average density for snow cover D_s (g cm^{-3}) is calculated by

$$D_s = W/(H - dH_m) \qquad (112)$$

The change in snow cover due to refreezing. The potential freezing of water F (cm) in a snowpack is calculated by the energy balance model presented in Chapter 7. The upper limit of the refreezing of water is the storage of liquid water in snowpack. The change in the ice concentration of snow due to freezing is

$$dR_i = F\ D_w/D_i\ 1/H \qquad (113)$$

The change in the water concentration is

$$dR_w = F/H \qquad (114)$$

Compaction of the snow cover. The changes in the density of the snow cover are due to the effect of wind on snow cover, compaction of overlying snow and metamorphic changes in the structure of snow cover.

Kojima (1967) and Yosida (1963) have presented similar quantitative expressions for compaction of the snow cover. According to them, the compaction of snow cover can be expressed as

$$1/D_s\ dD_s/dt = W/n \qquad (115)$$

where
n = viscosity coefficient, which depends on the temperature and density of snow (cm h^{-1})

According to Kojima (1967), the relationship between n and the density of snow can be expressed as

$$n = n_c \exp(C_2 D_s) \quad (116)$$

where

n_c = the hypothetical viscosity coefficient with zero density (cm h^{-1})

C_2 = parameter (cm^3 g^{-1}) to be determined from observations; according to Kojima (1967): 21 cm^3 g^{-1}

The results reported by Kojima (1967) are based on many observations of the change in the depth of various layers in seasonal snow cover with no change in the water equivalent.

With the help of Eq. 116, Eq. 115 can now be expressed in the following form

$$1/D_s \, dD_s/dt = C_1 \, W \exp(-C_2 D_s) \quad (117)$$

where

$C_1 = 1/n_c$ = the fractional increase in density per centimeter water equivalent of load per hour; according to Kojima (1967): 0.026 – 0.069 cm^{-1} h^{-1}

Kojima (1967) reported that Eq. 117 performed generally well against the observed data except for cases of low-density new snow, wind-packed snow and depth-hoar layers. Low-density snow and wind-packed snow layers increased in density at a faster rate than expressed by Eq. 117.

Mellor (1964) presented another equation for the viscosity coefficient n, which takes into account the temperature and type of snow by

$$n/n_o = \exp [AC/R \, ((T_c - T)/T \, T_c)] \quad (118)$$

where

T_c = 0 °C temperature in Kelvin degrees (273 K)

n_o = the viscosity coefficient at temperature of 0°C

AC = the activation energy of the snow (4 10^4 J mol^{-1})

R = the gas constant (about 8 J mol^{-1} K^{-1})

For a normal temperature range during the snow cover period, Eq. 118 can be presented as

$$n/n_o = \exp [C_3 (T_c - T)] \quad (119)$$

$$C_3 = AC/(R \, T \, T_c) = \text{about } 0.08 \; K^{-1}$$

After the temperature dependency of Eq. 119 has been taken into account, Eq. 117 is now

$$1/D_s \, dD_s/dt = C_1 \exp(-0.08(T_c - T)) \, 0.1 \, W \exp(-C_2 D_s) \quad (120)$$

According to Mellor (1964), the value of C_1 varies due to the differences in temperature and snow type. Instead of a constant C_1, which Kojima (1967) used in Eq. 117, we now have $C_1 \exp(-0.08(T_c - T))$. Eq. 120 is used in a snow cover simulation model for simulation of compaction. Instead of snow density D_s, the concentration of ice in snow R_i is used in Eq. 120.

The change in depth due to compaction is calculated now

$$dH_c = R_i/(R_i - dR_i) \, H \quad (121)$$

The change in the water concentration of the snowpack, due to compaction, is

$$dR_w = R_w \, dH_c/H \quad (122)$$

Water yield from the snow cover. Before any liquid water is released from the snow cover, the retention capacity of water must be fulfilled. The maximum retention capacity of snow WHL (in volume percentage) can be calculated using a function presented by Kuzmin (1957):

$$WHL = 0.11/D_s - 0.11 \quad (123)$$

When retention capacity is expressed as the maximum water concentration in snow R_{wm}, Eq. 120 is in the form (Kuchment et al. 1983):

$$R_{wm} = \frac{0.11(1 - D_i/D_w \, R_i)}{1.11 - 0.11(D_w/D_i \, R_i)} \quad (124)$$

Water yield from snow cover WQ (cm) is now

$$WQ = 0, \text{ if } R_w < R_{wm} \quad (125)$$

$$WQ = (R_w - R_{wm}) \, H, \text{ if } R_w > R_{wm}$$

The water yield, WQ, from snowpack diminishes the water equivalent W by the same value, and the density of snow D_s (g cm^{-3}) after water yield and compaction is

$$D_s = (W - WQ)/(H + dHc) \quad (126)$$

8.2 Results from simulation of snow cover characteristics

The energy balance snowmelt model used together with the physically based snow cover model presented above is much the same as that presented

in Chapter 7. The differences between the energy balance models and the results obtained with the energy balance model are presented in Chapter 8.3.

Snow density simulation. This physically based snow cover model had only one parameter that was calibrated against density observations. That parameter was the fractional increase in density per water equivalent load per hour C_1 in Eq. 120 (and originally Eq. 117). The other parameter, in Eq. 120, C_2 was taken as presented by Kojima (1967), i.e. 21 $cm^3 g^{-1}$. For parameter C_1, Kojima (1967) gave the value range of 0.026—0.069 $cm^{-1} h^{-1}$. In calibration for the Tujuoja basin, the best results were obtained with a value of 0.010 $cm^{-1} h^{-1}$ for parameter C_1. In the case of Loimijoki, the best value was 0.019 $cm^{-1} h^{-1}$. These values were considerably lower than those reported by Kojima.

The value of ice density R_i used in the models was 0.92 g cm^{-3} in the Tujuoja model and 0.93 g cm^{-3} in the Loimijoki model. The ice density values were adjusted slightly during calibration, although the model was not specially sensitive for the density of ice.

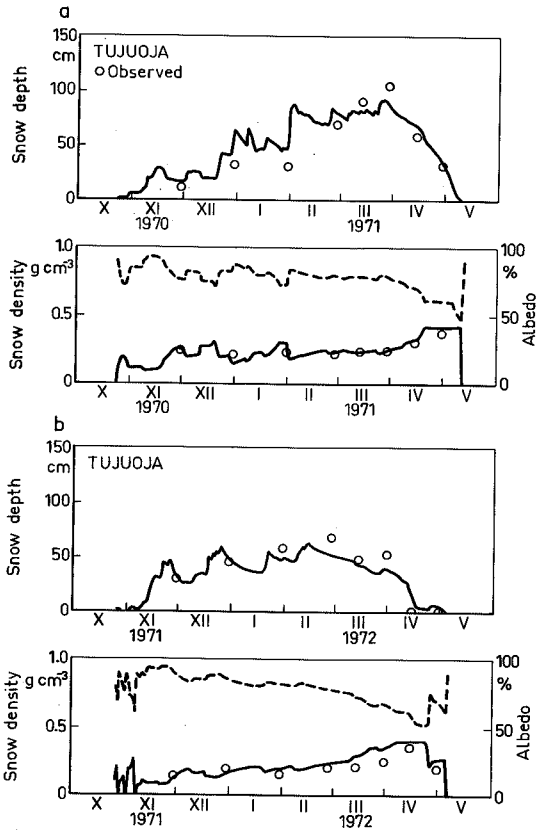

Fig. 25. Simulation of the density (——), depth (——) and albedo (- - -) of snow in the Tujuoja basin during the winters of 1970—1971 (a) and 1971—1972 (b). The observed values from one snow course are marked by (o).

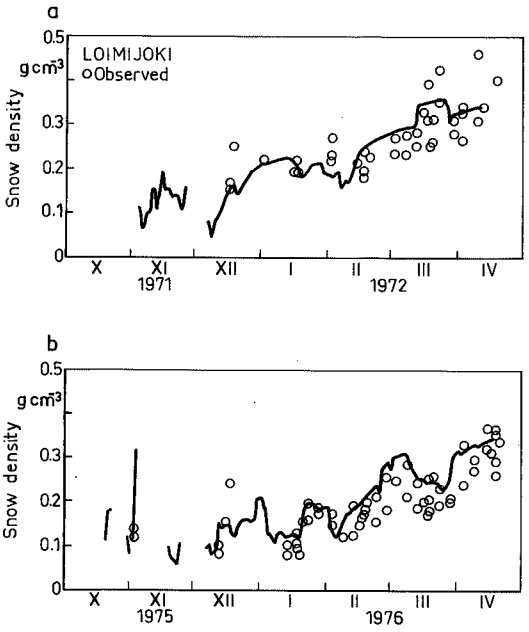

Fig. 26. Loimijoki basin: Simulation of snow density during the winters of 1971—72 (a) and 1975—76 (b). The observed values from snow course and snow stake stations are marked by (o).

Fig. 25 gives the best (1970—1971) and worst (1971—1972) results from snow density simulation for the Tujuoja basin in the verification period. The performance criterion determined by Eq. 20 was 0.525 for density in the calibration period (1976—1981) and 0.201 in the verification period (1970—1976). The low values of the performance criterion are due more to the low variance and F_o^2 of the observed density values than to the validity of the model. The results for density simulation at the Tujuoja basin were satisfactory, as can be judged from Fig. 25. There was some tendency for overestimation of the density in the 'worst' winter of 1971—1972.

Fig. 26 shows the simulation results of density for the Loimijoki basin also from the verification period with the best (1971—1972) and worst (1975—1976) winters, although the results did not differ very much from year to year. There was also some tendency for overestimation of density, especially at the end of snowmelt.

In both cases, the whole model was finally calibrated against discharge in a manner that did not allow the performance of the model worsen significantly against other observed variables.

Depth and water equivalent. For the Tujuoja basin, the performance criteria against snow depth and water equivalent were

Tujuoja	R^2(water equivalent)	R^2(depth)
Calibration	0.807	0.850
Verification	0.620	0.618

Fig. 27 presents the simulation of water equivalent over two winters; of these the winter of 1975—1976 is the best and the winter of 1974—1975 is the worst example. The simulation error in the winter of 1974—1975 is made mainly in January 1975. The error is due to simulation of both precipitation form and snowmelt. At the end of December 1974, there was abundant precipitation in both liquid and solid forms (Fig. 28) and the temperature fluctuated radically at the end of December 1974 and the beginning of January 1975 (Fig. 28). The wind speed, too, was very high in the middle of January 1975 (Fig. 29), and it was

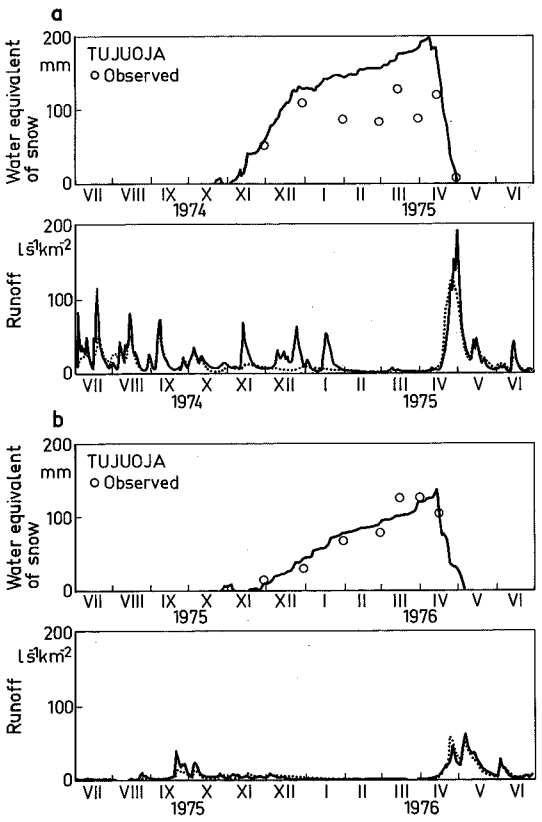

Fig. 27. Simulation of the water equivalent of snow and runoff in the Tujuoja basin during the winters of 1974—1975 a) and 1975—1976 b). The observed snow depth is marked by (o), the observed runoff by (——) and the simulated runoff by (···).

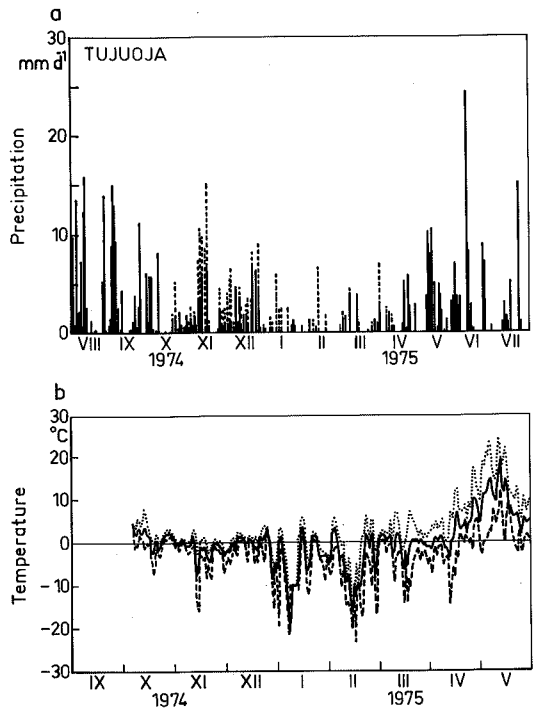

Fig. 28. Tujuoja basin during 1974—1975. a) Total precipitation with simulated precipitation form (snow - - -, water ——). b) The observed mean (——), maximum (···) and minimum (- - -) temperatures.

accompanied by very moist air (Fig. 29), with temperatures over zero both day and night (Fig. 28). High wind speed, moist air and a temperature over zero gave quite high values of sensible (300 J $cm^{-2}d^{-1}$) and latent heat (200 J cm^{-2}) exchange and positive long-wave radiation (100 J $cm^{-2}d^{-1}$) in the middle of January (Fig. 30). This means about 20 mm of melt per day, but the snow cover retained nearly all the liquid water. The simulated precipitation was mainly snow, and no peak of discharge was simulated as should have been (Fig. 27).

For the Loimijoki basin, the performance criterion against water equivalent was

Loimijoki	R^2 (water equivalent)
Calibration period	0.857
Verification period	0.833

Fig. 31 presents results for two winters of simulation of the water equivalent in the verification period. In the winters of 1971—1972 and 1973—1974, the simulation is quite correct. The simulation of water equivalent and discharge were

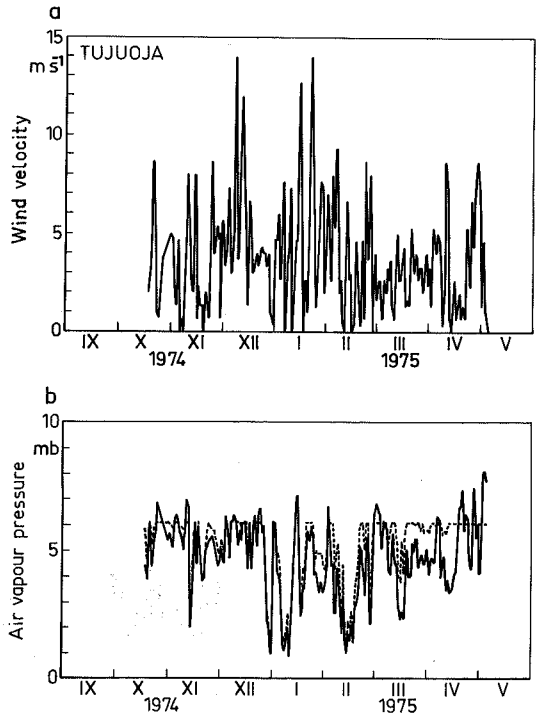

Fig. 29. a) The observed wind velocity and b) the observed air vapour pressure (——) with simulated saturation pressure (- - -) on the snow cover during the winter of 1974—1975 in the Tujuoja basin.

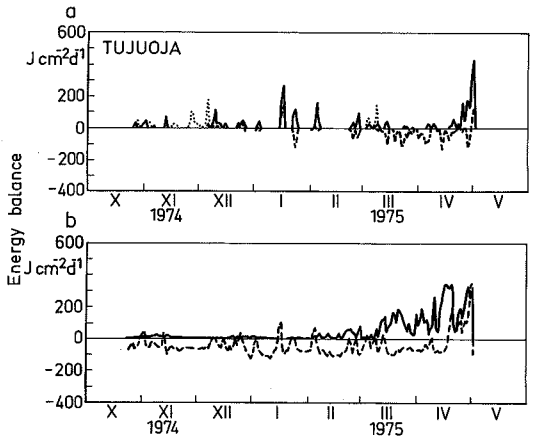

Fig. 30. The Tujuoja basin during the winter of 1974—1975. Simulated snowmelt energy balance terms: a) sensible heat (——), latent heat (- - -), precipitation heat (···); b) short-wave radiation (——), long-wave radiation (- - -).

now a little better than with the model without the physical snow cover model presented in Chapter 7. The main difference between these two models is in the calculation of snow albedo. Now albedo is calculated as a function of density and depth (Eqs. 77 and 78); earlier it was calculated as a function of the water equivalent (Eq. 79). The method based on water equivalent does not take into account changes in the albedo due to metamorphosis and compaction of snow, which decrease the albedo. This is true especially when the water equivalent remains constant. Fig. 32 presents the simulation of snow albedo with these two methods. The difference is considerable. The snow albedo calculated from snow density and depth varied more than the albedo calculated according to the water equivalent depletion. Because Eqs. 77 and 78 are based on measurements made in the field, their results should be more realistic. Also the per-

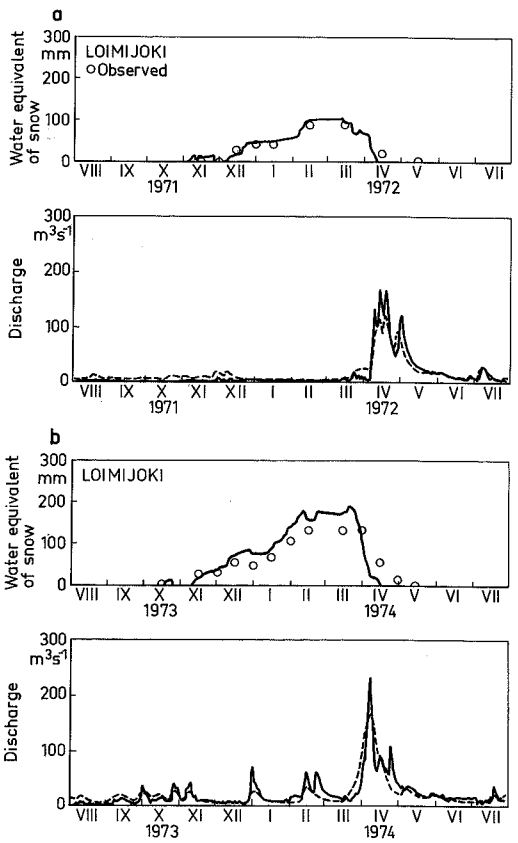

Fig. 31.The simulation of water equivalent (——) and discharge (- - -) in the Loimijoki basin during the winters of 1971—1972 (a) and 1973—1974 (b) with the snow model based on the energy balance model and the physical snow cover model. The observed water equivalent is marked by (o), the observed runoff by (——).

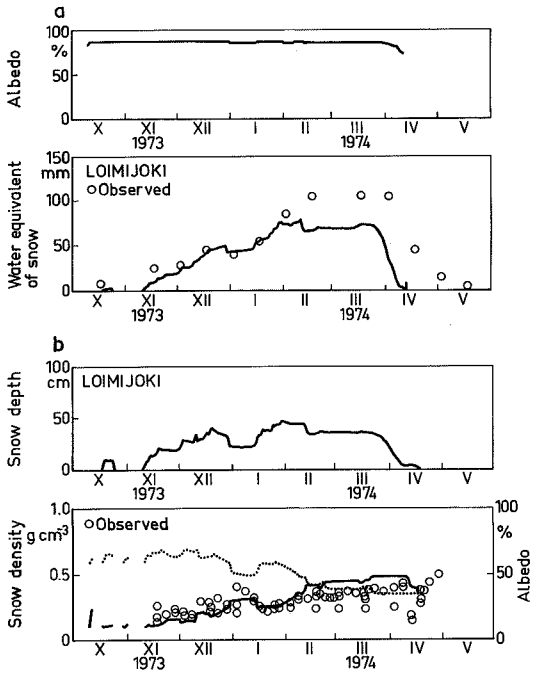

Fig. 32. a) Simulation of snow albedo in the Loimijoki basin as a function of water equivalent depletion, Eq. 79, and b) as a function of snow density (——) and depth, Eqs. 77 and 78, during the winter of 1973—1974. The observed water equivalent and density are marked by (o). In Fig. 32b, simulated albedo is marked by (···).

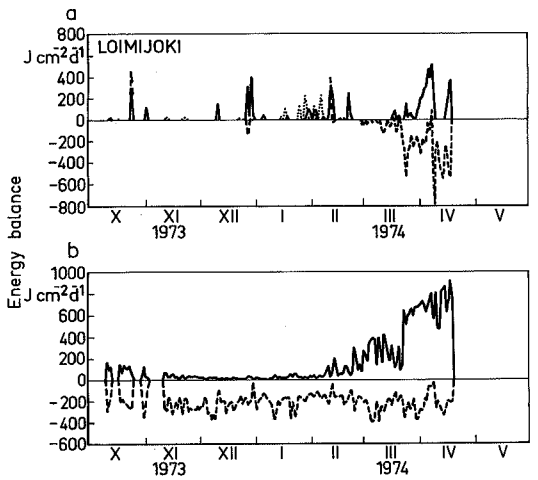

Fig. 33. Loimijoki basin during the winter of 1973—1974: Simulation of the snowmelt energy balance terms with a snow model based on the physical snow cover model. a) Sensible heat (——), latent heat (- - -), precipitation heat (···). b) Short-wave radiation (——), long-wave radiation (- - -).

formance criterion against the water equivalent in the verification period was much better (R^2 = 0.833) than when the albedo was calculated as a function of the water equivalent ($R^2 = 0.539$).

Fig. 33 presents simulation of the energy balance terms with the physically based snow cover model included at the Loimijoki basin during the winter of 1973 — 1974. The level and variation of short-wave radiation, and other energy balance terms as well, are now greater than in Fig. 22, where the energy balance terms, and especially the snow albedo, were simulated without the physical snow cover model presented in this chapter.

8.3 Results from energy balance simulations

The energy balance model used with the physical snow cover model was much the same as that presented in Chapter 7.8. The only essential difference was that the snow albedo calculations are now based on snow density and snow depth (Eqs. 77 and 78). Also Eqs. 86 and 88 (instead of Eqs. 82 and 83), which include the effect of cloudiness and forest in the simulation of long-wave radiation, are used. An example of the effect of cloudiness and forest on the simulation of long-wave radiation is presented in Fig. 36.

Short-wave radiation. With the physically based snow cover model, snow albedo is now calculated with Eqs. 77 and 78, in which snow albedo is a function of snow density and depth instead of water equivalent (Eq. 79) as in Chapter 7.8. The parameter values from calibration were

	C_{a1}	C_{a2}	H_{lim}	AL_{min}
Tujuoja	1.03	0.90	10 cm	0.35
Loimijoki	0.84	0.73	23 cm	0.24

The snow albedo values at the beginning (snow density 0.15 g cm^{-3}) and end (0.35 g cm^{-3}) of the snow cover period were now

	AL (new snow)	AL (old snow)
Tujuoja	0.88	0.55 (0.35)
Loimijoki	0.69	0.49 (0.38)

For the Tujuoja basin, the albedo decreases from 0.88 to 0.55 and to 0.35, when the snow cover is only a few centimetres thick. With Eq. 79, the albedo was a constant 0.62 over the whole snow cover period. For the Loimijoki basin, the snow albedo value is about 0.70 with new snow, being in the range of 0.49 — 0.38 at the end of the melt

period, depending on the snow depth according to Eqs. 77 and 78. These values are lower than calculated with Eq. 79 in Chapter 7.8. Fig. 34 presents the simulated albedo values for the Loimijoki basin.

Comparison with Fig. 18 reveals some correlation between albedo values calculated with these two methods. However, the range of albedo calculated from snow density is greater than that calculated from the cumulative snowmelt and the maximum water equivalent.

In particular, the snow albedo simulated with the water equivalent does not change during the accumulation period, as can be seen in Fig. 32a. Even the snow albedo does not change if snow melts, but refreezes again in the case of albedo simulation dependent on the water equivalent. This is unrealistic.

The higher albedo, which remained unchanged during the accumulation period, diminishes the net short-wave radiation (Fig. 35 compared to Fig. 19), which further changes the level of net long-wave radiation, sensible and latent heat. This may be the main reason why the energy balance snowmelt model does not perform as well as the energy balance model with the physically based snow cover model in the verification period.

The forest transmission coefficient CF is calculated by the same Eq. 72 as before, and the parameter values of canopy density CD with short-wave radiation and forest transmission with a 100 % canopy density CF1 were now

	CF1	CD	CF
Tujuoja	0.94	0.32	0.31
Loimijoki	0.88	0.14	0.54

For the Tujuoja basin, the canopy density value was the same as before; in the case of the Loimijoki basin, the canopy density and forest transmission coefficient values were a little lower than in Chapter 7.8.

In the following is presented the incoming short-wave radiation above forest RS (Eq. 76), below forest canopy RS_f (Eq. 73) and the net short wave radiation into the snowpack RSN (Eq. 71) at the beginning and end of snow cover period

	RS	RS_f	RSN (beginning)	RSN (end)
Tujuoja	100 %	31 %	4 %	12 % (21 %)
Loimijoki	100 %	54 %	17 %	28 % (35 %)

At the Tujuoja basin, the net short-wave radiation is now lower in the beginning of the snowmelt season than with the albedo simulated with cumulative snowmelt, when it was constant at 12 %. At the end of the snowmelt period, when the snow is less than 10 cm deep, the net short-wave radiation increases up to 21 % of incoming solar radiation.

At the Loimijoki basin, the net short-wave radiation is 40—50 % greater than before, when the albedo was simulated with cumulative snowmelt.

Long-wave radiation. The upward long-wave radiation is simulated by Eq. 81, the downward energy flux by Eq. 86 with combined atmospheric and forest emissivity simulated by Eq. 88. At the Tujuoja basin, the effect of clouds was not taken into account. The parameter values obtained from calibration were

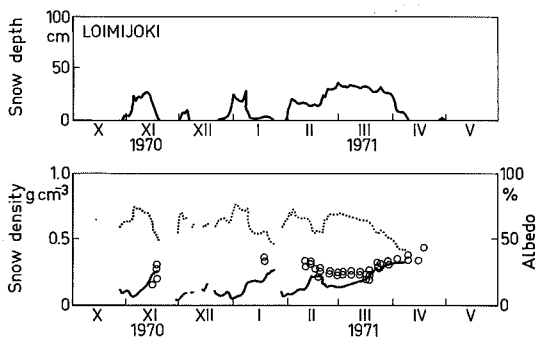

Fig. 34. Simulation of the snow albedo (···) with Eqs. 77 and 78 in the basin of Loimijoki during the winter of 1970—71. Simulated snow depth (——) and density (——) values are also presented. The observed densities from snow courses are marked by (o).

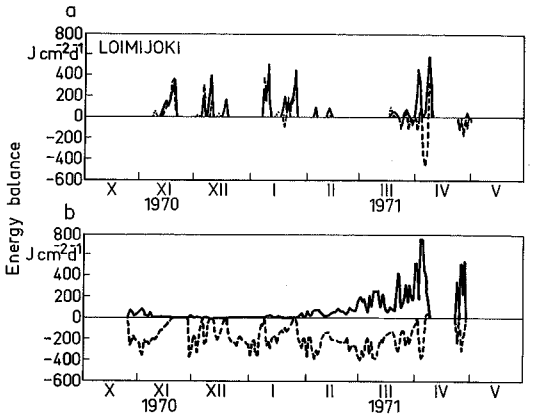

Fig. 35. Simulation of the snowmelt energy balance terms in the basin of Lomijoki during the winter of 1970—71. Snow albedo is calculated from the simulated snow density. a) Sensible heat (——), latent heat (- - -), precipitation heat (···). b) Short-wave radiation (——), long-wave radiation (- - -).

	E_s	a	b	CD_f	C_L	E_{ff}
Tujuoja	0.92	0.73	0.040	0.41	—	1.0
Loimijoki	0.96	0.66	0.053	0.22	0.12	1.0

Again, the canopy density values for long-wave radiation are greater than those for short-wave radiation. The snow emissivity E_s is now greater at the Loimijoki basin, and it is closer the values presented in the literature: 0.96—1.00. Parameters a and b in the atmospheric emissivity function are now lower at the Loimijoki basin, perhaps due to inclusion of the effect of clouds in long-wave simulation; again, the values are now closer to the values proposed by Kuzmin (1961): a = 0.62 and b = 0.05.

The contribution of cloudiness and forest to the downward flux of long-wave radiation at the Loimijoki basin is presented in Fig. 36. The effect of cloudiness is not very great, at most 10 %. The effect of forest is greater, being about 30 % of the downward flux.

Sensible and latent heat. In both research basins, the two sets of sensible and latent heat Eqs. 91, 95 and 102, 103 were tested. Eqs. 91, 95 performed better at the Tujuoja basin and Eqs. 102, 103 at the Loimijoki basin. The parameter values from calibration were

	CSEN	CLAT	a_s	b_s	c_s	c_L
Tujuoja	1.4	3.0	—	—	—	—
Loimijoki	—	—	0.22	0.075	0.033	2.74

The parameters of Eqs. 91, 95 were considerable lower than in Chapter 7.8 for the Tujuoja basin. The parameters of Eqs. 102, 103 for the Loimijoki basin were quite near the previous values.

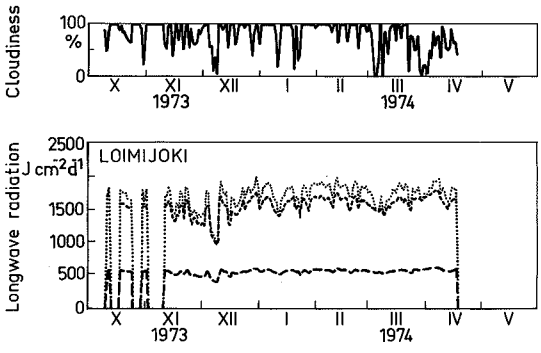

Fig. 36. Simulation of the downward flux components of long-wave radiation during snow cover in the Loimijoki basin. The atmospheric long-wave radiation during clear sky (- - -) is RLD0 = $(1-CD_f)\ E_a\ SF\ T_K^4$ (Eq. 82). The atmospheric component with cloud effect included (···) is RLDC = $(1-CDf)\ E_c\ SF\ T_K^4$ (Eq. 84) and the downward long-wave radiation from the forest canopy (—— ——) is RLDF = $CD_f\ E_{ff}\ SF\ T_K^4$ (see also Eqs. 86 and 88).

8.4 The physical snow cover model compared to the energy balance and temperature index models

The watershed model performance criterion R^2 against runoff and areal water equivalent with the physical snow cover model is compared to the best temperature index model and to the energy balance model without the physical snow cover model in Table 12.

The watershed model with the physically based snow cover model was slightly better than the energy balance approach without the snow cover model, especially at the Loimijoki basin. Apps. 16 and 17 present the simulation results obtained with these two models in the verification period. The differences in the simulations are concentrated mainly in two winters: the energy balance model with the physical snow cover model performed better in the winters of 1972—1973 and 1973—1974 when assessed according to the snow simulations. Also, the tendency for too early snowmelt and increase in discharge in the beginning of the springs of 1974 and 1976 at the Loimijoki basin did not exist in simulation with the physically based snow cover model.

The clearest difference between these two energy balance snow models is in the simulation of snow albedo (Fig. 32). With the simpler (physical snow cover model not included) energy balance model, the simulated snow albedo remains more or less constant, and high, throughout the period of snow accumulation and diminishes quite moderately only during the snowmelt period in spring (Fig. 32a). The albedo simulated with the physical snow cover model in Fig. 32b changes as a function of snow density, and this simulation takes the changes in snow albedo due to snow metamorphosis into account better.

It is difficult to see any direct connection between these differences in albedo simulation and

Table 12. The watershed model R^2-criterion against runoff (q), discharge (Q) and water equivalent (W) with the energy balance model, the combined energy balance and physical snow cover model and the best temperature index model in the calibration and verification periods.

	Tujuoja		Loimijoki	
	Calibr. q	Verific. q	Calibr. Q	Verific. Q/W
Energy balance model	0.821	0.708	0.821	0.723/0.757
-with snow cover model	0.850	0.710	0.842	0.758/0.833
Temperature index	0.847	0.737	0.856	0.780/0.837

the differences in simulation of the snow cover or discharge. The effect of different albedo simulations most probably comes out by changing the levels of the differe the melted water in the simpler energy balance model (Fig. 22). A more detailed example of the physical snow cover model simulation for the Loimijoki basin in the winter of 1973—1974 is presented in Figs. 31 and 33. These results can be compared to the first energy balance approach in Figs. 20 and 22.

The temperature index model (Apps. 14 and 15) is the best in both basins according to the R^2 values for the verification period. For the Loimijoki basin, the simulation results of peak discharges in spring were better with the best temperature index model when compared to the best energy balance model (Apps. 14 and 17). The reason for this is obviously the simulation of snow cover differently for open and forested areas. This improves the simulation of discharge at the end of the snowmelt period, when there is snow only in the forested area.

For the Tujuoja basin, the differences between the best temperature index model and the energy balance model with the physical snow cover model are slight, as shown by visual inspection of Apps. 15 and 18.

8.5 The contribution of different energy balance terms

Tables 13, 14, 17 and 18 present the contribution of different energy balance terms to the snow surface energy balance over the whole simulation period of 1970—1981 at the Tujuoja and Loimijoki basins.

The short-wave term dominates in spring. Long-wave radiation is negative practically throughout the snow cover period; May and September at the Tujuoja basin are an exception, as then the long-wave radiation was quite strongly positive. This is due to the high downward long-wave radiation from the forest canopy. The forest density for long-wave radiation is 0.41 at the Tujuoja basin. In late spring, when temperatures are high, this long-wave component is an important source of energy for snowmelt.

At the Tujuoja basin, the sensible heat term is the greatest positive energy term in September, November, December and January, i.e. during the period when short-wave radiation is very low. The case for the Loimijoki basin is the same, only the time period is shorter: November, December.

At both basins, the latent heat term is negative

Table 13. The Tujuoja basin: Mean and standard deviation (S.D.) of monthly energy balance terms on the snow surface over the period 1970—1981. Frk = number of months included.

			Monthly mean and S.D. of energy balance terms (J cm^{-2})					
Month	Frk		RSN	RLN	RSEN	RLAT	RP	RTOT
January	11	mean	148	−2409	178	8	85	−1990
		S.D.	166	446	264	80	77	762
February	11	mean	434	−2400	62	−18	110	−1813
		S.D.	158	368	127	59	194	615
March	11	mean	1797	−2060	283	−230	148	−62
		S.D.	438	599	232	215	123	803
April	11	mean	3966	−514	626	−875	18	3219
		S.D.	1312	704	274	441	12	1124
May	9	mean	740	351	183	−67	2	1209
		S.D.	877	381	180	95	2	1335
June	—		—	—	—	—	—	—
July	—		—	—	—	—	—	-
August	—		—	—	—	—	—	—
September	2	mean	34	8	44	11	14	111
		S.D.	45	72	10	63	8	108
October	11	mean	178	−558	95	42	48	−195
		S.D.	116	287	90	75	42	406
November	11	mean	136	−1526	146	24	122	−1097
		S.D.	81	446	100	73	140	617
December	11	mean	144	−2160	326	21	108	−1561
		S.D.	137	739	577	104	96	1408

in spring (evaporation) and positive in autumn (condensation). According to the results, the latent heat term is usually the smaller of the two wind induced turbulent heat transport terms. The contribution of latent heat to the snowmelt is greatest from October to January when latent heat accounts for 2 — 12 % of the total positive energy balance at the Tujuoja basin and for 13—35 % (75 %) at the Loimijoki basin. The snow evaporation/condensation values calculated using this model are discussed later in this chapter.

The precipitation heat is greatest in mid-winter, when rain is frozen in cold snow and latent heat is released into the snow cover. In spring, when melting snow has no cold content — the snowpack temperature being zero — the precipitation heat is

Table 14. The Tujuoja basin: The relative contribution of energy balance terms expressed as the percentage of the sum of positive energy balance terms during the period of 1970—1981. Frk = number of months included.

		Contribution of energy balance terms (%)				
Month	Frk	RSN	RLN	RSEN	RLAT	RP
January	11	35	−575	42	2	20
February	11	72	−397	10	−3	18
March	11	81	−93	13	−10	7
April	11	86	−11	14	−19	0
May	9	58	28	14	−5	0
June	—	—	—	—	—	—
July	—	—	—	—	—	—
August	—	—	—	—	—	—
September	2	31	7	40	10	13
October	11	49	−154	26	12	13
November	11	32	−357	34	6	29
December	11	23	−342	57	3	17

Table 15. The Tujuoja basin: Mean and standard deviation (S.D.) of monthly energy balance terms for days when the energy balance is positive over the period of 1970—1981. Frk = number of months included.

			Monthly mean and S.D. of energy balance terms (J cm^{-2})					
Month	Frk		RSN	RLN	RSEN	RLAT	RP	RTOT
January	7	mean	15	53	254	32	83	437
		S.D.	15	98	269	75	71	422
February	6	mean	37	−36	95	−18	179	257
		S.D.	49	96	125	43	197	249
March	11	mean	722	−187	258	−158	127	762
		S.D.	473	313	208	126	113	540
April	11	mean	3417	−101	604	−671	15	3264
		S.D.	1195	566	270	356	10	1048
May	9	mean	715	372	183	−61	2	1211
		S.D.	788	399	170	84	2	1262
June	—		—	—	—	—	—	—
July	—		—	—	—	—	—	—
August	—		—	—	—	—	—	—
September	2	mean	25	52	43	10	1	130
		S.D.	23	40	6	43	0	67
October	9	mean	61	83	94	60	24	323
		S.D.	70	139	90	68	29	327
November	9	mean	28	63	146	46	69	353
		S.D.	19	155	71	65	74	242
December	10	mean	19	41	305	40	83	487
		S.D.	19	185	558	102	72	834

small.

Tables 13 and 17 also give the standard deviations (S.D.) of different monthly energy balance terms. These S.D. values reveal the same picture as did the energy balance terms: the short-wave and long-wave terms are less variable, especially in spring, than are the sensible, latent and precipitation heat terms. The three heat terms appear more occasionally than do the radiation terms.

Energy balance during snowmelt days. In order to emphasize the importance of different energy balance terms during snowmelt, Tables 15, 16, 19 and 20 present the contribution of different snow surface energy balance terms only during those days when the total surface energy balance was positive, i.e. when surface snowmelt occurred.

The contribution of sensible and latent heat to snowmelt now becomes clearer. From September to January, sensible and latent heat accounts for

Table 16. The Tujuoja basin: The relative contribution of energy balance terms expressed as the percentage from the sum of positive energy balance terms. Only days when the total energy balance is positive are included. Period of 1970—1981. Frk = number of months included.

		Contribution of energy balance terms (%)				
Month	Frk	RSN	RLN	RSEN	RLAT	RP
January	7	4	8	55	2	31
February	6	11	−13	28	−5	61
March	11	64	−17	24	−15	12
April	11	85	−3	15	−17	0
May	9	56	29	15	−5	0
June	—	—	—	—	—	—
July	—	—	—	—	—	—
August	—	—	—	—	—	—
September	2	19	40	33	8	0
October	9	18	29	28	18	7
November	9	8	18	41	13	20
December	10	2	8	64	8	18

Table 17. The Loimijoki basin: Mean and standard deviation (S.D.) of monthly energy balance terms on the snow surface over the period of 1970—1981. Frk = number of months included.

			Monthly means and S.D. of energy balance terms (J cm^{-2})					
Month	Frk		RSN	RLN	RSEN	RLAT	RP	RTOT
January	11	mean	645	−6439	351	197	167	−5079
		S.D.	240	1820	406	308	199	2229
February	11	mean	2333	−6857	262	100	107	−4054
		S.D.	416	969	382	270	161	1695
March	11	mean	6850	−7011	971	−875	112	37
		S.D.	2454	1933	579	1086	92	1232
April	11	mean	3336	−1441	914	−1146	8	1671
		S.D.	2164	892	495	997	15	955
May	1	mean	1319	−101	760	−189	4	1793
		S.D.	—	—	—	—	—	—
June	—		—	—	—	—	—	—
September	1	mean	918	−540	0	2524	0	2902
		S.D.	—	—	—	—	—	—
October	9	mean	729	−1747	314	232	22	−451
		S.D.	526	1090	280	202	26	922
November	11	mean	549	−3419	719	747	125	−1302
		S.D.	364	1666	455	524	101	1341
December	11	mean	329	−5420	641	266	128	−4056
		S.D.	114	1868	443	243	196	1935

40—70 % at the Tujuoja basin and for 70—90 % at the Loimijoki basin. Thus from September to January, sensible and latent heat are the dominating energy sources for snowmelt at both basins, and especially at the Loimijoki basin, where there are more open areas.

In spring the contribution of short-wave radiation increases strongly, being over 50 % in March at both basins. The net short-wave term reaches its peak in April: 85 % at the Tujuoja basin and 69 % at the Loimijoki basin.

In late spring, the contribution of sensible and latent heat drops to 10 % at the Tujuoja basin and to 15 % at the Loimijoki basin. At the same time, latent heat is negative, i.e. evaporation from the snow cover prevails, which further diminishes the combined effect of turbulent mixing terms for snowmelt.

Table 18. The relative contribution of energy balance terms expressed as the percentage of the sum of positive energy balance terms during the period of 1970—1981. Frk = number of months included.

		Contribution of energy balance terms (%)				
Month	Frk	RSN	RLN	RSEN	RLAT	RP
January	11	50	−499	24	13	13
February	11	85	−252	8	3	4
March	11	86	−88	13	−11	1
April	11	79	−31	21	−27	0
May	1	63	−5	37	−9	0
June	—	—	—	—	—	—
July	—	—	—	—	—	—
August	—	—	—	—	—	—
September	1	27	−16	0	73	0
October	9	56	−135	24	18	2
November	11	26	−161	34	35	6
December	11	25	−404	46	19	10

Table 19. The Loimojoki basin: Mean and standard deviation (S.D.) of monthly energy balance terms for days when the energy balance is positive over the period of 1970—1981. Frk = number of months included.

			Monthly means and S.D. of energy balance terms (J cm^{-2})					
Month	Frk		RSN	RLN	RSEN	RLAT	RP	RTOT
January	6	mean	38	−280	446	343	130	677
		S.D.	29	135	349	367	146	564
February	5	mean	184	−337	446	190	88	570
		S.D.	129	204	383	369	153	762
March	11	mean	1522	−1027	810	−222	81	1170
		S.D.	1698	853	514	721	66	669
April	11	mean	1975	−645	870	−514	4	1690
		S.D.	1616	549	448	757	5	894
May	1	mean	1130	−6	714	−49	4	1793
		S.D.	—	—	—	—	—	
June	—		—	—	—	—	—	—
July	—		—	—	—	—	—	—
August	—		—	—	—	—	—	—
September	1	mean	918	−540	0	2524	0	2902
		S.D.	—	—	—	—	—	—
October	6	mean	86	−57	422	348	4	803
		S.D.	57	98	201	120	3	347
November	11	mean	46	−208	659	734	22	1253
		S.D.	29	141	420	511	40	891
December	9	mean	18	−253	495	373	27	661
		S.D.	6	125	233	164	65	352

The exaggeration of the short-wave radiation contribution seen in Tables 13, 14, 17 and 18 especially in mid-winter, is due to the fact that the short-wave term is positive throughout the year, and there is at least slight positive short-wave term every day even in mid-winter, whereas a greater amount of latent and sensible heat occurs only occasionally. The contribution of short-wave radiation to snowmelt from November to February is only 2—10 %.

Snow evaporation. Table 21 presents the mean monthly values of evaporation/condensation at the Tujuoja and Loimijoki basins in different months according to the best energy balance model. At both basins, the latent heat term is negative in spring, when evaporation prevails and positive in autumn, when condensation prevails.

Table 20. The Loimijoki basin: The relative contribution of energy balance terms expressed as the percentage of the sum of positive energy balance terms. Only days when the total energy balance is positive are included. Period of 1970—1981. Frk = number of months included.

		Contribution of energy balance terms (%)				
Month	Frk	RSN	RLN	RSEN	RLAT	RP
January	6	5	−35	42	33	20
February	5	20	−37	49	21	10
March	11	63	−42	33	−17	3
April	11	69	−23	31	−9	0
May	1	61	0	39	−3	0
June	—	—	—	—	—	—
July	—	—	—	—	—	—
August	—	—	—	—	—	—
September	1	27	−17	0	73	0
October	6	10	−6	48	40	2
November	11	3	−14	45	50	1
December	9	2	−29	55	41	3

Table 21. Monthly mean and standard deviation (S.D.) of snow evaporation/condensation according to the results of the physically based snow cover and energy balance model. The period is 1970—1981. Frk = number of months included.

	Tujuoja			Loimijoki		
Month	Frk	Snow evaporation mm per month		Frk	Snow evaporation mm per month	
January	11	mean	−0.0	11	mean	−0.7
		S.D.	0.3		S.D.	1.2
February	11	mean	0.1	11	mean	−0.4
		S.D.	0.2		S.D.	1.1
March	11	mean	0.1	11	mean	3.1
		S.D.	0.9		S.D.	4.3
April	11	mean	3.1	11	mean	4.0
		S.D.	1.8		S.D.	4.0
May	9	mean	0.2	1	mean	0.7
		S.D.	0.4		S.D.	—
June	—		—	—		—
July	—		—	—		—
August	—		—	—		—
September	2	mean	−0.0	—		—
		S.D.	0.3			
October	11	mean	−0.1	9	mean	−0.8
		S.D.	0.3		S.D.	0.8
November	11	mean	−0.1	11	mean	−2.6
		S.D.	0.3		S.D.	2.1
December	11	mean	−0.1	11	mean	−0.9
		S.D.	0.4		S.D.	1.0

At the Tujuoja basin, the evaporation from snow is 0.1—3.1 mm per month in spring. In autumn and winter, the condensation is 0.0—0.1 mm per month. At the Loimijoki basin, the phenomenon is the same: evaporation from the snow surface is 0.7—4.0 mm per month in spring, and condensation is 0.4—2.6 mm per month in autumn and winter. The standard deviation is as large or larger than the mean value of snow evaporation, which means that the range of variation of snow evaporation/condensation is great.

Snow evaporation measurements have also been made in Finland. According to Kaitera (1939) snow evaporation ranged from -0.7 mm d^{-1} to 1.9 mm d^{-1} in March and April during two springs, 1937 and 1938, in southern Finland. According to Kaitera and Teräsvirta (1972), condensation prevails from December (3 mm per month) to February (1.5 mm per month) and evaporation in the snowmelt period, the values being 5.7—13.5 mm per month in southern and northern Finland. Lemmelä and Kuusisto (1974) reported that the evaporation from snow during the snowmelt period is 9 mm per month in southern Finland. The results from the energy balance simulation and snow evaporation measurements well agree each other.

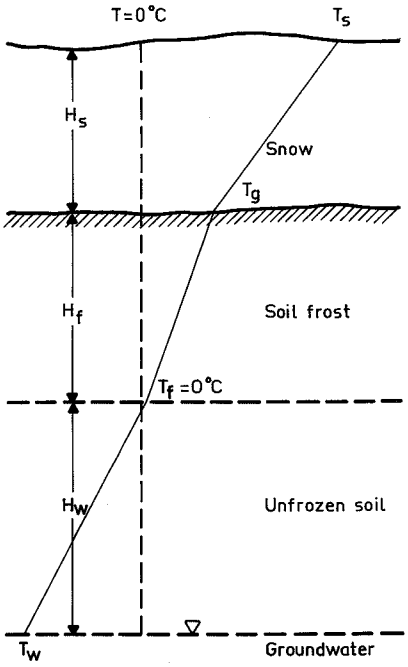

Fig. 37. Schematic soil section and temperature distribution.

9 SIMULATION OF SOIL FROST DEPTH AND EFFECT ON RUNOFF

This chapter presents a simple physically based soil frost depth model which is usable with conceptual runoff models and which can be used with air temperature and precipitation as input data. Snow depth is calculated by using the physical snow cover model presented in Chapter 8. The soil frost depth model is tested in the small basin of Tujuoja (Chapter 2), with a calibration and verification period of five years.

In the second stage, the simulated frost depth data were used to develop a HBV model version where the possible effect of soil frost on runoff is taken into account by means of a simple empirical model.

9.1 Soil frost model

Fig. 37 presents the winter situation in a schematic soil section during frost formation with snow cover. Snow cover and soil form a three layer system, through which the heat flux from snow surface to soil is calculated by the basic heat conduction equation:

$$q = -k\, dT/dz \qquad (127)$$

q = heat flux through a layer dz
k = thermal conductivity of the layer dz
T = temperature
z = depth

If we assume that all moisture in the zone of negative temperature in soil turns to ice during soil freezing, and that phase transitions occur only at the freezing or thawing front, we can distinguish between layers of frozen and unfrozen soil. Several frozen layers can form during repeated air temperature transitions through zero degrees centigrade.

When meltwater enters a frozen layer, it remains unfrozen, because phase transitions are assumed to occur only at the freezing or thawing front.

In the model to be developed, the inflow of heat from below is disregarded, and the distribution of temperature in the frozen layer and snow cover is assumed to be linear.

Under the assumption of linear temperature distribution in soil and snow, Eq. 127 is used to calculate the heat flux through the snow cover (q_1), frozen soil (q_2) and unfrozen soil (q_3):

$$q_1 = -k_1 (T_g - T_s)/H_s \quad (128)$$

$$q_2 = -k_2 (T_f - T_g)/H_f \quad (129)$$

$$q_3 = -k_3 (T_w - T_f)/H_w \quad (130)$$

where
k_1, k_2, k_3 = the thermal conductivity of snow, frozen soil and unfrozen soil
T_s = the snow surface temperature
T_g = the ground surface temperature
T_f = the temperature at the bottom of the frozen soil layer ($T_f = 0$ °C)
T_w = the temperature at the groundwater surface
H_s = snow cover depth
H_f = soil frost depth
H_w = the depth of the layer of unfrozen ground above the groundwater level

If we assume that there is no latent heat loss in the border between snow and ground, then

$$q_1 = q_2 \quad (131)$$

Further, the temperature at the border between frozen and unfrozen soil is zero: $T_f = 0$ °C. With these assumptions, we get the following equation for the temperature of soil surface T_g:

$$T_g = T_s H_f/(H_f + k_2/k_1 H_s) \quad (132)$$

In the border between the frozen and unfrozen soil layer, when the depth of frozen soil increases and the water in soil is freezing, the latent heat loss is calculated by the following equation:

$$q_2 = q_3 - Q\, dH_f/dt \quad (133)$$

where
$Q = L (w - w_l)$
L = the latent heat of fusion of ice (334 J g^{-1})
w = soil moisture in volumetric units
w_l = unfrozen water in frozen soil in volumetric units
t = time

The amount of unfrozen water in frozen soil is a function of soil temperature, but in frost depth calculations it can be kept constant at about 0.05—0.10 $m^3\ m^{-3}$. Assuming that the heat flux over the unfrozen soil layer q_3 is small compared to the latent heat exchange in the freezing border, Eq. 133 can be simplified assuming that $q_3 = 0$. Then, by solving Eq. 133 with the help of Eq. 132, we get the following function for the increase of depth of frozen soil H_f:

$$H_f = -S + ((S + H_f)^2 - 2 k_2 T_s\, dt/Q)^{0.5} \quad (134)$$

where
$S = k_2/k_1 H_s$

To compute the rate of soil thawing, the same approach is used as for soil freezing. It is assumed that the temperature of the meltwater penetrating into the soils is equal to zero and that the amount of cold in the soil is negligible. It is also assumed that, at soil temperature above zero, all the water is in the liquid state.

With allowance for these assumptions and also for the assumptions made in deriving Eq. (134), a similar expression for computing the movement of the thawing boundary H_m is obtained:

$$H_m = (H_m^2 + 2 k_3 T_g\, dt/Q)^{0.5} \quad (135)$$

The term S (Eq. 134) including snow depth is now cancelled out, because snow depth is assumed to be zero ($H_s = 0$) during soil thawing and thus $T_g = T_s = T_{air}$ (Eq. 132). The thermal conductivity used is k_3, the conductivity of the unfrozen soil layer.

If freezing and thawing periods are followed by each other in early winter, several frozen and unfrozen layers develop (Fig. 38). Later, if the freezing period continues, frozen layers may combine and the number of layers decreases. This phenomenon is taken into account in the simulation.

Thermal conductivies. Eqs. 134 and 135 are the basic equations for calculating the frost and thaw depth in soil. The thermal conductivity of frozen soil is higher than the thermal conductivity of unfrozen soil in the same moisture content, because the conductivity of ice is about four times the conductivity of water. The proportion of thermal conductivies of frozen soil and unfrozen soil is taken as 1.3 (Kuchment et al. 1983):

$$k_2 = 1.3\, k_3 \quad (136)$$

The thermal conductivity of unfrozen soil is a function of soil moisture and soil type. In this study the following equation is used (Kuchment et al. 1983):

$$k_3 = a \log w_p + b \quad (137)$$

where
w_p = soil moisture in per cent of weight
= 100 w/D
D = volume density of soil (1.2)
a = parameter (0.00085 J s^{-1} cm^{-1} °C^{-1})
b = parameter (−0.000023 J s^{-1} cm^{-1} °C^{-1})

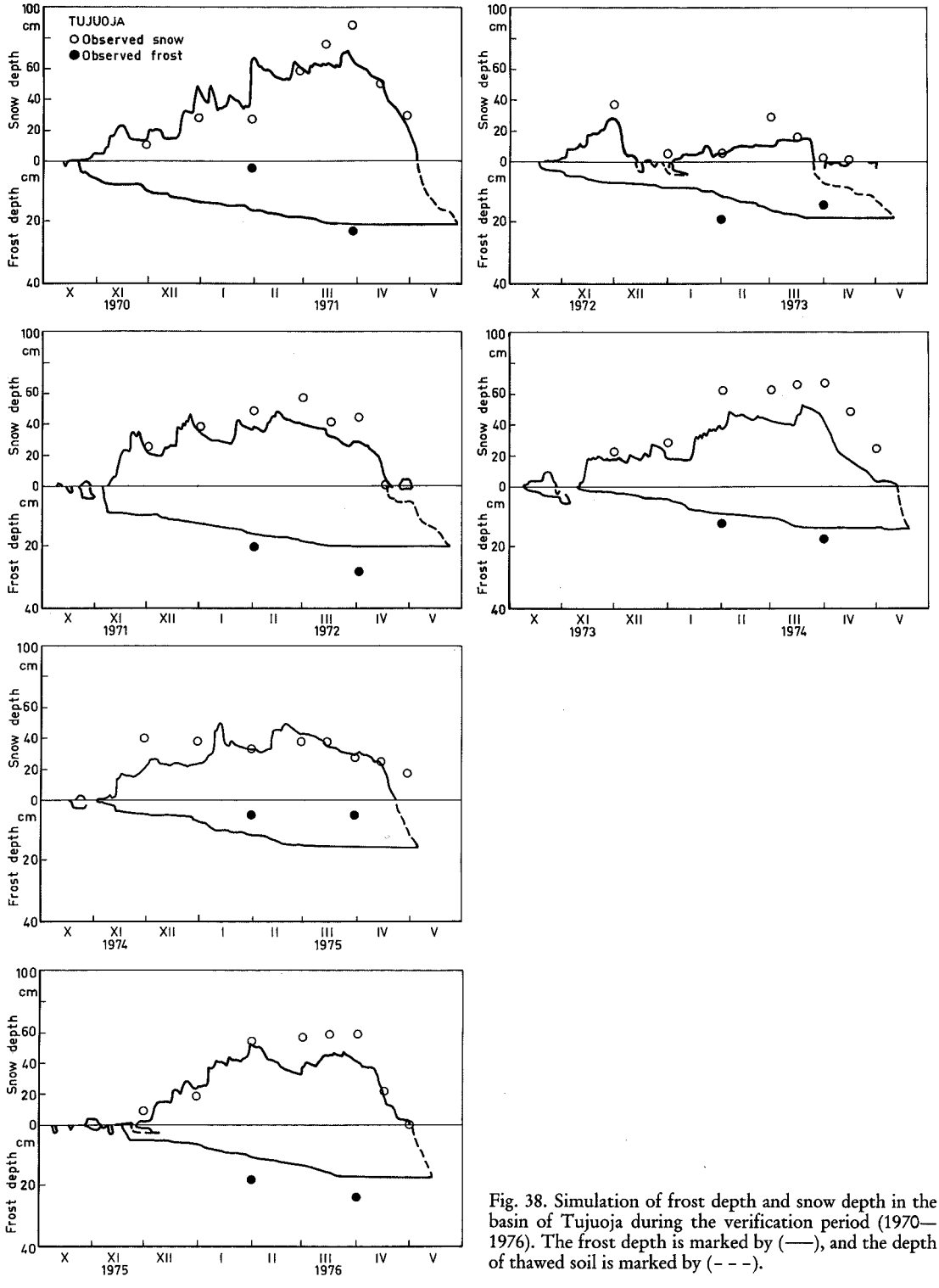

Fig. 38. Simulation of frost depth and snow depth in the basin of Tujuoja during the verification period (1970—1976). The frost depth is marked by (——), and the depth of thawed soil is marked by (- - -).

The thermal conductivity of snow is a function of the density, temperature and microstructure of snow. Most functions of thermal conductivity of snow include only snow density as an independent variable. The function given by Abels (1892) is used:

$$k_1 = c\, D_s^2 \qquad (138)$$

where

c = parameter with a value 0.0284 J cm^5 s^{-1} °C^{-1} g^{-2}

D_s = snow density g cm^{-3}

Snow cover model. The accumulation and ablation of the snow cover is simulated in this case with the physically based snow cover model presented in Chapter 8. This model simulates snowmelt by using the energy balance model. Potential melt and freezing of snow and precipitation are then used as input for a physically based snow cover model, which simulates the density, depth, water retention and water yield from snowpack. Density and depth are essential values for simulation of the thermal conductivity of snow (Eq. 138) and the depth of frozen and unfrozen soil (Eqs. 133 and 134).

9.2 Connection of the frost depth model to the HBV-model

The frost model is built on the basis of Eqs. 134 and 135 so that it is capable of simulating several layers of frozen and unfrozen soil following cold and warm periods. This frost/thaw depth model is then connected to a modified version of the HBV-model (Bergström 1976); Fig.3. In simulation of frost/thaw depth, the connection to the HBV-model is made through the soil moisture model by using the soil moisture storage MVS as the amount of water taking part in the formation of frost in the upper active soil layer. On the basis of calibration against observed frost depth values, the depth of the active soil layer is 67 cm. The volumetric soil moisture w is calculated now by equation

$$w = MVS/H_a \qquad (139)$$

MVS = soil moisture storage in the HBV-model, in centimetres of water

H_a = depth of the active soil layer which contains the soil moisture storage; a value of 67 cm is used for the Tujuoja basin

9.3 Results from frost depth simulation

The period of 1976—1981 was used for the calibration of frost depth and other components of the runoff model, for verification the period of 1970—1975. The performance criterion of simulation of snow cover, frost depth and the whole runoff model was R^2 (Nash and Sutcliffe 1970), presented with Eq. 20 in Chapter 4.2.

The performance criterion and the number of observations (N) during both periods were:

Variable	Calibration R^2	Calibration N	Verification R^2	Verification N
Water equivalent	0.922	38	0.684	43
Snow density	0.505	38	0.463	43
Snow depth	0.831	38	0.553	43
Soil frost depth	0.121	17	0.156	12

The performance criterion does not tell very much about the goodness of the model between different sub-models, because its value depends on the variance or F_0^2. The results based on R^2 are better with large variance (water equivalent) than with a smaller one (density), but R^2 can be used to evaluate the consistency of model between the calibration and verification periods. For water equivalent, model performance drops from 0.922 to 0.684, which reveals some over-calibration and inconsistency. The model performance of the frost depth model is 0.121 in the calibration period and 0.156 in the verification period. One can thus say that the frost depth model is at least consistent, but whether it simulates the frost depth properly cannot be judged. The effectivity of the frost depth model can be evaluated partly by visual inspection of Fig. 38, which gives the simulation results for frost and snow depth in the verification period. The largest errors during calibration period occur in the winter of 1978—1979 and also that of 1979—1980. The errors were derived from the snow cover formation and heat conduction through the snow cover at the beginning of winter. Incorrect simulation of the start of the snow cover period causes great error in frost depth simulation.

In the verification period (Fig. 38), the performance criterion was higher, which indicates good model consistency, but the value, 0.156, is rather low. It is low partly because of the low variance in frost depth measurements and, of course, due to errors. In the winter of 1974—1975, the error in frost depth simulation is the same as in the calibration period: the simulation of frost depth at the very beginning of winter and the snow cover period. The error in the first measurement in the winter of 1970—1971 may be measurement error,

because the simulated and measured frost depth were equal in the later measurements and the snow depth simulation was also correct between measurements. In January 1970, there were two warm periods with a good deal of snowmelt. Some of the melted water was conveyed to the river. In this period, reduction of the frost depth may have occurred.

The calibration and verification period revealed the importance of correct simulation of the beginning of snow cover accumulation. This is clear, because without snow cover the frost depth grows quickly during cold periods owing to the absence of effective insulator.

Although there were some errors in the calibration and verification period, the overall simulation capacity of the frost depth model was adequate during this ten-year period except in winter 1974—1975, when the simulated frost depth was 10 cm too deep. Some of the detected errors may also be due to observation errors. The frost depth model is quite simple, needing only daily precipitation and air temperature data (snow depth and density are simulated), and it can be run with operational watershed models.

9.4 The effect of soil frost on runoff

In forested areas with moraine, the effect of soil frost on runoff is considered to be small (Kuusisto 1984, Schwarz 1984). In the Tujuoja basin, 41 per cent of the area is moraines and graded soils consisting of 40 per cent gravel and sand and only one per cent silt and clay. Thus it is obvious that below the predominantly thin peat soils (59 % of the whole area is peat of which 28 % is 30—49 cm, 18 % is 50—99 cm and 13 % is over 100 cm thick peat), the underlying soil is mostly gravel and sand. So 70—80 per cent of the area of Tujuoja basin can be considered to be moraines or graded soils. More than half of the bog area is drained, and frozen water does not easily cause unpermeable ice layers to form on the surface at the beginning of winter.

Sand and Kane (1986) tested a modified HBV-3 model where parameters of soil moisture routine were varied seasonally in winter and summer due to the different hydraulic properties between frozen and unfrozen soils. The study basin was the Chena River in Alaska (5 125 km^2). The parameters to vary were maximum soil moisture storage (MVAK, Eq. 1), empirical coefficient EX in a function which simulates the water yield (INF, Eq. 3) from soil moisture storage and limit for potential evaporation (LP, Eq. 2); see also Fig. 3 :

$$INF = YIELD\ (MVS/MVAK)^{EX} \quad (3)$$

$$Es = HP\ MVS/LP\ ,\ \text{if } MVS < ALP \quad (2)$$
$$Es = HP\ ,\ \text{if } MVS > ALP$$

where

INF = water yield from soil moisture storage to upper storage (mm d^{-1})
YIELD = water yield from snowpack and rainfall into soil moisture storage (mm d^{-1})
MVAK = maximum soil moisture storage (480 mm)
EX = exponent (15)
Es = actual evaporation (mm d^{-1})
HP = potential evaporation (mm d^{-1})
LP = the soil moisture storage value after which actual evaporation equals potential evaporation (411 mm)

At the Chena River basin, the parameters MVAK, EX, LP differ considerably between frozen soil and unfrozen soil periods:

	MVAK	LP	EX
Unfrozen soil	320	320	2
Frozen soil	190	190	8

At the Tujuoja basin, we are looking for similar effects of soil frost on parameters in soil moisture model and in the model part below it; the formation of runoff (Fig. 3) as detected by Sand and Kane (1986) in Alaska. For the soil model, the parameters in Eq. 3 which determine the water yield were modified by soil frost as follows:

$$MVAK = MVAK + C1_f\ ICE \quad (140)$$

$$EX = EX + C2_f\ ICE \quad (141)$$

$$LP = LP + C1_f\ ICE \quad (142)$$

ICE = frozen water in soil (mm), about 20—100 mm

With Eq. 140, an assumption of a decreasing maximum storage capacity of soil with increasing soil frost is made. Accordingly, the threshold value of soil moisture storage for potential evaporation also decreases (Eq. 142). With Eq. 141, the water yield from soil moisture storage is assumed to be more peaky with increasing soil frost.

Furthermore, the equations for outflow (Q1) from upper storage (SUZ), for percolation (PERC) to lower storage and for outflow (SO) from temporary storage (SV) were modified. The basic functions were

$$Q_1 = K_1\ SUZ \quad (5)$$

$$PERC = PC\ SUZ \quad (143)$$

$$SO = SC\ SV \quad (33)$$
$$SO = SO + (SV - SVM)\text{, if } SV > SVM$$

where
SUZ, SV = storages (mm)
Q_1, PERC, SO = outflows (mm d^{-1})
K_1, PC, SC = parameters: 0.38, 0.001, 0.06 (d^{-1})
SVM = maximum temporary storage (55 mm)

The modifications were made by changing the parameter values as follows:

$$K_1 = K_1 + C3_f\ ICE \quad (144)$$
$$PC = PC + C4_f\ ICE \quad (145)$$
$$SC = SC + C5_f\ ICE \quad (146)$$
$$SVM = SVM + C6_f\ ICE \quad (147)$$

The assumption with Eqs. 144—147 is that soil frost increases runoff and thus the outflow from different storages by increasing the storage runoff coefficients (K_1, PC, SC) or by decreasing storage (SVM).

The calibration of this modified model version was made over the period of 1976—1981. The best values for the parameters, which reflect the possible effect of frozen soil on runoff obtained from the calibration were (Eqs. 140—142 and 144—147)

$C1_f = 0.00001$
$C2_f = 0.145$
$C3_f = 0.000001$
$C4_f = 0.00009$
$C5_f = 0.0$
$C6_f = 0.0$

The only case when soil frost seems to have an effect on model parameters was in Eq. 141 used to simulate the water yield from soil moisture storage. Although the effect of frost on parameter EX is quite large — with 60 mm frozen water in soil, the value of parameter EX increases from 15 up to 24 — the effect on the water yield from soil moisture storage is only 2—3 mm d^{-1} at best. Figs. 39 and 40 present the simulation of the water yield from soil moisture storage with the modified model in cases when soil frost is simulated and without soil frost simulation in winter (i.e. the parameter EX stays at the summer value of 15). Judged from Figs. 39 and 40 according the effect of soil frost is minimal. This is also obvious from the runoff

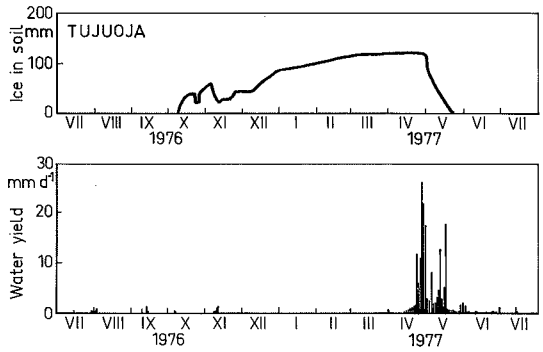

Fig. 39. Simulation of water yield from soil moisture storage and frost ice in soil with the modified soil moisture model (Eq. 141 included: $C2_f = 0.145$).

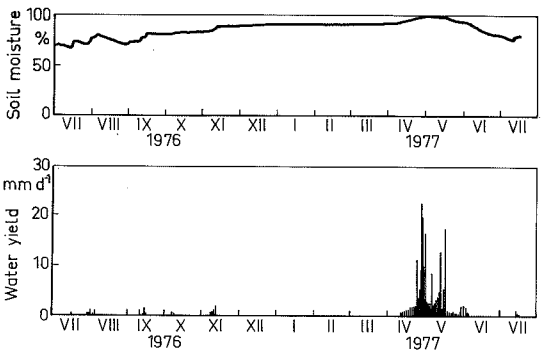

Fig. 40. Simulation of soil moisture and water yield from soil moisture storage without the soil frost model. All soil water is in the liquid stage, and the value of parameter EX is 15 (unfrozen soil value).

curves. There are not many deviations which can be corrected by assuming that soil frost increases runoff at the beginning of spring runoff, for example, in 1976 (Figs. 41 and 42). The situation is similar for the other years in the calibration period. Or if there were errors in discharge simulation, soil frost modification did not correct them. This was the case especially in the verification period.

The modified model did not perform better during the verification period (1970—1976) compared to unmodified model. The performance criteria R^2 against observed runoff were:

Model	Calibration	Verification
Unmodified	0.856	0.635
Modified	0.857	0.629

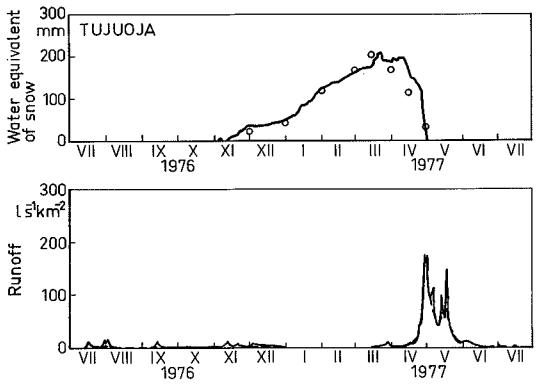

Fig. 41. Simulation of runoff (- -) with the modified model where the effect of soil frost on runoff is taken into account by Eq. 141. The areal water-equivalent is also simulated. Observed runoff: (——). Observed areal water equivalent: (o).

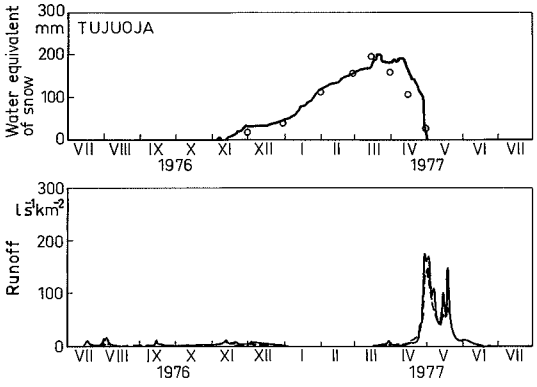

Fig. 42. Simulation of snow and runoff (- - -) without the effect of frozen soil on runoff. Observed runoff: (——). Observed areal water equivalent: (o)

10 THE OPERATIONAL USE OF SNOW COVER MODELS WITH WATERSHED MODELS

This chapter discusses experiences of the calibration and use of the degree-day based snow cover models (developed in Chapter 6) in operational watershed models. These snow models are used for real-time snow cover simulation during the accumulation period, and for snowmelt forecasting in spring in large watersheds ranging from 100 to 30 000 km^2. The watersheds concerned in this study are presented in Fig. 2.

10.1 Estimation of areal snow cover

Finland has an extensive snow course network (160 snow courses), which has been the basis for estimation of areal water equivalent for fifty years. The data gathered by this network are also a valuable source for developing areal snow cover models and for evaluating the usability of these models for the estimation of areal values of snow cover. The areal water equivalent maps based on snow course measurements, are presented in the Monthly hydrological report published by the Hydrological Office of the National Board of Waters and the Environment. Examples of the results from simulation of snow cover characteristics compared to this snow course data are presented in Figs. 43 and 44 and in Apps. 14—18.

10.1.1 Estimation of areal precipitation and temperature

The input data for snow cover model are precipitation and temperature. Therefore errors in estimation of areal precipitation are also errors in estimation of the areal water equivalent of snow. Wind, wetting and evaporation cause errors in the quantitative measurement of precipitation with a gauge. The common method to correct this is to use correction factors depending on the form of precipitation, presented earlier in Chapter 5.

Another very important factor associated with estimation of areal precipitation in operational work with models is the density of the precipitation station network. The error of the estimate of areal precipitation decreases with increasing network density (Fig. 5).

The time over which areal precipitation is estimated has a very strong effect on the accuracy. Estimation of daily values is quite inaccurate compared to monthly estimates especially with low network density. The situation is still better with areal snow cover simulation, when the accumulation time is 4—5 months.

App. 3 gives the number and the network density of precipitation stations in all main watersheds. The mean of number of stations per watershed is nine and the density one station per 465 km^2. According to Fig. 5 the mean square-error (RMS-error) is below 5 % with monthly precipitation values, which is good enough for estimation of areal snow cover. Another fact that is favorable for model simulation is: the watersheds concerned are usually quite large, the mean area being 7 000 km^2 (Table 3). It is thus justified to expect good areal snow water equivalent estimates

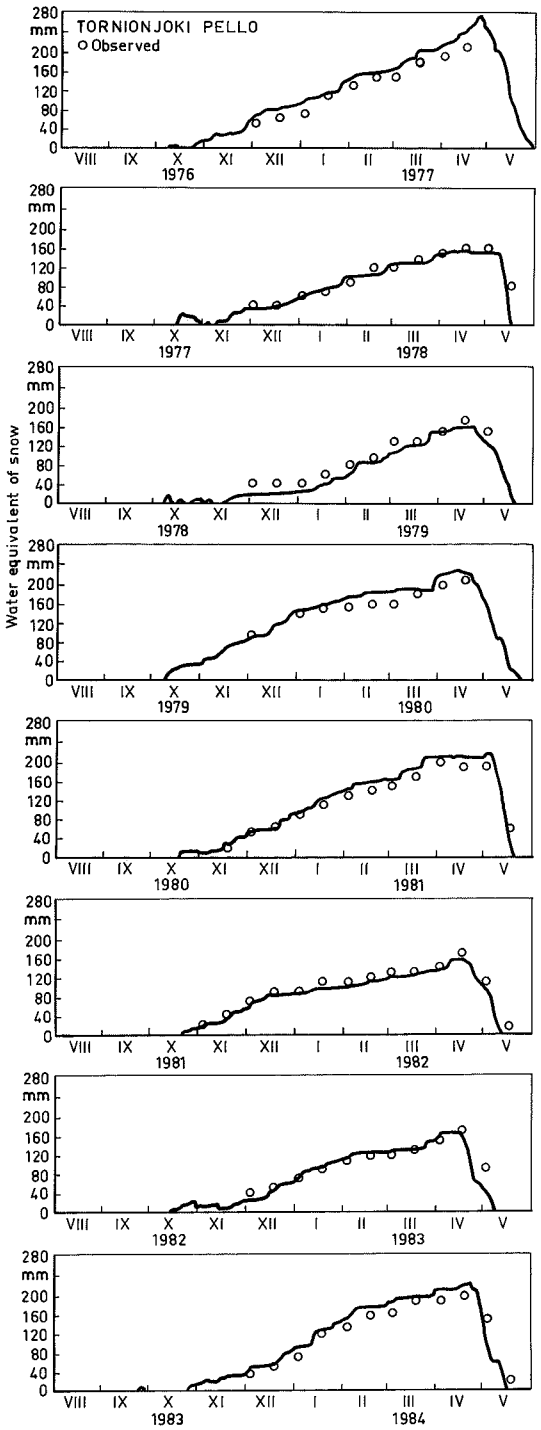

Fig. 43. Simulation of areal water equivalent in the sub-basin between Kallio and Pello in the Tornionjoki basin during the calibration period. The observed values based on five snow course measurements are marked by (o).

with snow cover models, as precipitation observations are concerned.

Temperature is more evenly distributed than precipitation, and fewer temperature stations are needed for simulation of snow cover than with precipitation. The mean number of precipitation stations is four per watershed (Table 4). Temperature observations become important when the temperature is near zero: estimation of the form of precipitation and of snowmelt is based on temperature. All the operational watershed models have temperature index based snowmelt models, which proved to be as good as physically based snow cover models in the study basins of Tujuoja and Loimijoki (Chapters 7 and 8). The ability of precipitation and snowmelt models to simulate the form of precipitation and snowmelt correctly is important for obtaining good areal precipitation and snow cover estimation. The largest errors in snow cover simulation usually come out in periods with near zero temperatures. But when the temperature is well below zero during the whole

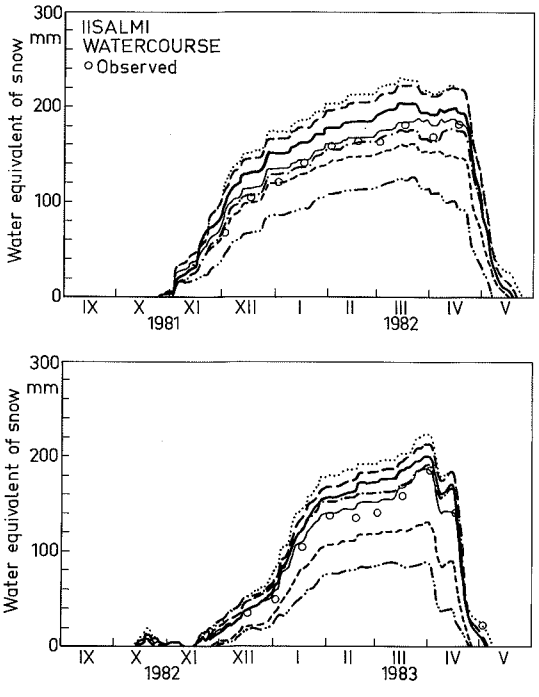

Fig. 44. Simulation of the areal snow water equivalent in the Iisalmi watercourse in six sub-basins between which the elevation difference is at most 150 m. The measured water equivalent for the whole area based on nine snow course measurements is marked by (o), and the corresponding simulated value is marked by (—).

winter period, as in northern Finland, estimation of the snow cover water equivalent rests on a firm base.

The areal water equivalent maps are based on observations from five snow courses/snow stake stations on the watersheds used in this study on the average and errors are possible. The possibility for serious errors due to snow maps is eliminated by checking the watershed models finally against discharge measurements i.e. against water balance.

10.1.2 Areal water equivalent of snow

The snow cover model for simulating the areal water equivalent of a watershed is based on the temperature index approach, which is the most commonly used method in operational watershed models. Division of large watershed into smaller sub-basin is essential in order to obtain relevant simulated snow cover values. Snow cover simulation separately for open and forested area also improves the results. All these aspects have been reviewed more thoroughly in Chapter 6.

The results are presented in the form of a criterion called the efficiency of a model R^2 (Nash and Sutcliffe 1970), presented in Chapter 4, Eq. 20. The main optimization method has been Rosenbrock's method (1960), which is also described in Chapter 4.

The practice of calibrating operational watershed models against areal water equivalents published in the Monthly hydrological reports have been in use for five years. These calibrations are not available for all the watersheds presented in Fig. 2. The results as R^2-values for the calibration period, and in two cases for the verification period are presented in App. 1. Calibration has been made against areal water equivalent. As can be seen from the values of the R^2-criterion, it is no problem to get a good snow cover model based on the temperature index approach. Of course, one must note that nearly all the results are from the calibration period, and verification has been made only in two cases, in Loimijoki and in Tujuoja. The verification results are also good, especially at the larger study basin of Loimijoki. The results were worse for the Tujuoja basin partly because there is only one precipitation station, compared to eight at the Loimijoki basin. Also, the error in the areal estimate of precipitation decreases with increasing area with the same gauging density Guschina et al. (1967). The verification result against snow observations for Loimijoki is good: $R^2 = 0.84$. Usually the R^2-value is about 0.75 for this five year verification period with the other snow model versions used for the Loimijoki basin. These good results are obtained with a temperature index model with separate simulation for open and forested areas; see Chapter 6.2. App. 14 presents the verification results for this model.

Generally, in northern Finland the simulation of the snow water equivalent is an easier task, because there are no long warm periods with abundant snowmelt in the middle of winter. These situations may increase the error in areal snow cover estimation. Because snowmelt periods do not commonly occur in the north, there is a good chance of getting accurate results. Large errors can occur only in the start of the snow cover period, but in winter the snow cover simulation is a plain accumulation of snow precipitation with corrections for the wind. Fig. 43 presents one example from the Tornionjoki watershed. Equally good results can be presented from any other northern watershed.

In Canada Goodison (1978) has also come to the conclusion that the accumulation of snow calculated from the precipitation gauge measurements by a mass balance method is in close agreement with snow course measurements stratified according to land use. Gardelin and Bergström (1987) compared simulated (by a watershed model) and measured snow water equivalents at one test basin (5 975 km^2) in Sweden. The use of measured water equivalents in the watershed model — instead of simulated values — did not improve the forecast results, because in most cases the observed and simulated values of the water equivalent were equal.

Another method used for measuring areal snow water equivalent in the Nordic countries is the gamma-radiation measurement from air (Kuittinen and Perälä 1984 , Bergström and Brandt 1984). Natural gamma-radiation from the ground is attenuated by water and snow over the ground. This method normally needs one calibration flight before the snow cover period in order to define the radiation level without snow. The areal water equivalent is estimated from the difference in radiation levels between the calibration flight and the snow cover flight. The advantages of the gamma-radiation method are its speed and the vast areal coverage, and it provides information on the areal variation of the snow water equivalent. The disadvantages are its costs (flights and measurement equipments) and the fact that ground measurements of the snow water equivalent have to be made to find the correct absolute level for gamma-radiation results.

For discharge forecasting purposes, the most valuable gamma-radiation measurement is made

during maximum snow cover. During snowmelt, the results cannot be used in a model because the differentiation of snow in solid and liquid form is not available from gamma-radiation measurements. This information is needed to update the snow model, which simulates snow both as solid ice and liquid water (Fig. 7).

10.1.3 The effect of elevation

The elevation differences in Finland are moderate, but they still have a considerable effect on the snow water equivalent values within a watershed. As an example, Fig. 44 presents simulation of the snow water equivalent in the Iisalmi watercourse (no. 8 in Fig. 2), which is divided into seven sub-basins. The elevation difference between the lowest and highest sub-basin is within 100—150 m, but the difference in the water equivalent can still be as much as 100 mm. The elevation has such a great effect through the combined effect of changes in temperature with elevation and changes in precipitation with elevation and slope in the windward direction. At higher elevation, the amount of solid precipitation is greater especially at the beginning of the snow cover period, due to the lower temperature. For the same reason, there is less snowmelt at higher elevation, which further increases the difference. The sub-basins on the eastern side of the watershed get more precipitation due to the westerly winds prevailing in weather fronts. The increase in precipitation with slope depends on the ascend rate, which is the product of wind velocity and slope rate more than elevation only.

The snow models of the sub-basins are calibrated against snow observations from the sub-basins. The whole watershed model, the snow cover model included, is checked against water level and discharge observations from four lakes (each one in a different sub-basin); this confirms whether the water balance and thus also the water equivalents are correct. The results of snow course measurements confirm that the overall picture of the distribution of water equivalent in these sub-basins is correct.

The effect of elevation is taken into account by dividing the area into homogenous sub-basins according to elevation. The other criterion for sub-basin division is the vegetation coverage or land use due to the different snow accumulation and snowmelt rate with different vegetation. For each sub-basin, the precipitation and temperature correction parameters, which take into account the elevation effect on precipitation, snow accumulation and snowmelt, are calibrated.

Large differences in areal snow cover have also been noticed in other flat watersheds during field snow measurements in spring during snowmelt. Within 20 km, an elevation increase of less than 100 m can increase the water equivalent from nearly zero to 100 mm, owing to the combined effect of increased precipitation and decreased temperature with elevation.

According to Ollila (1984), hills clearly higher than the surrounding area increase the water equivalent by approximately 50—60 mm/100 m in eastern Finland and by 40 mm/100 m in Lapland. Solantie (1975) studied the slope effect on precipitation and snow depth, which in Finland is about 20 % at best on the macroscale (100 km). According to Bergström (1990), the increase in precipitation is 10 % per 100 m increase in elevation in southern Sweden and 10—17 % in northern Sweden.

10.1.4 Simulation of other snow cover characteristics

If necessary it is possible to estimate snow density and depth by means of the snow cover model using the daily air temperature and precipitation as input data. Chapter 8 presented the physically based snow cover model, by which estimation of depth and density is possible with these input data. This snow cover model simulates water equivalent, density, depth, water retention and compaction due to overlaying layers and the metamorphosis dependent on temperature. The need to estimate snow density and depth is not great in operational use. The need for density values appears when energy balance models are used for simulation of snowmelt. Snow albedo is clearly dependent on snow density and also on snow depth if snowpack is shallow.

10.1.5 Real-time simulation of snow cover

The results presented above are based on all the precipitation and temperature observations that can be obtained from the watershed. This is seldom possible in real-time estimation of the areal water equivalent. On a daily basis, it is possible to get observations only from a couple of synoptic stations, and that inevitably worsens the results. During winter, however the need for up-to-date information is not urgent. It is enough if the areal snow cover observations are updated once a month. Observers send observation blanks from

standard precipitation stations once a month; updating can be done from these blanks. The work takes about a few hours per watershed. In this way the areal water equivalent can be kept correct till spring, when the water equivalent values are needed for watershed forecasting.

The other method for updating, made possible by watershed models, is to use discharge and water level observations. The watershed model, and especially the snow cover model, can be updated against these observations. In this way we can control that snowmelt is simulated correctly during warm spells in winter and in spring during the most intensive melt period. Discharge and water level observations can be obtained from automatic stations (over 30 operative stations in 1991) every day, from limnigraphs at one or two week intervals, or from observers by telephone.

Thus estimation of the areal water equivalent with the watershed model, also in real time, is very much possible both in theory and practice with the same accuracy as provided by the method based on snow course measurements. The cost of estimation of the areal water equivalent with model will also be very moderate compared to any other possibility.

10.2 Experiences from operational snowmelt flood forecasting with temperature index snow models

The temperature index snow model presented in Chapter 6 in connection with the watershed model in Chapter 4.1 has been in use for operational spring flood forecasting in Finland since 1981 (Vehviläinen 1982). These temperature index snow models and watershed models are now in operational use for over twenty watersheds (Fig. 2) ranging in size from 500 to 30 000 km^2. The experiences of these models in forecasting have revealed the most common difficulties and errors in real-time estimation of the areal snow cover and forecasting of water level and discharges in a watershed during snowmelt.

The main difficulties in forecasting encountered during the snowmelt period in spring in Finnish conditions have been varying parameters of the snowmelt model and evaluation of the areal water equivalent of snow. Also heavy rainfall and ice jams in rivers cause problems in updating areal snow cover, owing to errors in discharge and water balance evaluation of the watershed.

The methods used to overcome these difficulties in operational forecasting tested during this work have been:

— the development of temperature index models (Chapter 6) and physically based snowmelt models (Chapters 7 and 8), in order to get more reliable snow models
— use of statistical error models in snowmelt-runoff simulation to correct the runoff forecast.

Automatic observation and data transfer of water level, discharge and meteorological data are highly essential in real-time forecasting, to update snow cover and the whole watershed models. Real-time forecasting is not accurate enough without good real-time information about watershed and meteorological data.

10.2.1 Snowmelt model in flood forecasting

Spring flood forecasting models are sensitive to relatively small errors during the initial part of the snowmelt period. Quite small errors in the degree-day factor or in forecasted temperature can cause a large error in discharge simulation, in both timing and volume. This is because snowmelt, and especially the yield of water from the snowpack, has an accelerating nature along the snowmelt phenomenon due to the decreasing albedo and the decreasing temporary storage and retention capacity of snow (Chapter 6.1). Particularly critical is the time when the retention storage of snowpack and the temporary storage of terrain are being filled.

Updating of the snow model is essential at this stage if one is to get satisfactory results. Errors in snowmelt simulation can be corrected by changing the observed temperature values so that the observed and simulated discharges/water levels are equal. An example of this is presented in Fig. 45. Changing of the observed temperatures is preferred to changing the parameter values, because it is not reasonable to calibrate parameters against a few days of unchecked data. During the latter part of the snowmelt period, the forecast is not as sensitive to errors in the snowmelt model, because the snowmelt processes are proceeding steadily and the ripening period of snow is over. Further, the discharge is now more a function of outflow from other storage (surface, sub-surface, rivers and lakes) than a function of snowmelt and outflow from snowpack.

A large error in the initial value of snow water equivalent can make all forecasts worthless also in the latter part of the snowmelt period. If the initial water equivalent differs very much from the true value, the forecasts may be correct during the

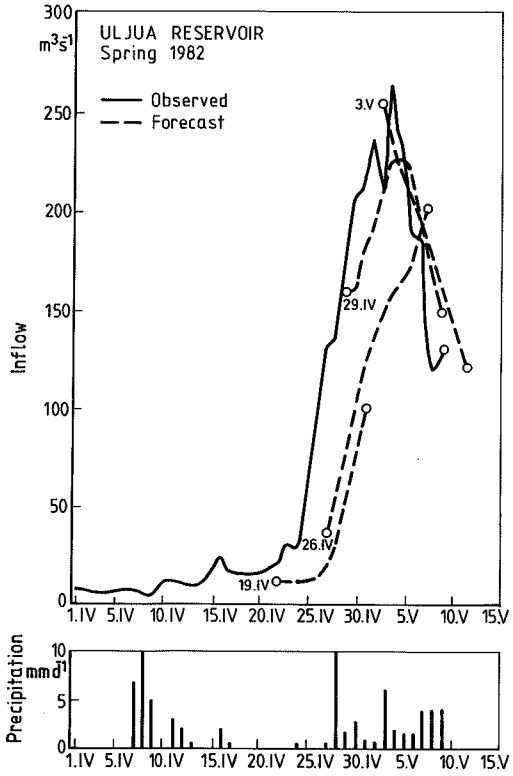

Fig. 45. An example of the effect of updating the forecasting model during the initial part of snow melt. Updating is made before the forecast of 29th April.

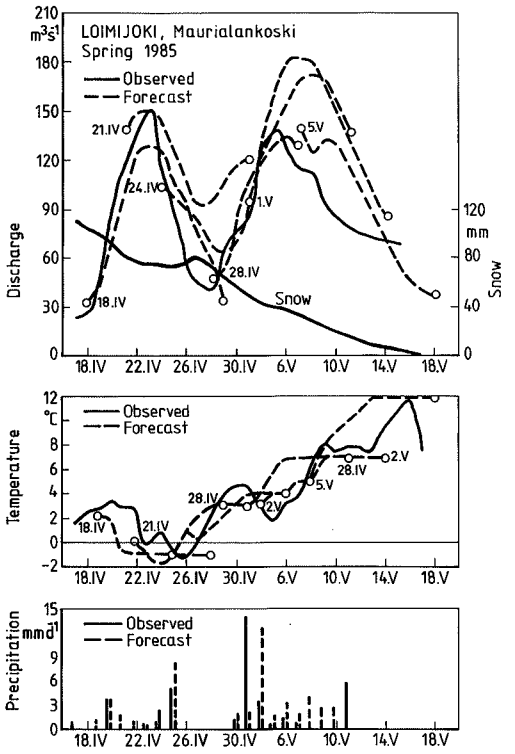

Fig. 46. An example of the effect of a wrong initial value for the areal snow water equivalent (about 30 mm too great). Following the large error, the forecast is corrected by the AR-model (forecast of 5th May).

Table 22. The number of precipitation (P) and temperature (T) stations used in real-time forecasting for watersheds. Zero means no stations in the watershed area. The number of stations used which are not in the watershed area are presented in brackets.

Watershed	Area(km²)	P	Area/P	Area/P_{all}	T
Säkylän Pyhäjärvi	635	0(1)	—	635	0(1)
Loimijoki	1 980	1	1 980	1 980	1
Ylä-Karvianjoki	988	0(1)	—	988	0(1)
Kyrönjoki Pitkämö	2 184	0(2)	—	1 092	0(2)
Lapuanjoki	3 690	1(1)	3 690	1 845	1(1)
Ähtävänjoki	1 715	0(2)	—	858	0(2)
Perhonjoki	1 390	0(2)	—	695	0(2)
Kalajoki	3 005	1	3 005	3 005	1
Siikajoki	3 470	0(3)	—	1 157	0(3)
Iisalmen reitti	5 574	1	5 574	5 574	1
Nilsiän reitti	4 135	0(1)	—	4 135	0(1)
Koitajoki	6 520	1	6 520	6 520	1
Hyrynsalmen reitti	8 635	1(1)	8 635	4 318	1(1)
Kuivajoki	1 270	0(2)	—	635	0(2)
Kemijoki	27 285	3	9 095	9 095	3
Ounasjoki	12 335	0(2)	—	6 178	0(2)
Raudanjoki	3 485	0(2)	—	1 743	0(2)
Tornionjoki*	22 442	3	7 480	7 480	3
Ivalonjoki	3 300	1	3 300	3 300	1
Mean		1(1)	5 475	3 223	1(1)

* for Tornionjoki at the Finnish-Swedish border (Muonionjoki and Tornionjoki between Pajala and Pello)

initial part of snowmelt, but the error may reveal itself at the very moment of the flood peak. The forecasted discharge peak differs considerably in timing, volume and magnitude from the observed peak (Fig. 46).

In order to get more stable snowmelt models, the basic degree-day snowmelt model presented in Chapter 6.1 has been developed towards physical direction by introducing variable degree-day constant and the liquid water retention capacity of snowpack into the snow cover model. Also the simulation of refreezing, depression storage, depletion of the snow covered area and different snowmelt in forested and open areas have been taken into account in operational snowmelt models. All these processes are relevant in Finnish conditions. These processes have been studied more thoroughly in Chapter 6.

10.2.2 Heavy rainfall during snowmelt

Heavy rainfall during snowmelt usually causes difficulties in the simulation and forecasting of discharges and water levels.

First, the number of real-time operating precipitation stations in all cases is too few to give reliable daily areal precipitation estimates; see Fig. 5. Table 22 presents the number of precipitation and temperature stations usable for real-time forecasting for the watersheds in Fig 2. The mean density of precipitation stations is very low, below one station per 5 400 km^2 in the watershed, or one station per 3 200 km^2, if the nearest stations outside the watershed are included.

Only two stations, on the average are used for estimation of areal precipitation in real time. This means that the average error for daily values according to Fig. 5 may be over 50 per cent. Estimation of areal precipitation for short intervals in the observation period is thus inaccurate. Further, errors in precipitation forecasting are still more significant. It is impossible to make accurate quantitative rainfall forecasts for longer periods than one or two days. Thus a heavy rainfall during real-time watershed forecasting inevitably leads to poor discharge and water level forecasts (Fig. 47). Also estimation of the areal snow cover is difficult: the watershed model cannot be used effectively to update areal snow cover against total water balance (discharge/ water levels) observations because the correct amount of precipitation is more or less unknown.

The possibilities to reduce these errors are very limited. The transfer of data on precipitation and, especially, discharge and water level observations

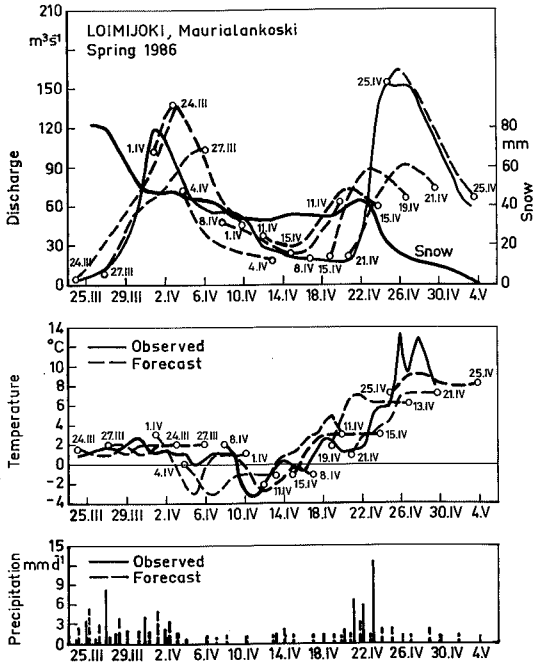

Fig. 47. An example of the effect of abundant precipitation during real-time fore casting of discharge. The three-day precipitation near 22nd April is not forecasted correctly and the final value of precipitation is estimated with the help of the watershed model by changing the observed precipitations so that the observed and simulated precipitations are equal. Forecast is marked by (- - -) and observation by (——).

can be speeded up by using automatic observation stations, because real-time observations of the watershed make it possible to update the model by changing the observed precipitation values, and thus also to estimate the areal precipitation through the watershed model (Fig. 47). Further, error models can be used to correct the simulated discharge and water level values, if observed real-time values are available (Fig 46). The use of error models is discussed later in this chapter.

10.2.3 Ice jams during snowmelt floods

Ice, and especially ice jams, cause discharge measurement difficulties in rivers; in consequence the updating of snow cover and the whole watershed model is impossible. Unnoticed and uncorrected ice jam effects in the discharge values may lead to incorrect updating of the watershed model, which may, in turn cause errors later.

Ice jams have caused flooding problems and damages in Finland nearly every spring in the 1980s. It is difficult to forecast the time, and especially the quantitative effects, of ice jams. In those cases when the flood peak rises very sharply, however, it is easy to make ice jam predictions. Ice jams occur during sharp flood rising which lasts only a few days in most Finnish rivers when there is a sudden and abrupt increase in air temperature. An exceptionally warm period causes breakup along the whole river, which causes ice jams, especially at the lower part of the river (Fig. 48). The situation is even worse in cases when there is a firm ice cover downriver.

When a spring has many warm spells, melt and none-melt periods follow each other, and it is difficult to predict ice-breakup; the ice cover may melt considerably before ice-breakup. In such cases, the threat of ice jams decreases all the time (Fig. 49).

Thus far there are no accurate enough physical models for forecasting ice jams, but statistical models have been developed (Beltaos 1983). A combined discharge and ice-breakup forecasting model is in use for the Tornionjoki river (Vehviläinen et al. 1988); its results for the springs of 1988—1990 were good. The error, in forecasting the time of ice-breakup one to two weeks in advance, has been one to two days. In this model, the ice-breakup forecast is based on the positive degree-day sum and discharge. Other indicators, e.g. the water level during ice-cover formation and during flood, ice thickness and the rate of rise in water levels before break-up, were tested, but they were not included in the ice-breakup model in this case (Forsius 1988, and Forsius and Granholm 1988).

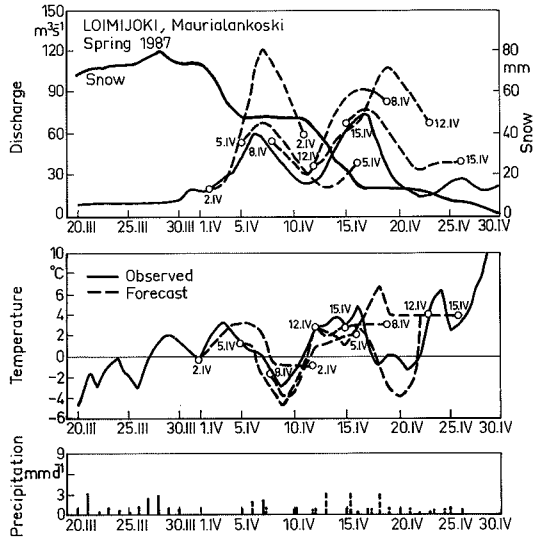

Fig. 48. An abrupt rise in temperature after 15th May caused effective snowmelt and sharp rise in discharge, which created difficult ice jams at the lower part of the Ivalojoki river. Note that practically all the snow melted in five days.

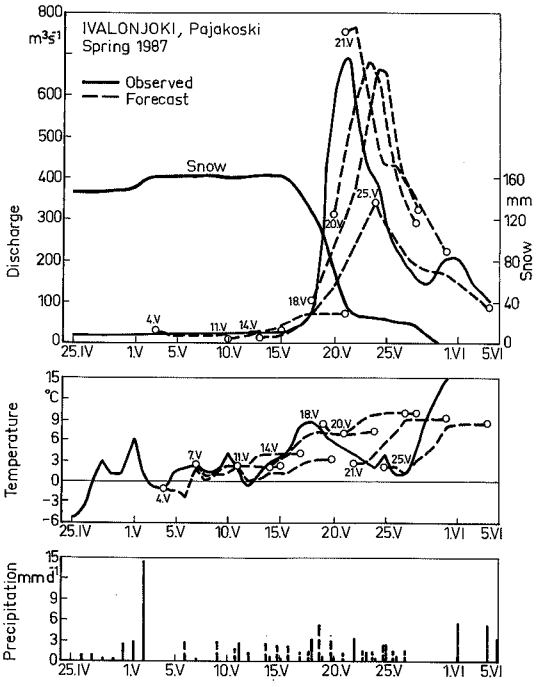

Fig. 49. Example of a spring with warm and cold periods alternating and with a moderate discharge as compared to the channel capacity of the river. In that spring, the ice cover nearly melted before ice breakup.

10.2.4 Experiences of error models in snowmelt flood forecasting

In cases when there is an error in estimation of the areal snow water equivalent which cannot be quantified, an autoregressive (AR) error model helps to make decent flood forecast for the coming few days (Fig. 46). An autoregressive error model corrects the forecast on the basis of the error made during the observation period. The parameters of the error model are estimated from the series of residuals during the calibration period. For the Loimijoki basin (1 980 km^2) (Fig. 2), a first-order autoregressive model of the following form has been tested:

$$z_i = p_1 z_{i-1} + a_i \qquad (148)$$

where
z_i = the current value of the error at time step i
p_1 = coefficient
a_i = the current shock at time step i from a random process with zero mean and known variance; a_i is usually omitted.

This model gave the following results, expressed as model efficiency R^2 (Eq. 20) with different lags. In this test, lag means how old the error in use is, i.e. how many days ahead the "forecast" is made:

Model	Model efficiency R^2
Basic hydrological model	0.864
With AR(1)-model, lag = 1 day	0.916
2 days	0.875
3 days	0.869
4 days	0.866
5 days	0.866

The error model considerably improves the results for the next one to two days, after which the effect diminishes very quickly. An example of the effect of AR(1)-model in a real forecasting situation is presented in Fig. 46 from Loimijoki. In this case, the most probable reason for the too high forecasted discharges at the end of the snowmelt period was the initially excessive areal water equivalent, which caused overestimation of peak discharge and the volume of flow. During operational real-time forecasting, location of the error source is a difficult task in a case of this kind; it is especially difficult to estimate how much too large the areal water equivalent is in the middle of the peak discharge; an AR-model is thus very helpful for correcting the forecast according to real-time observations. At the beginning of the snowmelt period, errors in simulated discharges are most probably due to snowmelt simulation; this can be corrected by changing the input temperatures. We can thus maintain the correct water balance (water equivalent) of the watershed, assuming that the initial values are correct. The error model is not very helpful in this period.

The use of an AR-model or some other model based on a time series requires accurate and rapidly transferred data. Error models are useless without daily observations of the forecasted components (discharge, water level). During ice jams, for example, discharge observations are very inaccurate, nor could error model be used to correct the discharge forecasts because the correct value of discharge was not known. This caused an error in simulated discharge during the observation period. Further, error models do not help before the error has revealed itself; by then it is often too late for the forecast to help rescue work or decisions how to regulate the watershed. Thus a reliable snow cover model and a conceptual hydrological watershed model are very important, especially in cases when the observations from the watershed are difficult or impossible to get.

Time series models, Autoregressive (AR) and Transfer-Function-Noise (TNF)-models, have also proved to be effective in real-time forecasting (Malve 1986, Lundberg 1982).

10.2.5 Data transfer

Real-time forecasting needs real-time data from hydrological and meteorological observation stations. In 1991, the National Board of Waters and the Environment had over thirty automatic water level measuring stations, many of which are situated in the watersheds forecasted in Fig. 2: Loimijoki, Säkylän Pyhäjärvi, Lapuanjoki, Ähtävänjoki, Perhonjoki, Siikajoki, Tornionjoki and Ivalojoki have one or more automatic stations each. These stations belong to the PROCOL-system (Puupponen et al. 1990), which observes water level data in real time and transfers it to the datanet of the National Board of Waters and the Environment, from which they are readily available for watershed forecasting models. If a discharge rating curve exists, the water levels are also used to calculate discharges. In these cases, real-time discharge data are available, but without a possible ice-reduction, which must be taken into account separately.

Furthermore, there are some automatic water level stations which are available over the telephone. The water level value is given by a voice-simulator from Ounasjoki (1 station) and Kemijoki (1 station) basins. These stations are also quite helpful for real-time forecasting. PROCOL-stations data are also available over the telephone.

As far as daily air temperature and precipitation values are concerned, the meteorological input data for watershed models in their operational use come through the datanet of the Finnish Meteorological Institute. Every day, the report of 50 synoptic stations is transferred into the datanet of the National Board of Waters and the Environment (NBWE). Simultaneously with the real-time data, the precipitation (quantitative) and temperature forecast for the next ten days made by the European Centre for Medium-Range Weather Forecast (ECMWF) in England is transferred through the datanet of the Finnish Meteorological Institute to the datanet in NBWE. Furthermore, the Finnish Meteorological Institute three times a week delivers a 5—10 day precipitation and

temperature forecast based on computer forecasts made in England, Germany, the USA and Finland.

The real-time data on precipitation, air temperature, water level and discharge are available to all District Offices of NBWE, through the NBWE datanet. Thus every District Office can operate its forecast model by itself.

11 SUMMARY AND CONCLUSIONS

The aim of this study was to develop a snowmelt model valid for large watersheds, using standard meteorological and hydrological data. Further, some other processes not directly part of the snowmelt were studied in order to determine their effect on the simulation of snowmelt runoff.

The starting point for the development of the snowmelt model was the widely used degree-day model, which is the main snowmelt simulation approach used in operational watershed models.

11.1 Development of the degree-day model

The basic degree-day model with a constant degree-day value, a constant water retention capacity and no distribution of snow cover was modified according to the following modifications:

1. The degree-day constant was increased during the progress of snowmelt in the spring as a function of cumulative melt. This increase in degree-day parameter can be explained by the decrease in the snow albedo, by soil warming through the shallow snowpack due to short-wave radiation at the end of snow cover period and by increased solar radiation at the end of the snowmelt period. According to the results from 76 watersheds and sub-basins, the mean value for the increasing degree-day factor was 1.4 mm $°C^{-1}d^{-1}$ and the standard deviation 0.52 mm $°C^{-1}d^{-1}$ at the beginning of the snowmelt period. At the end of the snowmelt period, the mean degree-day factor was 4.7 mm $°C^{-1}d^{-1}$ and the standard deviation 1.9 mm $°C^{-1}d^{-1}$. The maximum value of the degree-day factor is reached after 77 mm of snowmelt on the average.

The mean threshold temperature for snowmelt was 0.3 °C. Inclusion of a changing degree-day in the snow model did not directly improve the results for the study basin of Loimijoki. During the verification period, the goodness of fit R^2 was 0.769 with a constant degree-day model and 0.768 with an increasing degree-day parameter in the snow model.

2. A model version with separate snowmelt simulation for open and forested areas considerably improved the results for the study basin of Loimijoki. During the verification period, the model performance value R^2 increased from 0.667 to 0.837 against snow observations and from 0.768 to 0.780 against discharge observations. This model version with different degree-day values for open and forested areas were also calibrated to 36 sub-basins in operational watershed models. According to the results from these calibrations the degree-day value during snowmelt increased in open areas from 1.7 mm $°C^{-1}d^{-1}$ to 7.8 mm $°C^{-1}d^{-1}$ and from 1.4 mm $°C^{-1}d^{-1}$ to 4.7 mm $°C^{-1}d^{-1}$ in forests.

The snowmelt threshold temperature was 0.2°C for open areas and 0.6°C for forested areas. The maximum degree-day value was reached after 109 mm of melt in open areas and after 83 mm of melt in forests. The standard deviation of the maximum degree-day value in forests was 1.9 mm $°C^{-1}d^{-1}$; in open areas it was 3.1 mm $°C^{-1}d^{-1}$. Another approach widely used is to increase the degree-day function seasonally according to day number. With this version of the model, the results were slightly worse than when the degree-day was a function of cumulative melt at the study basin of Loimijoki.

3. The retention capacity of snowpack is not constant during the snowmelt period. When the grain size of snowpack increases during snowmelt period, the water retention capacity decreases because there are less voids and grain surface layer to which the liquid water can be attached. Also vertical and horizontal drains develop in snowpack during the melting period, which further decrease the liquid water storage in snow. According to these considerations, the simulation results, as indicated by the R^2-value, improved from 0.753 to 0.768 when a model with decreasing retention capacity was included in the snowmelt model at the study basin of Loimijoki (1 900 km^2). When the results for all 76 sub-basin calibrations were considered, the retention capacity decreased from 17 % to 5 % by weight on the average during snowmelt. But the retention capacity reached the minimum value after 7 mm of snowmelt on the average, which means that the retention capacity is

practically constant over most of the snowmelt period. In 30 % of the calibrated basins, the decreasing retention capacity was a more valid process, with the retention capacity changing from 16 % to 5 % during 20 mm of cumulative melt.

The reason for the weak response of the retention capacity process in the snow model calibration is probably the depression storage described in the next paragraph. This storage delays the outflow of melt water form snowpack in a manner similar to the snow retention capacity. The depression storage is larger and may thus cover the effect of the retention storage. Thus it seems to be possible to omit the retention capacity from the snowpack model without deteriorating the model simulation in most cases, especially in large basins.

4. The other storage process connected to the snowmelt period found to be important at the watersheds studied and at the other modelled watersheds (about seventy, including sub-basins), is called here depression storage. This is the storage of meltwater in depressions, ditches and snowdrifts at the beginning of the snowmelt period before the meltwater is released into rivers. The depression storage process is important, especially in flat areas, as most of the tested watersheds were.

The main effect of this depression storage is, first, to store and delay the snowmelt runoff and, later, to increase the yield of water from snowpack over the value of daily snowmelt and rainfall together. Thus the water yield from snowpack exceeds the daily snowmelt due to the release of earlier melted water from depression storage. At the Loimijoki basin (1 900 km^2), the R^2-value increased from 0.759 to 0.768, and at the Tujuoja basin (20.6 km^2) from 0.717/0.709 (two different verification periods 1970—1976/1963—1976) to 0.730/0.717, when the depression storage was included in the snow model.

The values of depression storage varies much from area to area. For 20 sub-basins, where a constant value for depression storage was used, the average was 24 mm (S.D. 11 mm) with outflow constant 0.16 d^{-1}. For 56 basin the amount of depression storage was calculated as the percentage of the areal snow water equivalent with a mean value of 54 % (S.D. 27 %) and an outflow constant of 0.19 d^{-1}. For example, with a water equivalent of 150 mm, the depression storage is 81 mm. The latter approach gave better results, and the behavior of the storage is closer to reality: the quantity of depression storage depends on the quantity of snow.

5. Simulation of the areal extent of the snow covered area also proved to be a factor which improved the results of watershed model performance R^2 from 0.759 to 0.768 at the Loimijoki basin. Simulation of the snow covered area was based first on the snow depletion curve (Chapter 6.1), which divides the area of watershed into snow free and snow covered areas according to the accumulated snowmelt. Further, a model version where snowmelt was simulated separately for open and forested areas with separate snow depletion curves considerably improved model performance at the larger study basin of Loimijoki (1 900 km^2). The model performance R^2 increased from 0.768 to 0.780 against discharge and from 0.667 to 0.837 against snow observations.

Especially in cases when snowmelt ceased for a few days during the snowmelt period, the distinction of snowmelt in open and forested areas improved the results. In that case, open areas were often free of snow while forested areas had a considerable amount of snow left. In contrast to the Loimijoki basin, separate snow melt simulation for forested and open areas made little improvement at the smaller study basin of Tujuoja (20.6 km^2).

A model with a statistical distribution of snow was tested at the Loimijoki basin. The distribution function was a 2-parameter gamma-distribution, and the simulation results were as good as in the case of snow simulation for open and forested areas, but not better.

6. Some modest improvements were also obtained by including refreezing of meltwater and different snowmelt functions for rainfall and snowfall situations.

The inclusion or omission of one of the previously presented modifications in the snowmelt model does not cause any dramatic change, but all of them together had a favourable effect on model performance when the comparison was made against the observed snow water equivalents or the observed discharge/runoff values during the verification period. For the Tujuoja basin, the model without any modifications presented above gave a model performance R^2 of 0.586/0.613, compared to the best modified model with an R^2 of 0.730/0.717 during the verification periods of 1970—1976/1963—1976. For the Loimijoki basin, the R^2-values were 0.763 with the unmodified model and 0.780 with the best modified model during the verification period of 1970—1976. For both basins, the model performance values presented above were calculated against observed discharge values. According to the results, the most important improvement was inclusion of the snow cover distribution in the snow cover simulation, through division into open and forested areas.

11.2 Combined degree-day and energy balance models

An approach to the energy balance snowmelt simulation was started by adding some terms connected to energy balance simulation to the best degree-day model, thus attempting to improve the results of snowmelt simulation in large watersheds. Components simulating short-wave and long-wave radiation, latent and sensible heat, heat from liquid precipitation and from the ground were tested in the snowmelt model, each alone and together with others, to improve the results of the degree-day approach. The heat deficit of snowpack (cold content) was also tested to see whether the results of the degree-day approach improved. Inclusion of energy balance terms did not improve the overall model performance significantly. In extreme situations, the latent heat (during strong wind and high air moisture) and short-wave radiation component (during high solar radiation) may become important, especially at the Loimijoki basin, where 55 per cent of the area is open. At the Tujuoja basin, with only 18 per cent of open areas, the degree-day component was always the most important component in this attempt.

Other modifications of the degree-day model were: inclusion of diurnal temperature difference in degree-day snowmelt model; calculation of the daily mean temperature separately, if the daily minimum temperature is below zero; use of degree-day hours. None of these modifications improved the results.

11.3 Snowmelt energy balance model

An energy balance model which simulates short-wave and long-wave radiation, latent, sensible and precipitation heat and the heat deficit of snowpack was constructed and tested in Chapter 6. For both of the study basins, the energy balance model was not as good as the best degree-day model.

In order to improve the net short-wave simulation, a physically based snow cover model was developed in Chapter 7, which could simulate the characteristics of snowpack: density, depth, liquid water retention capacity and, most of all, snow albedo. The snow albedo was simulated now as a function of density and depth. This approach improved the overall results of energy balance simulation. At the Loimijoki basin, this physically based snow cover and snowmelt model gave snow cover simulation results as good as the best degree-day model. At the Tujuoja basin, the results were not as good as with the best degree-day approach. The physically based snow cover model simulates snow density and depth well. Due to the modest need for input data, this model can even be used operationally, to obtain areal snow depth and density values.

The energy balance approach gives valuable information about the contribution of various energy balance terms to snowmelt during different periods of the year. Latent and sensible heat are the most important energy balance terms from September to January. During this period, the contribution of latent and sensible heat is 40—70 % at the Tujuoja basin and 70—90 % at the more open Loimijoki basin. In spring, the contribution of short-wave radiation increases strongly and in March is over 50 % at the Tujuoja and Loimijoki basins. The net short-wave component reaches its maximum at both basins in April: 85 % at the Tujuoja and 69 % at the Loimijoki basin. In late spring, the contribution of sensible and latent heat drops to 10 % at the Tujuoja and to 15 % at the Loimijoki basin. In April, latent heat is mainly negative, i.e. evaporation from the snow cover prevails and the amount of snow evaporation is 3.1 mm per month at the Tujuoja and 4.0 mm per month at the Loimijoki basin. The condensation prevailing in autumn and mid-winter is only 0.1—0.5 mm per month.

11.4 The effect of soil frost on runoff

A simple physically based soil frost model, which can be included in the modified HBV-runoff model and needs only daily precipitation and temperature data, was developed in Chapter 9. The performance of the soil frost model against observed frost depth observations was fairly good. This soil frost model was connected to the hydrological model through soil moisture model.

The effect of soil frost depth on runoff formation was taken into account by modifying the parameters of the runoff model according to the simulated soil frost depth. No significant effect of soil frost on runoff was detected in the forested study basin of Tujuoja, with moraine soils. It was concluded that in forested areas with moraine soils, the infiltration capacity will not significantly be decreased during the snowmelt period with soil frost.

11.5 Dependence between snow and runoff models

It is obvious that the best snow models, and especially the calibrated parameters in snow models, are more or less specific for the runoff model (HBV) used. This interdependency was also noted in the intercomparison of snowmelt runoff models arranged by WMO (WMO 1986). In this study, presented here, the interdependency is minimized through calibration and verification of snow models against areal snow observations. Snow observations are scarce during the most active snowmelt period in spring. In this period, the active parameters in the snow model are calibrated more against the total water balance (discharge/runoff) than against snow observations. During the long snow accumulation period (5 months), the situation is the opposite. However, the best snow models give the highest model performance both when verification is made against snow observations or against total water balance, i.e. against discharge.

11.6 Simulation of areal snow cover

Chapter 10 discussed the possibilities and accuracy of the snow cover model — the modified degree-day model — to simulate the areal water equivalent of snow throughout the whole winter season in large watersheds. The results obtained from calibration and verification of models over periods of five to ten years at the study basin of Loimijoki and other 39 sub-basins calibrated for operational use gave a model performance of $R^2 = 0.90$, on the average, against observed areal snow water equivalents. It was concluded that compared to other available methods, the snow cover model is a good, reliable and less expensive way to estimate the areal water equivalent for large basins.

The key points for good results are, first, the time scale. Daily precipitation observations are inaccurate; the error may be as much as 50 %. When the time span increases, the error in precipitation measurements decreases considerably; with monthly values, the error in precipitation measurement decreases well below 10 %. In snow cover simulation, the time scale is four to five months. Two other facts important to snow cover simulation are the size of watersheds and the number of precipitation stations. The accuracy of areal estimates increases with increasing precipitation station density and with increasing watershed size with the same station density. The precipitation station density in this study is one station per 465 km^2. The number of stations per watershed is nine on the average.

The results of operational real-time simulation of areal snow water equivalent have been good in both southern and northern Finland. In real-time simulation, the crucial point is to check the snow simulation against discharge and water level observations, i.e. against the total water balance of the watershed. Possible errors in snowmelt simulation can be detected by comparing the observed and simulated discharge and water level values. The error is corrected by updating the snow model so that the observed and simulated discharge and water level values are equal.

The physically based snow cover model presented in Chapter 7 makes it possible to simulate also areal values of snow density and snow depth. These variables are seldom simulated with snow cover models.

11.7 Snowmelt flood forecasting

As revealed by this study, the modified degree-day model is thus far the best snow model for a large watershed, especially if we take into account the larger need for data characteristic for the combined physically based energy balance and snow cover model presented in Chapters 6 and 7. Real-time forecasting models developed for large watersheds in Finland use the degree-day approach for snow simulation.

When water levels and discharges are forecasted in real time, the snow cover simulation can be corrected according to discharge and water level observations. In cases when updating of model storage is not possible, an error model based on autoregressive or autoregressive moving average models is used to correct the forecast.

Essential for real-time forecasting is a good real-time data transfer system for the forecasted variables.

11.8 Concluding remarks

As the discussion above reveals, the snow cover model can be developed in many different directions in order to improve the results for large watersheds. This was also revealed in the intercomparison of different snowmelt models (WMO

1986), where a large variety of snowmelt models was tested; most of them were found to simulate snowmelt runoff satisfactorily. The two main research directions in this study have been to develop the temperature index and the physically based snow models. For the watershed, the temperature index models seems to be better, especially when the distribution of the snow cover is taken into account. In short, the key point in simulation of snow for the watershed is to know where the snow is, i.e. to simulate the snow distribution correctly in space.

ACKNOWLEDGEMENTS

Many people have influenced my studies in recent years. My initial interest in snow studies was waken long ago by Dr. Esko Kuusisto and his many excellent snow studies done at the Hydrological Office. Both his research and his advice have given me many ideas on how to continue my work. The same can be said of the many discussions I had with Mr. Jaakko Perälä concerning snow and snow modelling in general. I am also very grateful to Professor Lev Kuchment for the opportunity to work at the Hydrological Laboratory of the Water Problems Institute in Moscow, where I collaborated, in particularly, with Dr. Yuri Motovilov. The work done with Dr. Motovilov has been very important for this paper. Dr. Motovilov has been a great help during my studies, guiding me by virtue of his vast experience of physical snow and runoff models.

In the final stages of preparing my dissertation I have been given valuable advice by Professor Seppo Mustonen, Professor Pertti Vakkilainen, Professor Juhani Virta, Dr. Risto Lemmelä and Dr. Pertti Seuna. I am very grateful to them for their assistance.

The illustrations were drawn by Ms. Tiina Anamo-Laaksonen and checked by Ms. Terttu Halme. The English language was revised by Ms. Sheryl Hinkkanen and the Finnish summary by Ms. Raija Leppäjärvi.

I wish to express my gratitude to everyone who has contributed to this work.

Helsinki, December 1991 Bertel Vehviläinen

YHTEENVETO

Tutkimuksen päämääränä oli Suomen oloihin sopivan lumimallin kehittäminen. Lähtökohtana oli vesistöennustemalleissa käytetty lumen lämpötilaindeksimalli, joka laskee lumen määrää vuorokauden lämpötila- ja sadantatietoja käyttäen.

Lämpötilaindeksimallin ohella kehitettiin lumipeitettä fysikaalisesti kuvaava malli. Fysikaalinen lumimalli, joka perustuu lumen energiataseeseen, kuvaa lumen kertymistä ja sulantaa sekä lumen fysikaalisia ominaisuuksia. Molempia malleja testattiin vesistöalueille meteorologisia ja hydrologisia perushavaintoja käyttäen. Tulokseksi saatiin, että vuorokauden keskilämpötilaan perustuva lumimalli antaa parempia tuloksia suurille vesistöalueille kuin fysikaalisesti tarkempi energiatasemalli.

Vesistömallin antamia tuloksia koetettiin parantaa ottamalla huomioon routa, koska se voi vaikuttaa valuntaan. Siksi kehitettiin routamalli, jota voidaan käyttää lämpötila- ja sadantahavaintojen avulla. Tulosten mukaan routa ei ollut metsäalueilla merkittävästi valunnan muodostumiseen vaikuttava tekijä.

Tutkimuksessa tarkasteltiin myös sulanta-valunta -mallien pohjalta kehitettyjen vesistömallien käyttöä reaaliaikaiseen virtaaman, vedenkorkeuden ja lumimäärän ennustamiseen.

Lämpötilaindeksimallin kehittäminen

Lämpötilaindeksimallia kehitettiin kahdella kohdevesistöllä: Loimijoella (1 900 km^2) ja Tujuojalla (20,6 km^2). Kehitystyö tehtiin liittämällä lämpötilaindeksimalliin osamalleja, jotka kuvaavat eräitä tärkeitä sulantaan liittyviä prosesseja. Uusien osamallien vaikutusta malliin arvioitiin vertaamalla laskentatuloksia lumi-ja virtaamahavaintoihin. Seuraavassa esitetään ne uudet, tärkeät sulantaan liittyvät prosessit, jotka on otettu huomioon kehitystyössä:

1. Lumen sulamisnopeus lisääntyy sulamisen edistyessä mm. lumen albedon pienenemisen takia. Tämä voidaan kuvata kasvattamalla mallin astepäivätekijää esimerkiksi kumulatiivisen sulannan funktiona. Astepäivätekijä ilmoittaa kuinka paljon lunta sulaa yhtä positiivista lämpötila-astetta kohti vuorokaudessa.

Vakioastepäivätekijää käyttäen Loimijoen mallin hyvyysluku R^2 oli 0,769, muuttuvalla astepäivätekijällä 0,768 molemmat virtaamahavaintojen avulla laskettuna. Jälkimmäinen mallityyppi on ollut käytössä kaikissa operatiivisissa vesistömalleissa. Vesistömallien kalibrointitulosten perusteella astepäivätekijän arvo on sulannan alussa keskimäärin 1,4

mm $°C^{-1}d^{-1}$ (keskihajonta 0,52 mm $°C^{-1}d^{-1}$) ja sulannan lopussa 4,7 mm $°C^{-1}d^{-1}$ (keskihajonta 1,9 mm $°C^{-1}d^{-1}$). Arvot ovat keskiarvoja 76 kalibroidulta valuma-alueelta. Astepäivätekijän maksimiarvo saavutetaan keskimäärin silloin kun kumulatiivinen sulanta on 77 mm. Sulannan rajalämpötilan keskiarvo oli 0,3 °C. Lumen sulamisen katsotaan alkavan, kun aluelämpötila ylittää rajalämpötilan.

2. Lumen sulannan laskenta erikseen aukeille ja metsäalueille paransi tuloksia Loimijoen vesistöalueella. Verifiointijaksolla lumihavaintojen perusteella laskettu hyvyysluku R^2 kasvoi arvosta 0,667 arvoon 0,837, virtaamahavaintojen avulla laskettuna arvosta 0,768 arvoon 0,780. Malliversiota, jossa lumen sulaminen on laskettu erikseen aukeille ja metsälle, käytettiin myös useissa operatiivisissa vesistöennustemalleissa. Astepäivätekijä kasvaa aukeilla keskimäärin arvosta 1,7 mm $°C^{-1}d^{-1}$ arvoon 7,8 mm $°C^{-1}d^{-1}$ ja metsässä arvosta 1,4 mm $°C^{-1}d^{-1}$ arvoon 4,7 mm $°C^{-1}d^{-1}$. Arvot perustuvat 36 osavaluma-alueen kalibrointituloksiin.

Lumen sulamisen rajalämpötila aukeilla oli keskimäärin 0,2 °C ja metsässä 0,6 °C. Astepäivätekijän suurin arvo saavutettiin, kun kumulatiivinen sulanta ylitti aukeilla 109 mm ja metsässä 83 mm. Astepäivätekijän maksimiarvojen keskihajonta oli aukeilla 3,1 mm $°C^{-1}d^{-1}$ ja metsässä 1,9 mm $°C^{-1}d^{-1}$.

Astepäivätekijän laskeminen vuodenajan funktiona on toinen sulantanopeuden muutosten kuvaamiseen käytetty menetelmä. Tällaisen mallin tulokset olivat kuitenkin hieman huonompia kuin jos menetelmänä oli astepäivätekijän kasvattaminen kumulatiivisen sulannan funktiona.

3. Lumen kyky pidättää nestemäistä vettä pienenee sulamisen edistyessä, koska lumen rakenne muuttuu. Lumen huokoisuus pienenee ja lumirakeiden koko kasvaa, mikä pienentää lumirakeiden vettä sitovaa pintaa. Lumeen syntyy vettä johtavia käytäviä sulamisen loppuvaiheessa. Loimijoen vesistömallin hyvyysluku R^2 kasvoi arvosta 0,753 arvoon 0,768, kun lumen vedenpidätyskyvyn simulointi otettiin malliin mukaan. Kaikkien 76 alueen kalibrointitulosten mukaan lumen pidätyskyky pienenee keskimäärin 17 painoprosentista 5 painoprosenttiin sulamisen aikana. Vedenpidätyskyky saavuttaa minimin heti sulannan alussa keskimäärin n. 7 mm sulannan jälkeen, mikä merkitsee, että se on käytännössä vakio sulamisen aikana. Noin 30 %:lla valuma-alueista pidätyskyvyn minimi saavutettiin 20 mm sulannan jälkeen. Pidätyskyky muuttui näillä alueilla 16 prosentista 5 prosenttiin.

4. Vesistömallien tulokset paranivat keväällä, kun huomioon otettiin lumesta sulaneen veden varastoituminen sulannan alussa soille, painanteisiin ja pelloille sekä varastoituneen veden purkautuminen näistä painannevarastoista sulannan loppuvaiheessa vesistöön. Kun painannevarasto jätettiin pois, laski vesistömallin hyvyysluku R^2 Loimijella arvosta 0,768 arvoon 0,759 ja Tujuojalla arvosta 0,730/0,717 arvoon 0,717/0,709.

Painannevaraston simulointi on sitä tärkeämpää mitä alavampia ja soisempia ovat sovellutusalueet. Syynä kohdassa 3 mainittuun lumen vedenpidätyskyvyn vähäiseen merkitykseen lumimallissa voi olla painannevarasto, joka vaikuttaa valuntaan samalla tavoin kuin lumen vedenpidätyskyky. Sekä lumipeite että painanteet varastoivat sulannan alussa vettä, aiheuttavat viivettä valunnassa ja purkavat sulannan lopussa vesivarastoja.

Painannevarastoa pidettiin vakiona 20 valuma-alueella ja sen keskiarvo oli 24 mm, keskihajonta 11 mm ja valuntakerroin 0,16 d^{-1}. Valuntakerroin ilmoittaa kuinka paljon varastosta poistuu vettä laskentajakson aikana. Painannevaraston suuruus laskettiin 56 valuma-alueelle prosenttiosuutena lumen vesiarvosta. Painannevaraston arvoksi tuli keskimäärin 54 % lumen vesiarvosta (keskihajonta 27 %) ja valuntakertoimeksi 0,19 d^{-1}. Jos lumen vesiarvo on 150 mm, on painannevaraston suuruus 81 mm. Jälkimmäinen mallintamistapa oli laskentatulosten mukaan parempi ja sen kuvaus lähempänä todellista prosessia.

5. Lumen alueellisen peittävyyden laskenta paransi mallien tuloksia. Loimijoella vesistömallin hyvyysluku laski verifiointijaksolla arvosta 0,768 arvoon 0,759, kun lumen alueellista jakaumaa ei kuvattu mallissa. Lumen peittävyys laskettiin kumulatiivisen sulannan funktiona. Edelleen lumimallia kehitettiin laskemalla lumen peittävyys erikseen metsälle ja aukealle (pellot,avosuot,metsänaukot). Tämä paransi tuloksia selvästi Loimijoen vesistöalueella. R^2 kasvoi arvosta 0,768 arvoon 0,780 virtaamaa vastaan verifioitaessa ja arvosta 0,667 arvoon 0,837 lumihavaintoja vastaan verifioitaessa.

Erityisesti tulokset paranivat keväinä, jolloin sulanta tapahtui kahden tai useamman jakson aikana. Tällöin ensimmäisen sulantajakson aikana lumi suli aukeilta usein jo kokonaan, mutta metsään jäi runsaasti lunta. Loimijoen alueella kokeiltiin lumen alueellisen jakauman laskemista 2-parametrisella gamma-jakaumalla. Simulointitulokset olivat yhtä hyviä kuin simuloimalla aukealla ja metsässä tapahtuvaa sulantaa erikseen.

6. Simulointitulokset eivät parantuneet, vaikka malliin otettiin mukaan sulaneen lumen uudelleen jäätyminen kylmän jakson aikana. Samoin tulokset eivät parantuneet, vaikka käytettiin eri astepäivätekijän arvoja laskettaessa sulantaa vesisateen ja lumisateen aikana.

Kaikkien yllä lueteltujen prosessien liittäminen

lumimalliin yksi kerrallaan ei aina parantanut tuloksia mainittavasti. Kun kaikki prosessit liitettiin lumimalliin, olivat laskentatulokset parempia kuin peruslumimallilla saadut tulokset. Verifiointijaksolla Tujuojan mallin hyvyysluku R^2 virtaamaa vastaan oli 0,730/0,717, kun kaikki kohtien 1—6 muutokset olivat mukana, ja 0,586/0,613 ilman muutoksia. Loimijoella R^2-arvot olivat parhaalla kehitetyllä mallilla 0,780 ja mallilla ilman muutoksia 0,763. Kalibrointijaksoa käytetään mallin sovittamiseen havaintojen perusteella ko. vesistöalueelle. Verifiointijaksoa käytetään, kun arvioidaan kalibroidun mallin todellista kykyä simuloida vesistön tapahtumia. Kalibrointi- ja verifiointijakso ovat ajallisesti eri jaksot.

Lämpötilaindeksimallin ja energiatasemallin yhdistäminen

Lämpötilaindeksimallin kehittäminen energiatasemalliksi aloitettiin lisäämällä energiatasemallin osamalleja parhaaksi osoittautuneeseen lämpötilaindeksimalliin. Lyhyt- ja pitkäaaltoinen säteily, latentin ja havaittavan lämmön vuo, vesisateen tuoma energia ja lämpövuo maakerroksista liitettiin lämpötilaindeksimalliin osamalleina. Myös lumen kylmäsisällön mallintamisen vaikutusta kokeiltiin mallin simulointituloksiin. Energiatasetermien liittäminen lämpötilaindeksimalliin ei parantanut tuloksia merkittävästi. Loimijoella testatun lämpötilaindeksi- ja energiatasemallin yhdistelmän mukaan latentin lämmön vuon tuoma energia muodostuu sulannan merkittäväksi energialähteeksi tuulisella säällä, kun myös ilmankosteus on suuri. Saman mallin mukaan lyhytaaltoisen säteilyn tuoma energia on suurin sulamisen energialähde pilvettömänä ja tyynenä kevätpäivänä. Loimijoella 55 % alueesta on aukeata peltoa ja suota. Tujuojan alueella, missä vain 18 % on aukeata, astepäivätekijän perusteella laskettu sulanta oli aina kokonaissulannan merkittävin tekijä. Muita menetelmiä, joilla lämpötilaindeksimallia yritettiin parantaa olivat astepäivätuntien käyttö; päivittäisen lämpötilavaihtelun käyttö lyhytaaltosen säteilyn kuvaamiseen; vuorokauden keskilämpötilan laskenta painottaen enemmän lämpötilan maksimiarvoja silloin, kun lämpötila laskee alle nolla-asteen. Mikään näistä lämpötilaindeksimallin muunnoksista ei kuitenkaan parantanut laskentatuloksia.

Lumen sulannan energiatasemalli

Lumen energiatasemallia, joka simuloi lyhyt- ja pitkäaaltoista säteilyä, latentin ja havaittavan lämmön vuota, vesisateen mukana ja maaperästä tulevan lämmön vuota sekä lumen kylmäsisältöä, kokeiltiin Tujuojan ja Loimijoen vesistömalleissa. Molemmilla alueilla energiatasemallin tulokset olivat huonompia kuin parhaan lämpötilaindeksimallin tulokset.

Lyhytaaltoisen nettosäteilyn simuloinnin tarkentamiseksi kehitettiin fysikaalinen lumimalli, joka simuloi lumen tiheyttä, syvyyttä, veden pidätyskykyä ja lumen albedoa. Albedo laskettiin lumen tiheyden ja syvyyden funktiona. Tämä malliversio paransi energiatasemallin tulokset parhaan lämpötilaindeksimallin tasolle. Loimijoella tällä mallilla saatiin hyvyysluvun R^2 arvoksi 0,758 laskentatuloksia virtaamahavaintoihin verrattaessa ja 0,833 lumihavaintoihin verrattaessa. Parhaan lämpötilaindeksimallin vastaavat hyvyysluvut olivat 0,780 ja 0,837.

Tujuojan valuma-alueella energiatasemallin hyvyysluku oli vain 0,710 valuntahavaintoja vastaan parhaalla energiatasemallilla, kun paras lämpötilaindeksimallin R^2-arvo oli 0,737. Fysikaalisen lumimallin kyky simuloida lumen tiheyttä ja syvyyttä osoittautui hyväksi ja lumimallia voidaan käyttää mm. vesistöalueen tiheyden seurantaa reaaliajassa. Malli vaatii lähtötiedoiksi pilvisyyden, lämpötilan ja sadannan.

Fysikaaliset lumimallit antavat tietoa sulannan energialähteiden suhteista eri vuodenaikoina. Nämä tiedot ovat hyödyllisiä lumen sulannan taustatietona kehitettäessä yksinkertaisempia lumimalleja. Latentin ja havaittavan lämmön vuot ovat tärkeimmät energiataseen termit syyskuusta tammikuuhun. Termien yhteenlaskettu osuus sulannan käyttämästä energiasta on 40—70 % Tujuojan alueella ja 70—90 % Loimijoen alueella. Loimijoen alueen suurempi aukeiden alueiden määrä näkyy tuloksissa. Keväällä lyhytaaltoisen säteilyn osuus kasvaa voimakkasti ja ylittää maaliskuussa 50 % molemmilla alueilla. Lyhytaaltoinen nettosäteily saavuttaa suurimmat arvonsa huhtikuun aikana. Tällöin sen osuus sulamiseen kuluvasta energiasta on 85 % Tujuojalla ja 69 % Loimijoella. Samaan aikaan havaittavan ja latentin lämmön vuon yhteisosuus pienee 10 %:iin Tujuojalla ja 15 %:iin Loimijoella. Huhtikuussa latentin lämmön vuo on pääasiassa negatiivinen eli lumipeitteestä haihtuu vettä ilmakehään. Haihdunta on mallilaskelmien perusteella Loimijoella 4,0 mm kuukaudessa ja Tujuojalla 3,1 mm kuukaudessa. Tiivistyntä on vallitsevana syksyllä ja keskitalvella. Se on keskimäärin vain 0,1—0,5 mm kuukaudessa. Vesisateen tuoma energia on keskimäärin 0—10 % sulamiseen kuluvasta energiasta.

Roudan vaikutus valuntaan

Tutkimuksessa kehitettiin myös yksinkertainen routamalli, jota voidaan käyttää valuntamallin yh-

teydessä. Routamalli toimii valuntamallin syöttötiedoilla, jotka ovat vuorokauden sadanta ja keskilämpötila. Roudan vaikutus valuntaan otettiin huomioon laskemalla tiettyjen valuntaan vaikuttavien parametrien arvot roudan syvyyden funktiona. Muunneltavat parametrit valittiin kirjallisuudesta saatujen tietojen perusteella. Merkittävää roudan vaikutusta valuntaan ei saatu esille Tujuojan pienellä valuma-alueella, jossa moreeni oli vallitseva maaperätyyppi. Tujuojalla saatujen tulosten mukaan maaperän infiltraatiokyky ei pienene merkittävästi roudan vaikutuksesta metsäisillä moreenimailla. Loimijoella routamallia ei kokeiltu.

Lumimallin ja valuntamallin keskinäinen riippuvuus

Paras lumimalli ja sen parametrit ovat riippuvaisia käytetystä valuntamallista. Tämä lumimallien ja valuntamallien riippuvuus toisistaan oli keskeinen tulos myös WMO:n järjestämässä erityyppisten sulanta-valuntamallien vertailussa (WMO 1986). Nyt tässä tutkimuksessa lumi- ja valuntamallin keskinäistä riippuvuutta pyrittiin vähentämään kalibroimalla ja verifioimalla lumimallit lumihavaintojen avulla. Lumihavaintoja oli kuitenkin vähän lumen sulantakaudelta. Sen vuoksi sulantaan vaikuttavat parametrit kalibroitiin havaitun virtaaman/vedenkorkeuden eli vesitaseen avulla. Talvella lumihavaintoja on riittävästi. Paras verifiointitulos sekä virtaama- että lumihavaintojen mukaan saatiin samalla vesistö-lumimallikokonaisuudella.

Lumen alueellisen vesiarvon laskenta

Kehitetyn lämpötilaindeksimallin käyttökelpoisuutta ja tarkkuutta lumen alueellisen vesiarvon laskennassa testattiin suurilla vesistöalueilla. Loimijoella ja 39:llä eri vesistöjen osavaluma-alueilla tehtyjen kalibrointien keskimääräinen hyvyysluku oli 0,90. Kalibrointijaksot olivat 5—10 vuotta. Hyvyysluvun arvo 1,00 vastaa täydellistä mallia: havainnot ja lasketut arvot ovat samat. Voidaankin todeta, että vesistömallien lumimallit ovat taloudellinen ja tarkka menetelmä arvioida lumen alueellista vesiarvoa suurilla vesistöalueilla. Käsitystä tukevat myös noin viiden vuoden ajan ennustekäytössä olleet vesistömallit. Selvästi virheellisiä tuloksia esiintyi alle 10 prosentilla lasketuista osavaluma-alueista. Kevään lyhyenä sulantakautena lumen mittaus maastossa on epätarkkaa lumipeitteen suuren vaihtelevuuden takia eikä mittaustuloksia ole useinkaan käytettävissä. Tällöin lumimallilla lasketut alueelliset vesiarvot ovat suureksi avuksi käyttäjille.

Laskennan aikajakso on tärkein lumilaskennan tulosten laatuun vaikuttava tekijä. Päivittäiset aluesadantahavainnot ovat talvella tuulisissa oloissa virheellisiä. Havaintovirhe voi olla jopa 50 %. Kun tarkasteltava aikajakso pitenee kuukausiin ja sadeasemien määrä vesistöalueilla lisääntyy sekä alueen koko kasvaa, pienenee aluesadannan ja lumen vesiarvon määritysvirhe keskimäärin alle 10 %:iin. Vesistömallien lumen vesiarvon laskennassa tyypillinen aikajakso on 4—5 kuukautta. Lumen alueellisen vesiarvon määritystarkkuus paranee sadeasematiheyden ja vesistöalueen koon kasvaessa. Sadeasematiheys oli tarkastelluilla alueilla yksi asema 465 km^2:ä kohti. Sadeasemien määrä vesistöaluetta kohti oli keskimäärin 9 asemaa ja vesistöalueiden keskikoko 7 000 km^2.

Kokemukset operatiivisesta lumen vesiarvon laskennasta ovat olleet yhtä hyvät sekä Etelä- että Pohjois-Suomessa. Olennaista on tarkistaa vesistömallin lumilaskenta virtaama- ja vedenkorkeushavaintojen eli vesitaseen avulla. Näin saadaan korjattua suurin osa lumen vesiarvon laskennassa syntyneistä virheistä ja ne voidaan korjata ennen ennusteajoja. Korjaus tapahtuu muuttamalla lumilaskentaa siten, että havaitut ja lasketut virtaamat ja vedenkorkeudet ovat samat, jolloin myös lumilaskenta vastaa paremmin todellisuutta.

Tutkimuksessa kehitetyllä fysikaalisella lumimallilla voidaan lumen vesiarvon lisäksi laskea lumipeitteen tiheys ja syvyys, koska mallin lähtötietoina tarvitaan vain vuorokauden sadanta- ja sulantatiedot.

Vesistöennusteet

Työssä kehitetty lämpötilaindeksimalli on paras vesistöalueiden lumilaskentaan soveltuva malli erityisesti, jos otetaan huomioon fysikaalisen lumimallin suurempi havaintojen tarve. Kaikki vesistömallit, joita Suomessa käytetään ennustamiseen, käyttävät lämpötilaindeksimallia lumilaskennassa.

Kuten edellä todettiin, korjataan vesistömallin laskentaa siten, että virtaaman/vedenkorkeuden laskentatulokset ja havainnot vastaavat toisiaan. Jos mallin virhettä ei saada näin korjatuksi, voidaan ennusteiden korjaukseen käyttää autoregressiivisiä (AR, ARMA) virhemalleja. Näiden mallien avulla otetaan ennusteessa huomioon aiemmin laskennassa tehty virhe. Virhemallit auttavat vain 2—5 päivää eteenpäin, minkä jälkeen alkuperäinen vesistömallin ennuste ja virhemallilla korjattu ennuste ovat samat. Virhemallien käyttö vaatii onnistuakseen hyvät reaaliaikaiset havainnot vesistöstä. Niitä saadaan automaattisten havaintoasemien välityksellä. Vesistömalleja on käytetty myös arvioitaessa il-

mastonmuutoksen vaikutuksia vesistöjen virtaamiin, vedenkorkeuksiin ja lumioloihin. Esimerkkinä näistä laskelmista voidaan käyttää GISS-ilmastomallin skenaariota, jossa lämpötila nousisi 5—6 °C talvella ja 2—4 °C kesällä, kuukausisadannat kasvaisivat 11—13 mm talvella ja 20—30 mm kesällä sekä haihdunta kasvaisi 1—3 mm talvella ja 20—30 mm kesällä. Tällöin oikea lumitalvi jäisi lähes kokonaan pois Etelä-Suomesta ja Pohjois-Suomessakin talvikuukausia olisivat vain helmi- ja maaliskuu. Tämän seurauksena talvialivirtaamat kasvaisivat 20—90 %. Kasvu olisi Pohjois-Suomessa suurempi kuin Etelä-Suomessa. Etelä-Suomessa lumen sulamisen aiheuttamat kevättulvat jäisivät pois ja syystulvat saattaisivat kasvaa. Pohjois-Suomessa lumen sulamisen aiheuttamat kevättulvat säilyisivät, mutta pienenisivät.

Loppupäätelmät

Kuten tutkimuksesta käy ilmi, lumimalleja voidaan kehittää monin eri tavoin, kun tavoitteena on vesistöalueiden lumilaskennan parantaminen. Sama asia kävi ilmi myös WMO:n järjestämässä operatiivisten lumimallien kansainvälisessä vertailussa vuonna 1986, missä testattiin hyvin erilaisia lumimalleja. Lähes kaikki lumimallit toimivat operatiivisen käytön kannalta riittävän hyvin.

Tämän tutkimuksen kaksi lumimallien pääkehityssuuntaa olivat lämpötilaindeksimallit ja lumen energiataseeseen perustuvat mallit. Suurille vesistöalueille kehitetty lämpötilaindeksimalli, jossa otettiin huomioon lumen alueellinen jakauma, osoittautui paremmaksi näistä kahdesta vaihtoehdosta. Lumilaskennan onnistumisen kannalta on tärkeää tietää, missä lunta on eli tuntea lumen alueellinen jakauma. Lumen sulannan laskenta on helpompi tehtävä. Näin on erityisesti keväällä sulannan loppuvaihessa.

LIST OF SYMBOLS

A = cross-sectional area (m^2), Eq. 18
a = the angle of the radiation with the horizontal
a_S = parameter in Eq. 102 and 103
AC = the activation energy of the snow, $4\ 10^4$ J mol^{-1}, Eq. 118
AL = the albedo of snowpack (0.4—0.9)
ALP = LP
AMIN = lower limit for the snow covered area SA (0.01—0.10), App. 6
B = coefficient of non-uniform velocity distribution, Eq. 18
b = storage width (m), Eq. 18
b_S = parameter in Eq. 102 and 103
C_{al} = parameter in Eq. 77
C_a = specific heat of air (kJ kg^{-1} $°C^{-1}$)
C_i = specific heat of ice (kJ kg^{-1} $°C^{-1}$)
C_L = parameter in Eq. 85
C_s = specific heat of snow (2 kJ kg^{-1} $°C^{-1}$)
C_v = specific heat of water vapor (kJ kg^{-1} $°C^{-1}$)
C_v = the coefficient of variation of the areal snow water equivalent, Chapter 6.3
C_w = specific heat of water (kJ kg^{-1} $°C^{-1}$)
C_1 = $1/n_c$, Eq. 117
C_2 = parameter in Eq. 116
C_3 = AC/R T T_c, Eq. 119
c_L = parameter in Eq. 103
c_S = parameter in Eq. 102 and 103
CC = parameter in Eq. 31
CD = canopy density, in per cent
CD_f = effective forest canopy density for long-wave radiation, in per cent
CF = forest transmission coefficient
CF1 = forest transmission coefficient with 100 per cent canopy density
CL = cloudiness (0—1)
CLAT = bulk transfer coefficient for latent heat exchange (kJ $(m^3 mb^{-1})^{-1}$)
CL1 = cloudiness of the lower clouds (0—1)
CMAX = liquid water retention capacity of snow at the beginning of snowmelt, percentage of weight: 0.10—0.30
CMIN = liquid water retention capacity of snow at the end of the melt period as the percentage of weight
CO = cold content of snowpack (J cm^{-2})
CPL = total correction constant for liquid precipitation (1.00—1.10)
CPLU = wind correction constant for liquid precipitation
CPS = total correction constant for solid precipitation (1.10—1.40)
CPSU = wind correction constant for solid precipitation
CS = parameter in Eq. 71
CSEN = bulk transfer coefficient for sensible heat exchange (kJ m^{-3} $°C^{-1}$)

CV1 = parameter in Eq. 39
CV2 = parameter in Eq. 39
CV3 = parameter in Eq. 40
CV4 = parameter in Eq. 40
CV5 = parameter in Eq. 39, 40
D = volume density of soil (m^3/m^3) in Eq. 137
d = declination
D_a = air density (kg m^{-3})
D_i = density of ice (kg m^{-3})
D_p = density of new snow (kg m^{-3})
D_s = density of snow (kg m^{-3})
D_v = density of water vapor (kg m^{-3})
D_w = density of water (kg m^{-3})
DP = the part of the day when temperature is over 0°C
e = exponent in Eq. 28
E_a = atmospheric emissivity for long-wave radiation (0.70—0.90)
E_{ff} = emissivity of the forest for long-wave radiation, Eq. 87
e_a = vapor pressure in air (mb)
eal = exponent in Eq. 46
E_s = emissivity of snow surface for long-wave radiation (0.97—1.00)
EKM = parameter in Eq. 48
e_s = saturation vapor pressure at the melting snow surface (mb)
ESC = evaporation from snow (mm d^{-1})
exs = exponent in Eq. 35
F = amount of liquid water frozen into ice in snowpack (mm)
F^2 = the sum of squares of residuals, Eq. 21
F_o^2 = defined in Eq. 20
f = latitude
FM = degree-day value for refreezing (mm °C^{-1} d^{-1}), Eq. 28
FMH = degree-hour value for refreezing (mm °C h^{-1}), Eq. 67
g = acceleration due to gravity (9.81 m s^{-1})
GM = snowmelt due to heat from the ground (mm d^{-1})
H = depth of snow (cm)
H_a = depth of the active soil layer in soil moisture formation, Eq. 139 (cm)
H_f = soil frost depth (cm)
H_{lim} = threshold value for snow depth Eq. 78 (cm)
H_m = depth of thawing soil, Chapter 9 (cm)
H_s = snow cover depth (cm)
H_w = depth of the layer of unfrozen ground above ground water level (cm)
h = sun's hour angle
H_+ = the sum of positive degree-hours during a day and night (°C)
H_- = the sum of negative degree-hours during a day and night (°C)
HA = actual evaporation (mm d^{-1})
HP = potential evaporation (mm per time unit)
HV = latent heat of vaporization (2 830 kJ kg^{-1} from the snow surface below 0°C, 2 500 kJ kg^{-1} from melting snow surface)
ICE = frozen water in soil, Chapter 9 (mm)
k = von Karman's constant (0.4)
k = thermal conductivity in Chapter 9 (J °C^{-1} cm^{-1} s^{-1})
k_g = thermal conductivity of surface ground (J °C^{-1} cm^{-1} s^{-1})
K_e = eddy diffusivity of latent energy transfer ($m^2 s^{-1}$)
K_h = eddy diffusivity for convective energy transfer (m^2 s^{-1})
KC = parameter in Eq. 29 for calculation of the degree-day value
K_m = eddy diffusivity for momentum ($m^2 s^{-1}$)
KLT = parameter in Eq. 60
KM = degree-day value (mm°C d^{-1})
KMAX = degree-day value at the end of the snowmelt period (mm °C^{-1} d^{-1})
KMH = degree-hour value for snowmelt (mm°C h^{-1})
KMIN = the initial degree-day value for snowmelt (mm°C d^{-1})
KST = parameter in Eq. 58
KST2 = parameter in Eq. 59
L = the latent heat of fusion of ice (334 J g^{-1})
LH = parameter in Eq. 45
LS = parameter in Eq. 36
LS2 = parameter in Eq. 38
LP = soil moisture threshold value after which actual evaporation equals potential evaporation (mm)
M = surface snowmelt (mm per time unit)
n = viscosity coefficient for snow (cm h)
n_c = hypothetical viscosity coefficient with zero density (cm h), Eq. 116
n_o = the viscosity coefficient at temperature of 0°C (cm h), Eq. 118
P = depth of precipitation (mm d^{-1})

P_{lim} = precipitation threshold value for rain-melt simulation, Eq. 42 (mm)
PKM = degree-day factor for melt due to heat in liquid precipitation Eq. 41 (mm $mm^{-1}\,°C^{-1}$)
PKM2 = degree-day factor during rainfall ($mm°C^{-1}d^{-1}$)
PL = liquid precipitation (mm)
PLIM = threshold value of precipitation Eq. 42 (mm)
PM = melt due to heat in liquid precipitation (mm $mm^{-1}°C^{-1}d^{-1}$)
PS = solid precipitation (mm)
Q = discharge (m^3s^{-1})
Q = latent heat loss in soil frost formation, Chapter 9
q = lateral inflow ($m^2\,s^{-1}$), Eq. 18
q = heat flux through the snow or soil layer ($J\,s^{-1}$), Chapters 8,9
R = the gas constant, about 8 $J\,mol^{-1}K^{-1}$
R_i = ice concentration of snow in volumetric units (m^3m^{-3})
R_w = water concentration of snow in volumetric units (m^3m^{-3})
R_{wm} = maximum water concentration of snow in volumetric units (m^3m^{-3})
RG = heat exchange at the ground surface ($J\,cm^{-2}s^{-1}$)
RLAT = latent heat exchange ($J\,cm^{-2}s^{-1}$)
RLD = downward long-wave radiation ($J\,cm^{-2}s^{-1}$)
RLN = long-wave radiation balance ($J\,cm^{-2}s^{-1}$)
RLT = effect of long-wave radiation on melt Eq. 60
RLU = upward long-wave radiation ($J\,cm^{-2}s^{-1}$)
RLUE = upward long-wave radiation due to snow emission ($J\,cm^{-2}s^{-1}$)
RLUR = upward long-wave radiation due to snow reflection ($J\,cm^{-2}s^{-1}$)
RKM = parameter in Eq. 44
RP = heat content of liquid precipitation
RS = incoming short-wave radiation ($J\,cm^{-2}s^{-1}$)
RS_f = incoming short-wave radiation through forest ($J\,cm^{-2}s^{-1}$)
RS_i = direct solar radiation above clouds incident upon a horizontal surface ($J\,cm^{-2}s^{-1}$)
RSB = transmitted short-wave radiation in snow ($J\,cm^{-2}s^{-1}$)
RSEN = sensible heat exchange ($J\,cm^{-2}s^{-1}$)
RSN = net short-wave radiation for snowpack ($J\,cm^{-2}s^{-1}$)
RSN2 = short-wave radiation balance ($J\,cm^{-2}s^{-1}$)
RSR = reflected short-wave radiation ($J\,cm^{-2}s^{-1}$)
RST = melt due to short-wave radiation calculated with the temperature difference, Eq. 58 (mm per time unit)
RST2 = short-wave melt calculated with the temperature difference, Eq. 59 (mm per time unit)
R^2 = the efficiency of model performance, Eq. 20
S_f = friction slope, Eq. 18
SA = snow covered area (0—1)
SF = Stefan-Boltzmann constant ($3.40\ 10^{-11}$ $J\,cm^{-2}\,min^{-1}\,K^{-1}$)
SD = snow density ($g\,cm^{-3}$)
SLR = solar constant ($J\,cm^{-2}\,min^{-1}$)
SLR2 = parameter in Eq. 69
SM = cumulative snowmelt (mm)
t = time
T = air temperature (°C)
T = temperature (°C) in Chapter 9
T_b = temperature of the bulk of snowpack (°C)
T_c = 0°C in Kelvin degrees: 273 K
T_f = temperature at the bottom of the frozen soil layer (°C)
T_g = ground surface temperature (°C)
T_K = absolute temperature (K)
T_p = temperature of precipitation (°C)
T_{pot} = potential temperature Eq. 89 (°C)
T_s = snow surface temperature (°C)
T_w = temperature at the groundwater surface (°C)
TF = threshold air temperature for refreezing
TM = threshold air temperature for snowmelt (°C)
TL = threshold air temperature for liquid precipitation (°C)
TR = parameter in Eq. 44
TR2 = parameter in Eq. 45
TS = threshold air temperature for solid precipitation (°C)
U = wind velocity ($m\,s^{-1}$)
UKM = parameter in Eq. 47
W = water equivalent of snow (mm)

w = soil moisture in volumetric units ($m^3 m^{-3}$), Chapter 9
w_p = soil moisture in per cent of weight, Chapter 9, Eq. 137
w_l = unfrozen water in frozen soil ($m^3 m^{-3}$), Chapter 9
WH = water retention capacity of snow, percentage from weight
WHL = water retention capacity of snow, percentage of volume
WMAX = maximum water equivalent of snow (mm)
WS = liquid water in snowpack (mm)
WQ = water yield from the snow cover (mm per time unit)
x = longitudinal space co-ordinate in the horizontal plane, Eq. 18
y = water surface elevation above datum (m)
z = depth of snow in Chapter 7 or soil in Chapter 9 (cm)
z, z_1, z_2 = measurement height (m)

REFERENCES

Abels, H. 1892. Beobachtungen der täglichen Periode der Temperatur im Schnee und Bestimmung des Wärmeleitungvermögens des Schnees als Function seiner Dichtigkeit. Rep. Meteorol. Bd. XVI, No. 1, p. 1—53.

Ahti, K. 1974. Sade- ja lumihavainto-ohjeet. Ilmatieteen laitos.

Allerup, P. & Madsen, M. 1980. Accuracy of point precipitation measurements. Nordic Hydrology, 11, 1980, p. 57—70.

Anderson, E. A. 1973. National Weather Service Forecast System-Snow Accumulation and Ablation model. NOAA Technical Memorandum NWS HYDRO-17, U.S. Dept. of Commerce, Silver Spring, MD, 217 p.

Anderson, E. A. 1976. A point energy and mass balance model of a snowcover. NOAA Tech. Rep. NWS-19, U.S. Dept. Commer., Washington, D.C.

Arner, E. 1991. Simulering av vårflöden med HBV-modellen. SMHI Hydrologi nr. 32.

Baumgartner, A. 1967. Energetic bases for differential vaporization from forest and agricultural land. Proc. Int. Symp. Forest Hydrol., p. 381—390. Pergamon Press.

Belchikov, V. A. and Koren, V. I. 1979. Model of the formation of direct runoff for wooded drainage basins. Soviet Hydrology: Selected Papers. Vol. 18, No. 3, 1979.

Beltaos, S. 1983. Guidelines for extraction of ice-breakup data from hydrometric station records. National Water Research Institute. Canada Center for Inland Waters.

Bengtsson, L. 1980. Evaporation from a Snow cover. Nordic Hydrology, 11, p. 221—234.

Bengtsson, L. 1982. The importance of refreezing on the diurnal snowmelt cycle. Nordic Hydrology, 13(1), p. 1—12.

Bengtsson, L. 1986. Snowmelt simulation models in relation to space and time. Modelling Snowmelt-Induced Processes. IAHS Publication no. 155. Budapest.

Bergström, S. 1975. Development of a snow routine for the HBV-2 model. Nordic Hydrology, 2, p. 73—92.

Bergström, S. 1976. Development and application of a conceptual runoff model for Scandinavian catchments. SMHI. Nr RH7. Norrköping.

Bergström, S. 1990. Parametervärden för HBV-modellen i Sverige. SMHI Hydrologi. Nr 29, 1990.

Bergström, S. & Brandt, M. 1984. Snömätningar med flygburen gammaspektrometer i Kultsjöns avrinningsområde. SMHI, HO rapport 21, Norrköping.

Braun, N.L. 1985. The simulation of Snowmelt-Runoff in Lowland and Lower Alpine regions of Switzerland. Züricher Geographische Schriften no 21. Geographisches Institut. Zürich.

Brechtel, H. 1984. Möglichkeiten und Grenzen einer Steuerung der Schneeansammlung und Schneeschmelze durch forstliche Massnahmen.Schneehydrologische Forschung in Mitteleuropa. Mitteilungen des Deutschen Verbandes für Wasser wirtschaft und Kulturbau e.V.Heft 7. Bonn.

Brooks, F.A. 1959. An introduction to physical microclimatology.264 p. illus. Davis,Calif.: Assoc. Students Store.

Brunt, D. 1952. Physical and Dynamical Meteorology. Cambridge Univ. Press, Cambridge, Mass.

Dunkle, R.V., Gier, J.T., Shimazaki, T.T. & Possner, L. 1949. Non-Selective Radiometers for Hemispherical Irradiation and Net Radiation Interchange Measurements. Univ. Calif. Dept. Engin., Thermal Radiation Proj. 9, Calif.

Eagleson, P.S. 1970. Dynamic Hydrology. McGraw-Hill. New York.

Engelmark, H. 1986. Infiltration and runoff during the period of snow melt (English Summary). Division of Water Resources Engineering (WREL). Rapport Serie A nr 145. Luleå, Sweden.

Erbel, K. 1969. Ein Beitrag zur Untersuchung der Metamorphose von Mittelgebirsschneedecken unter besonderer Berücksich tung eines Verfarens zur Bestimmung der thermischen Schneequalitet. Mitt. aus dem Inst. für Wasserwirtschaft, Grundbau aun Wasserbau der Univ. Stuttgart, Heft 12. 251 p.

Fitzgibbon, J. & Dunne, T. 1980. Snowmelt prediction in a subarctic drainage area. Nordic Hydrology 11, 4, p. 243—254.

Forsius, J. 1984. Computing unsteady flow and tracer movement in a river. Publications of the Water Research Institute, National Board of Waters. Finland.

Forsius, J. 1988. Predicting River Ice Breakup Using Hydrometric Station Records. 7th Northern Research Basins Symposium, Illulissat, Greenland, 25 May — 1 June 1988.

Forsius, J. & Granholm, G. 1988. Statistical Model for Predicting of Ice Breakup in River Torneälven. Proceedings of the Nordic Expert Meeting on River Ice, Espoo 2—4 November 1987, NHP-Report No 21, Helsinki.

Gates, D.M. 1965. Energy, plants and ecology. Ecol. 46, p. 421—13.

Gardelin, M. & Bergström, S. 1987. Snötaxering och hydrologiska prognoser — ett diskussionsinlägg. Vannet i Norden Nr 3—1987.

Geiger, R. 1961. Das Klima der bodennahen Luftschicht (The Climate Near the Ground). (English Transl. by Scripta Technica Inc., Harvard University Press, Cambridge, Mass.)

Goodison, B.E. 1978. Comparability of snowfall and snowcover in Southern Ontario basin. Proc., Modelling Snow Cover Runoff (S. C. Colbeck and M. Ray eds.), U.S. Army Cold Reg. Res. Eng. Lab., Hanover, N. H., p. 34—43.

Gushchina, M.V., Kagan, R.L. & Polishchuch, A.I. 1967. Accuracy in determining the mean precipitation depth over an area. Trudy GGO. No 208, Trans. in Soviet Hydrology. Selected Papers. Issue no 6, 1967, p. 49—63.

Gurevich, M.I. 1950. Dependence of the snow melting rate on air temperature. Meteorology and Hydrology (Meteorologiya i gidrologiya), No. 3, p. 44—48.

Gürer, I. 1973. Long term forecasting of seasonal inflows to Kemihaara artificial lake. National Board of Waters Report 50. 82 p.

Gürer, I. 1974. Pielisen eri vuodenaikojen tulovesimäärien ennustaminen. Summary: Long term forecasting of seasonal inflows to Lake Pielinen. Vesitalous 3, p. 10—16.

Gürer, I. 1975. Hydrometeorological and water balance studies in Finland. Helsinki University of Technology. Research Papers 49.

Hankimo, J. 1976. Sateen olomuodon prediktoreista. Ilmatieteen laitos, tutkimusseloste 57.

Hatfield, J.L., Reginato, R.J. & Idso, S.B. 1983. Comparison of Long-Wave Radiation Calculation Methods Over the United States. Water Resources Research, Vol. 19, No. 1. p. 285—288.

Harstveit, K. 1984. Snowmelt modelling and energy exchange between the atmosphere and a melting snow cover. Geophysical Institute, Meteorological Division, University of Bergen. Scientific Report no 4.

Heino, R. & Hellsten, E. 1983. Climatological statistics in Finland 1961—1980. Supplement to the meteorological yearbook of Finland. Volume 80 part 1a-1980. Helsinki.

Hooli, J. 1973. Korkeussuhteiden ja viettosuunnan vaikutuksesta lumipeitteen vesiarvoon Lapin tuntureilla ja vaaroilla talvella 1971/72 suoritettujen mittausten valossa. helsingin teknillinen korkeakoulu, tieteellisiä julkaisuja 43. 67 p.

Hiitiö, M. 1982. Lumen sulannasta ja sen aiheuttaman valunnan arvioinnista. Diplomityö, Teknillinen korkeakoulu, rakennusinsinööriosasto. English summary. 96 p.

Huovila, S. 1971. Inversiotutkimuksia Lapissa. Geofysiikan Seura, Helsinki, p. 57—65.

Hydrologiset havainto- ja mittausmenetelmät. 1984. Publications of The National Board of Waters 47. Helsinki.

Jansson, P-E. & Halldin, S. 1980. Soil water and heat model. Tecknical description. Technical Report 26, Swedish Coniferous Forest Project, Uppsala, Sweden.

Kaila, M. 1977. Hydrologiset ennusteet Saimaan säännöstelyä varten. Summary: The forecasting of inflow into Lake Saimaa. Helsinki Univ. of Technology Dept. of Civil Engineering. 191 p.

Kaitera, P. 1939. Lumen kevätsulamisesta ja sen vaikutuksesta vesiväylien purkautumissuhteisiin Suomessa. Maataloushallituksen kulttuuriteknillisiä tutkimuksia. No 2. Helsinki.

Kaitera, P. 1949. On the melting of snow in springtime and its influence on the discharge maximum in streams and rivers in Finland. Scientific Researches of Helsinki University of Technology 1, p. 75—98.

Kaitera, P. & Teräsvirta, H. 1972. Snow evaporation in South and North Finland, 1969/70 and 1970/71. Aqua Fennica 2, p. 11—19.

Karvonen, T. 1980. Sadanta-valuntamallin soveltaminen Kyrönjoen vesistösuunnitteluun. Vesihallituksen monistesarja 28. Helsinki.

Karvonen, T. 1988. A model for predicting the effect of drainage on soil moisture, soil temperature and crop yield. Helsinki University of Technology. Publications of the Laboratory of Hydrology and Water Resources Engineering. Espoo, Finland.

Killingtveit, Å. & Aam, S. 1978. En fördelt modell för snöackumulering og -avsmeltning. EFI-Institut för Vassbyggning, NTH, Trondheim, Norway.

Kojima, K. 1967. Densification of seasonal snow cover, Physics of snow and ice, Proceedings of International Conf. on Low Temperature Science, Sapporo, Vol. I, Part 2. The Institute of Low Temperature Science, Hokkaido University, Sapporo, p. 929—952.

Kondratyev, K.Ya. 1969. Radiation Energy of the Sun. Gidromet., Leningrad.

Korhonen, V. 1914a. Kaksi Suomessa v. 1912 sattunutta harvinaista ilmastollista ilmiötä. Suomalaisen tiedeakatemian toimituksia, Sarja A, 6, 2. 54 p.

Korhonen, V. 1914b. Über die Bildung der Monatsmittel der Schneehöhen. Meteorologische Zeitschrift, p. 397—399.

Korhonen, V. 1915. Die Ausdehnung und Höhe der Schneedecke. Helsinki. 199 p.

Korhonen, V. 1917. Lumisateista Suomessa. Suomalaisen tiedeakatemian esitelmät ja pöytäkirjat, Helsinki. 43 p.

Korhonen, V. 1918. Kevättulvasta ja kesäkauden sateista maanviljelysoloja silmälläpitäen. Maataloushallituksen tiedonantoja no. 123, Helsinki. 36 p.

Korhonen, V. 1923. Beobachten über die Dichte der Schneedecke in vershiedenenartigen Gelände und in verschieden Tiefen. Mitteilungen der Meteorologischen Zentralanstalt des finnischen Staates 11. 58 p.

Korhonen, V. 1926a. Über die Dichte des Neuschnees. Mitteilungen der Meteorologischen Zentralanstalt des finnischen Staates 18, 11 p.

Korhonen, V. 1926b. Untersuchungen über die Dichte und das Schmelzen der Schneedecke in Finland. Annales Academiae Scientiarum Fennicae, Serie A, 26, 3.

Korhonen, V. 1927. Linienmessungen der Höhe und Dichte der Schneedecke in Finnland. Annales Aca-

demiae Scientiarum Fennicae, Serie A, 26, 17.
Korhonen, V. 1936. Der mittlere Wassergehalt der Schneedecke in Finnland am 15. März in der Jahren 1919—34. Fünfte hydrologische Konferenz der Baltischen Staaten, Bericht 18 A. 7 p.
Kuchment, L.S., Demidov, V.N. & Motovilov, Yu.G. 1983. Formirovanie Rechnogo Stoka (River runoff formation — physically based models). Nauka, Moskva.
Kuchment, L.S., Demidov, V.N. & Motovilov, Yu.G. 1986. A physically based model of the formation of snowmelt and rainfall runoff. Modelling Snowmelt-Induced Processes. Proceedings of The Budapest Symposium July 1986. IAHS Publ. no. 155.
Kuittinen, R. & Perälä, J. 1984. Resultat av undersökningar med flygburen gammaspektrometer, som utfördes i Finland åren 1981—1984 för att utveckla operativ snötaxerings metod, NHP-rapport nr. 8.
Kuittinen, R., Autti, M., Perälä, J. & Vironmäki, J. 1985. Lumen vesiarvon määrittäminen luonnon gammasäteilyn ja satelliittikuvien avulla. Technical Research Centre of Finland. Research reports 370.
Kuittinen, R. 1988. Determination of Areal Snow Water Equivalent Using Satellite Images and Gamma Ray Spectrometry. Acta Polytechnica Scandinavica. Civil engineering and building construction series No. 91. Helsinki.
Kuusisto, E. 1973. Lumen sulamisesta ja sulamiskauden vesitaseesta Lammin Pääjärvellä 1970—72. Summary: On snowmelt and water balance during snowmelt period in Pääjärvi representative basin in 1970—72. Helsinki. Vesihallituksen tiedotus 46. 115 p.
Kuusisto, E. 1977a. Konseptuaallisten valuntamallien soveltamisesta Suomessa. Vesitalous 1, p. 16—20.
Kuusisto, E. 1977b. Suur-Saimaan vesitase ja tulovirtaaman ennustaminen. Summary: Conceptual modelling of inflow into lake Suur-Saimaa from the surrounding watersheds. Helsinki. Publ. of the Water Research Institute 26, 66 p.
Kuusisto, E. 1978. Optimal complexity of a point snowmelt model. Symposium on the Modelling of Snow Cover, Hanover, New Hampshire 26—28 September 1978, p. 205—210.
Kuusisto, E. 1980. On the values and variability of degree-day melting factor in Finland. Nordic Hydrology 11, 4, p. 235—242.
Kuusisto, E. 1981. Lumen vesiarvon vähenemisestä Suomessa. Vesitalous 2, p. 33—35.
Kuusisto, E. 1984.Snow accumulation and snowmelt in Finland. Publ. of the Water Research Institute 55. Helsinki.
Kuzmin, P.P. 1957. Fizitsheskije svojstva sneznogo pokrova (The physical properties of snow cover). Gidrometeoizdat, 179 p.
Kuzmin, P.P. 1961. Melting of snow cover. Leningrad. Israel Program for Scientific Translations. Jerusalem 1972.
Lang, H. 1984. Forecasting meltwater runoff from snow-covered areas and from glacier basins. Real-time river flow forecasting. Landbouwhogeschool. Report 6. Editor J. R. Moll. Wageningen.
Lavila, T. 1949. Lumisademäärän alueellinen jakautuminen Suomessa. Referat: Die regionale Verteilung der Schnee-niederschlagsmenge in Finnland. Turun yliopiston maantieteellisen laitoksen julkaisuja 21. 116 p.
Leavesley, G.H. 1973. A mountain watershed simulation model: Fort Collins, Colo., Colorado State University, Ph.D. dissertation.
Lemmelä, R. 1970. Lumen sulamisesta aiheutuvasta valunnasta sekä pohjaveden muodostumisesta hiekkaperäisellä alueella. Helsingin yliopisto, geofysiikan laitos. 119 p.
Lemmelä, R. 1971. Snowmelt and water yield from a snow cover. Nordic IHD Report 1, p. 80—95.
Lemmelä, R. 1972. Measurements of evaporation-condensation and melting from a snow cover. IAHS Proceedings of the Banff Symposia 1, p. 670—679.
Lemmelä, R. 1990. Water balance of a sandy aquifer at Hyrylä in southern Finland. Turun Yliopisto julkaisuja, ser. A, II. Biologica-Geographica-Geologica, 73. Turku, 340 p.
Lemmelä, R. & Kuusisto, E. 1974. Evaporation from snow cover. Hydrological Siences Bulletin 19, 4, p. 541—548.
Light, P. 1941. Analysis of high rates of snowmelting. Trans. Am. Geophys. Union, Part I, p. 195—205.
Linsley, R., Kohler, M. & Paulhus, J. 1975. Hydrology for engineers. McGraw-Hill. Second edition.
Lundberg, A. 1982. Combination of a conceptual model and an autoregressive error model for improving short time forecasting, Nordic Hydrology, Vol. 13, No. 4, p. 233—246.
Male, D.H. & Gray, D.M. 1981. Snowcover ablation and runoff. Handbook of Snow. Pergamon Press.
Malve, O. 1986. Konseptuallisten valuntamallien ja aikasarjamallien käyttö lyhytaikaisten tulvaennusteiden tekemisessä. (English abstract: The use of conceptual rainfall-runoff models and time series models in real time flood forecasting). Vesihallituksen monistesarja Nro 430. The National Board of Waters, Helsinki.
Mantis, H.T. 1951. Rewiev of the properties of snow and ice. SIPRE Report 4.
Martinec, J. 1960. The degree-day factor for snowmelt runoff forecasting. IAHS Publ. 51, p. 468—477.
Mellor, M. 1964. Properties of snow, Cold Regions Science and Engineering Monograph III-A1. Cold Regions Research and Engineering Laboratory, Hanover, N. H., 105 p.
Meteorological yearbook of Finland 1974. Vol. 74, part 1a-1974. Published by the Finnish Meteorological Institute.
Meteorological yearbook of Finland 1982. Vol. 71—1980, part 4:1. Published by the Finnish Meteorological Institute.
Monthly hydrological reports, 1963—1981. Hydrological office, Water Research Institute, National Board of Waters. Finland.
Morris, E. and Godfrey, J. 1978. The European Hydrological System snow routine. Symposium on the Modelling of Snow Cover, Hanover, New Hampshire 26—28 September 1978, p. 269—278.
Motovilov Yu.G. 1979. Simulation of Meltwater Losses through Infiltration into Soil. Soviet Hydrology: Selected Papers Vol. 18, No. 3, 1979.
Motovilov Yu.G. & Vehviläinen B. 1987. Snow cover and snowmelt runoff model in the forest zone. Proceedings of the International Soviet-Finnish Symposium in Water Research in Moscow, 1986. VYH monistesarja Nro 27. Helsinki.

Mustonen, S. 1965a. Hydrological investigations by the Board of Agriculture during the years 1957 to 1964. Soil and hydrological investigations no. 11. Helsinki.

Mustonen, S. 1965b. Ilmasto- ja maastotekijöiden vaikutuksesta lumen vesiarvoon ja roudan syvyyteen. Summary: Effect of meteorologic and terrain factors on water equivalent of snow cover and frost depth. Acta Forestalia Fennica 79.

Mustonen, S. 1965c. Meteorologisten ja aluetekijöiden vaikutuksesta valuntaan. Effects of meteorologic and basin characteristics on runoff (Enghlis abstract). Maa- ja vesiteknillisiä tutkimuksia 12. Helsinki.

Mustonen, S. & Seuna, P. 1969. Daily values of meteorological evaporation index for hydrological research basins of the Board of Agriculture in summertime during 1958...1967. Soil and hydrotechnical investigations 15.

Nash, J.E. & Sutcliffe, J.V. 1970. River flow forecasting through conceptual models. Part I — a discussion of principles. Journal of Hydrology, 10 (3).

NHP, 1986. Estimating of Areal Precipitation. NHP-Report no. 18. The Co-ordinating Commitee for Hydrology in Norden (KOHYNO).

Nisula, T. 1988. Suon vesitase keväällä. Water balance of aapamire in spring time (abstract). Diplomityö. Teknillinen korkeakoulu, Maanmittaus- ja rakennustekniikan osasto.

Obled, C. & Rosse, B. 1977. Mathematical models of a melting snowpack at an index plot. Journal of Hydrology 32, p. 139—163.

Ollila, M. 1974. Lumipeitteen vesiarvosta Lapin tuntureilla ja vaaroilla. Diplomityö. Helsingin teknillisen korkeakoulun rakennusinsinööriosasto. Espoo. 152 p.

Ollila, M. 1984. Tykyn esiintymisestä sekä korkeusaseman ja viettosuunnan vaikutuksesta lumipeitteen vesiarvoon. Helsinki University of Technology, Department of Civil Engineering, Division of Water Engineering. Report 35. Espoo. 121 p.

Perälä, J. 1971. On snow surveying in Finland. Nordic IHD Report 1, p. 24—32.

Prandtl, L. 1932. Meteorologische Anwendung der Strömungslehre. Beitr. Phys. d. freien Atmos., Vol. 19, p. 188—202.

Price, A. G. & Dunne, T., 1976. Energy Balance Computations of Snowmelt in a Subarctic Area. Water Resources Research 12, p. 686—694.

Puupponen, M., Heikkilä, H., Järvinen E., Sevola P., Vehviläinen, B. & Vuolas, E. 1990. Procol-kaukomittausjäjestelmän kehittämisohjelma 1988—89. Vesi- ja ympäristöhallituksen monistesarja, Nro 257. Helsinki.

Päivänen, J. 1973. Harvennuksen vaikutus lumi- ja routasuhteisiin nuoressa turvemaan männikössä. Summary: The effect of thinning on the snow cover and soil frost conditions in a young Scots pine stand on drained peat. Silva Fennica 7, 2, p. 114—128.

Quick, M. & Pipes, A. 1975. Nonlinear channel routing by computer. Journal of the hydraulics division. Vol. 101. No HY6.

Rapeli, P. 1971. Energiförbrukning vid snösmältning. Nordic IHD Report 1, p. 100—107.

Reifsnyder, W.E. 1965. Wind profiles in a small isolated forest stand. For. Sci. 1, p. 289—297.

Reifsnyder, W.E. & Lull, H.W. 1965. Radiant energy in relation to forests U.S.D.A. Technical Bulletin. No. 1344.

Rosenbrock, H.H. 1960. An automatic method for finding the greatest or least value of a function. Computer Journal 3.

Sand, K. 1990. Modelling snowmelt runoff process in temperate and arctic environments. Universitetet i Trondheim. Norges teknisk hogskole. IVB-rapport B-2—1990—1.

Sand, K. & Kane, D.L. 1986. Effects of seasonally frozen ground in snowmelt modelling. Proceedings of the Symposium: Cold Regions Hydrology. University of Alaska-Fairbanks, Fairbanks, Alaska. Edited by D. L. Kane. AWRA.

Schwarz, O. 1984. Schneeschmelze und Hochwasser Ergebnisse eines forstlichen Schneemessdiensten im Schwarzwald. Schnee-hydrologische Forschung in Mitteleuropa, editor Brechtel, H.-M. Deutscher Verband für Wasserwirtschaft und Kulturbau. Heft 7.

Seppänen, M. 1961a. On the influence of trees on accumulation of snow in pine dominated forest in Finland. IAHS Publication 64, p. 64—68.

Seppänen, M. 1961b. On the accumulation and the decreasing of snow in pine dominated forest in Finland: Hydrologian toimiston tiedonantoja 20. Helsinki.

Seppänen, M. 1963. On the influence of the amount of snow, slope of terrain, and position of trees on the rate of decrease of the snow in pine-dominated forest. Geophysica 8, 3, p. 213—224.

Seppänen, M. 1964. Lumen syvyyden jakautuminen pienellä alueella. Metsätaloudellinen aikakauslehti 4, p. 17—17.

Seppänen, M. 1965. Erisuuruisten metsänaukkojen lumipeitteestä. Metsätaloudellinen aikakauslehti 4, p. 1—2.

Seppänen, M. 1967. Average depth of snow in undulating land in Finland. Geophysica 9, 4, p. 277—286.

Seppänen, M. 1969a. Tarkoitukseensa sopivista lumenmittauspaikoista. Geofysiikan päivät, Oulu 18—19.6.1968, p. 102—107.

Seppänen, M. 1969b. Vesistöalueen lumipeitteen vesiarvojen ilmoittamisesta. Geofysiikan päivät, Helsinki 28—29.5.1969, p. 67—75.

Seuna, P. 1971. Om bestämning av snöns vattenekvivalent ur snömätningvärden på små hydrologiska områden. Nordic IHD Report 1, p. 33—35.

Siren, A. 1936. Bestimmungen des Wasserwertes der Schneedecke. V. Hydrologische Konferenz der Baltischen Staaten, Helsinki, Bericht 18 B. 15.

Slaughter, C.W. 1969. Snow albedo modification. A review of literature. CRREL, Technical report 217, 25 p.

Solantie, R. 1975. Talvikauden sademäärän ja maaliskuun lumensyvyyden alueellinen jakautuma Suomessa. Summary: The areal distribution of winter precipitation and snow depth in March in Finland. Ilmatieteen laitoksen tiedonantoja 28. 66 p.

Solantie, R. 1977. Valuman kevätnousun alkaminen Kyrönjoessa. Geofysiikan päivät 10—11.3. Helsinki. p. 19—28.

Solantie, R. 1978. On the variation of snow depth on 15th March in Finland. Nordic Hydrological Conference, Hanasaari, Papers of sessions II, p. 110—119.

Sucksdorff, Y. 1982. Lämpötilavaihtelut maaperän pintakerroksessa (The variation of temperature in the upper soil layers). MSc-thesis, Univ. of Helsinki, Dept. of Geophysics. 55 p.

Taivainen, L. 1952. Pohjois-Suomen tuoreiden kangasmetsien kasvillisuudesta. Referat: Über die Vegetation der frischen Heidewälder in Nordfinnland. Vanamo 25, p. 77—84.

Tulvakomitean mietintö, 1939. Komiteamietintö No 14. Helsinki.

USCE, 1956. Snow Hydrology; Summary Report of the Snow Investigations. North Pacific Division, Corps of Engineers, U.S. Army, Portland, Oregon. 437 p.

Vakkilainen, P. & Karvonen, T. 1982. Adaptive rainfall-runoff model, SATT-I. Acta Polytechnica Scandinavica. Civil Engineerig and Building Construction Series No. 81. 54 p.

Valmari, A. 1969. Havaintoja tuiskulumen kasaantumisesta sekä tummennusaineen vaikutuksesta lumen sulamiseen. Geofysiikan päivät, Oulu 18.-19.6.1968, p. 83—101.

Valmari, A. 1971. Om snömängden i olika terräng. Nordic IHD Report 1:108.

Vehviläinen, B. 1982. Valuntamallin sovellutus ennustekäyttöön Kala-, Ähtävän- ja Lapuanjoella. Vesihallituksen monistesarja, Nro 145. Helsinki.

Vehviläinen, B. 1986a. Modelling and forecasting snowmelt floods for operational forecasting in Finland. IAHS publ. no 155. Modelling Snowmelt Induced Processes.

Vehviläinen, B. 1986b. Operational spring time forecasting difficulties and improvements. Nordic Hydrology vol. 17, no. 4/5, p. 363—370.

Vehviläinen, B. 1987. Tulvan reaaliaikainen ennustaminen. Rakennustekniikka 1987. Helsinki.

Vehviläinen, B. 1989. Operational snow accumulation and snowmelt modelling. New directions for surface water modelling. Proceedings of the Baltimore symposium, May 1989. IAHS Publ. no. 181.

Vehviläinen, B. 1990. Vesistömalliennusteet keväällä 1990 ja lumen vesiarvon laskenta. Vesi- ja ympäristöhallituksen monistesarja Nro 265. Helsinki.

Vehviläinen, B. 1991. Physically Based Snowcover Model. Recent Advances in the Modelling of Hydrologic Systems. Editors: Bowles/O'Connell. NATO ASI. Kluwer Academic Publishers, the Netherlands.

Vehviläinen, B., Forsius, J., Zachrisson, G. & Häggström, M. 1988. Transboundary co-operation on flood forecasting and ice control in the river Torneälven/Tornionjoki XV Nordisk hydrologisk konferens, NHK-88. Rovaniemi 1—3 August, 1988.

Vehviläinen, B. & Kuusisto, E. 1984. The application of simple snowmelt models in three different terrain types. Proceedings of the fifth northern research basin symposium. Vierumäki Finland.

Vehviläinen, B. & Lohvansuu, J. 1991. The effects of climate change on discharges and snow cover in Finland. Hydrological Sciences Journal — des Sciences Hydrologiques, 36, 2, 4/1991.

Vehviläinen, B. & Motovilov, Yu.G. 1989. Simulation of soil frost depth and effect on runoff. Nordic Hydrology, vol. 20, p. 9—24.

Virta, J. 1987. Determination of the spring runoff for a basin with abundant lakes using a stepwise linear storage model. Aqua Fennica 17, 2, p. 115—121.

Westerberg, A. 1982. Snösmältningen i Bensbyn åren 1981 och 1982. WREL. Forskningsrapport 1982:23. Serie A Nr. 102. Luleå.

WMO/IHD, 1973. Annotated bibliograbhy on precipitation measurement instruments. WMO No 343.

WMO, 1974. Guide to hydrological practices. Third edition. WMO No. 168. Geneva.

WMO, 1982. Operational Hydrology Reports No 21. Methods of correction for systematic error in point precipitation measurement for operational use. WMO No 589.

WMO, 1986. Intercomparison of models of snowmelt runoff. Operational Hydrology. Report No. 23.

Ylinen, J. 1968. Lumen vähenemisestä keväällä sateettomina päivinä. Ilmatieteen laitos, tutkimusseloste 17. 6 p.

Yli-Vakkuri, P. 1961. Pälvien muodostumisesta metsäisessä maastossa. Summary: The formation of bare spots in the snow on woody terrains. Suomen Riista 14, p. 43—52.

Yosida, Z. 1963. Physical properties of snow. Ice and snow, W.D. Kingery, editor, the M.I.T. Press, Cambridge Mass., p. 485—527.

Appendix 1. The R^2 model performance values for operational watershed models against observed discharge and areal snow water equivalent.

Basin	R^2		Calibration period
	discharge	snow	
Säkylän Pyhäjärvi			
— Yläneenjoki	0.76	—	1976—81
— Pyhäjoki	0.75	—	1976—81
Loimijoki	0.87	0.86	1976—81
Ylä-Karvianjoki			
— Vatajankoski	0.89	0.85	1973—82
— Vahokoski	0.84	0.82	1973—82
— Kirkkojärvi	0.62	—	1973—82
— Karvianjärvi	−1.16	0.93	1973—82
Kyrönjoki Pitkämö	0.93	0.94	1973—82
— Jalasjoki	0.92	0.87	1973—82
Lapuanjoki			
— Kuorasjärvi	0.44	—	1976—81
— Hirvijärvi	0.43	—	1976—81
— Kuortane	0.72	—	1976—81
— Pappilankari	0.86	—	1976—81
Ähtävänjoki			
— Alajärvi	0.69	—	1973—81
— Lappajärvi	0.43	—	1973—81
— Evijärvi	0.43	—	1973—81
Perhonjoki			
— Venetjärvi	−12.8	0.90	1973—81
— Tunkkari	0.75	0.91	1973—81
— Ullavanjoki	0.72	0.89	1973—81
— Pelo	0.93	0.88	1973—81
Kalajoki			
— Reis-Vuohtojärvi	0.75	—	1976—81
— Hautaperä	0.84	—	1976—81
— Settijärvi	0.56	—	1976—81
— Haapajärvi	0.54	—	1976—81
— Pidisjärvi	0.47	—	1976—81
— Niskakoski	0.95	—	1976—81
Tujuoja	0.86	0.86	1976—81
Siikajoki			
— Iso-Lamujärvi	−24.9	0.91	1976—81
— Kortteinen	0.36	0.96	1976—81
— Lamujoki	0.92	0.94	1976—81
— Uljua	0.73		1976—81
— Harjunniva	0.93	0.90	1976—81
Iisalmen reitti			
— Salahmi	0.72	0.86	1977—84
— Onkivesi	0.36	0.92	1977—84
Nilsiän reitti			
— Karjalankoski	0.64	0.85	1977—84
— Alaluosta	0.04	0.91	1977—84
— Keyritty	0.97	0.95	1977—84
— Atro	0.72	0.91	1977—84
— Jyrkka	0.65	0.94	1977—84
— Laakajärvi	0.41	0.93	1977—84

Appendix 1. Continued.

Basin	R^2		Calibration period
	Discharge	Snow	
Koitajoki		0.93	1974—83
— Pamilo	0.63	0.82	1974—83
— Lylykoski	0.95	0.84	1974—83
— Möhkö	0.96	0.89	1974—83
Kuivajoki	0.95	0.82	1976—82
Kemijoki			
— Kummaniva	0.90	—	1976—81
— Ylä-Kemijoki	0.80	—	1976—81
Oulujoki Hyrynsalmen			
— Hossanjärvi	0.93	0.93	1976—86
— Kiantajärvi	−0.59	0.95	1976—86
— Aittokoski	0.86	0.92	1976—86
— Seitenoikea	0.67	0.86	1976—86
— Koirakoski	0.96	0.88	1976—86
— Pyhäntä	0.50	0.85	1976—86
— Uvajärvi	0.95	0.95	1976—86
— Leppikoski	0.80	0.88	1976—86
Ounasjoki			
— Köngäs	0.93	—	1976—81
— Kaukonen	0.97	—	1976—81
— Marraskoski	0.98	—	1976—81
Raudanjoki	0.86	0.93	1976—81
Tornionjoki			
— Karesuvanto	0.91	0.86	1975—84
— Muonio	0.99	0.85	1975—84
— Kallio	0.95	0.90	1975—84
— Pello	0.96	0.90	1975—84
Ivalonjoki	0.86	—	1976—81
Mean	—	0.90	—
Number of values	—	41	—
Standard deviation	—	0.04	—

Appendix 2. The temperature ranges between which a change in precipitation from solid to liquid takes place according to the results of sub-model calibrations. TS is the temperature below which all precipitation is solid, and TL is the temperature above which all precipitation is liquid.

Basin	Area km²	TS °C	TL °C
Säkylän Pyhäjärvi			
— Pyhäjoki	76	−2.4	1.6
— Yläneenjoki	195	−3.2	2.0
Loimijoki	1 980	−4.1	1.9
Karvianjoki			
— Nummijoki	154	−0.3	3.2
— Karvianjärvi	159	−4.3	1.1
— Suomijärvi	168	−6.1	0.0
— Vahokoski	157	−5.2	0.2
— Vatajankoski	350	−4.2	0.7
Kyrönjoki			
— Pitkämö	95	−1.9	3.1
— Ala-Jalasjoki	318	−3.0	1.5
— Hirvijoki	299	−3.4	1.4
— Mustajoki	332	−2.1	1.2
— Ala-Kauhajoki	285	−2.2	1.5
— Ikkelänjoki	212	−4.2	2.2
— Hyypänjoki	205	−0.3	0.3
— Päntäneenjoki	209	−0.2	0.4
— Kainastonjoki	420	−0.9	0.6
Lapuanjoki			
— Kuorasjärvi	249	−6.0	1.5
— Hirvijärvi	385	−3.0	1.5
— Kuortane	1 652	−3.0	1.5
— Pappilankari	1 444	−2.6	2.1
Ähtävänjoki			
— Alajärvi	478	−4.2	2.8
— Lappajärvi	1 052	−4.2	3.0
— Evijärvi	175	−2.0	3.0
Perhonjoki			
— Venetjärvi	196	−3.1	0.2
— Tunkkari	1 131	−4.0	0.8
— Ullavanjoki	422	−5.8	2.8
— Köyhänjoki	266	−6.5	1.7
— Vissavesi	39	−5.0	2.4
— Pelo	262	−6.0	1.1
Kalajoki			
— Reis-Vuohtojärvi	372	−2.4	2.9
— Hautaperä	589	−2.0	3.2
— Settijärvi	193	−2.2	3.5
— Haapajärvi	294	−2.2	3.5
— Pidisjärvi	754	−2.0	3.5
— Niskakoski	865	−2.0	3.5
— *Tujuoja*	21	−2.3	3.2
Siikajoki			
— Iso-Lamujärvi	188	−0.3	0.1
— Kortteinen	179	−4.2	1.4
— Lamujoki	620	−2.9	0.0
— Uljua	1 453	−2.1	1.6
— Harjunniva	895	−1.7	2.0
Iisalmen reitti	5 574	−2.7	1.3
— Salahminjärvi	450	−1.6	0.6

Appendix 2. Continued.

Basin	Area km²	TS °C	TL °C
Nilsiän reitti			
— Laakajärvi	475	−1.7	3.0
— Kiltuanjärvi	245	−1.8	1.7
— Sälevä	410	−0.5	1.1
— Ala-Tiilikanjoki	300	−0.1	3.0
— Ylä-Tiilikanjoki	200	−4.1	1.7
— Keyritynjoki	530	−2.6	1.4
— Luostanjoki	545	0.0	0.4
— Syväri	800	−0.8	3.1
— Vuotjärvi	605	−4.1	0.4
Kuivajoki			
— Ala-Kuivajoki	369	−4.7	0.8
— Hamarinjoki	195	−1.5	0.8
— Kivijoki	705	−2.4	1.0
Hyrynsalmen reitti			
— Hossa	890	−1.6	0.0
— Ämmäkoski	2 560	−0.2	0.0
— Aittokoski	1 355	−4.0	0.0
— Seitenoikea	1 415	−2.3	0.1
— Koirakoski	690	−3.5	0.0
— Iso-Pyhäntä	550	−2.2	1.4
— Uvajärvi	277	−2.9	2.7
— Leppikoski	783	−3.4	1.2
— Alanteenjärvi	115	−3.9	0.8
Kemijoki			
— Kummaniva	8 715	−5.5	3.0
— Ylä-Kemijoki	18 570	−5.2	4.0
Ounasjoki			
— Köngäs	4 515	−4.0	−0.1
— Kaukonen	3 505	−3.5	0.0
— Marraskoski	4 315	−3.1	0.0
Raudanjoki	3 537	−4.0	0.0
Tornionjoki			
— Karesuvanto	5 915	−5.1	0.0
— Muonio	3 600	−5.0	0.0
— Kallio	4 825	−5.0	1.0
— Pello	2 237	−2.0	0.7
Ivalonjoki	3 300	−5.0	0.0
Mean		−3.0	1.5
Standard deviation		1.6	1.2

Appendix 3. Correction factors for solid (CPS) and liquid (CPL) precipitation obtained from calibrations of different sub-basins. The density of precipitation network (A/N) and the number of precipitation stations (N) on main watersheds are also given.

Basin sub-basin	CPS	CPL	A/N km²	N
Säkylän Pyhäjärvi			160	4
— Yläneenjoki	1.20	1.06		
— Pyhäjoki	1.20	1.06		
Loimijoki	1.26	1.09	250	8
Ylä-Karvianjoki			123	8
— Nummijoki	1.11	1.06		
— Karvianjärvi	1.44	1.01	154	1
— Suomijärvi	1.33	1.02		
— Vahokoski	1.40	1.02		
— Vatajankoski	1.18	1.09		
Kyrönjoki			218	10
— Pitkämö	1.10	1.04		
— Ala-Jalasjoki	1.16	1.08		
— Hirvijoki	1.38	1.09		
— Mustajoki	1.08	1.05		
— Ala-Kauhajoki	1.20	1.02		
— Ikkelänjoki	1.12	1.07		
— Hyypänjoki	1.18	1.08		
— Päntäneenjoki	1.26	1.07		
— Kainastonjoki	1.16	1.02		
Lapuanjoki			410	9
— Kuorasjärvi	1.30	1.06		
— Hirvijärvi	1.30	1.06		
— Kuortane	1.30	1.06		
— Pappilankari	1.32	1.07		
Ähtävänjoki			350	5
— Alajärvi	1.30	1.06		
— Lappajärvi	1.30	1.06		
— Evijärvi	1.30	1.06		
Perhonjoki			331	7
— Venetjärvi	1.35	1.02		
— Tunkkari	1.15	1.02		
— Ullavanjoki	1.24	1.11		
— Köyhänjoki	1.04	1.03		
— Vissavesi	1.11	1.09		
— Pelo	1.20	1.06		
Kalajoki			370	8
— Reis-Vuohtojärvi	1.20	1.07		
— Hautaperä	1.30	1.06		
— Settijärvi	1.30	1.06		
— Haapajärvi	1.30	1.06		
— Pidisjärvi	1.20	1.04		
— Niskakoski	1.35	1.14		
Tujuoja	1.30	1.13	20	1
Siikajoki			500	7
— Iso-Lamujärvi	1.17	1.00		
— Kortteinen	1.50	1.20		
— Lamujoki	1.33	1.18		
— Uljua	1.20	1.06		
— Harjunniva	1.17	1.13		
Iisalmen reitti			348	16
— Salahminjärvi	1.23	1.18		
— Iisalmen reitti	1.11	1.11		

Appendix 3. Continued.

Basin sub-basin	CPS	CPL	A/N km²	N
Nilsiän reitti			376	11
— Laakajärvi	1.09	1.01		
— Kiltuanjärvi	1.08	1.03		
— Sälevä	1.09	1.08		
— Ala-Tiilikanjoki	1.22	1.07		
— Ylä-Tiilikanjoki	1.11	1.08		
— Keyritynjoki	1.10	1.08		
— Luostanjoki	1.18	1.02		
— Syväri	1.09	1.02		
— Vuotjärvi	1.19	1.02		
Kuivajoki			181	7
— Ala-Kuivajoki	1.22	1.10		
— Hamarinjoki	1.10	1.09		
— Kivijoki	1.15	1.10		
Hyrynsalmen reitti			617	14
— Hossa	1.27	1.09		
— Ämmäkoski	1.10	1.01		
— Aittokoski	1.27	1.06		
— Seitenoikea	1.29	1.03		
— Koirakoski	1.33	1.08		
— Iso-Pyhäntä	1.17	1.08		
— Uvajärvi	1.19	1.08		
— Leppikoski	1.10	1.02		
— Alanteenjärvi	1.27	1.06		
Kemijoki			1 600	18
— Kummaniva	1.27	1.04		
— Ylä-Kemijoki	1.30	1.03		
Ounasjoki			880	14
— Köngäs	1.29	1.26		
— Kaukonen	1.37	1.14		
— Marraskoski	1.17	1.04		
Raudanjoki	1.40	1.22	580	6
Tornionjoki			1 360	14
— Karesuvanto	1.41	1.18		
— Muonio	1.20	1.15		
— Kallio	1.11	1.11		
— Pello	1.23	1.17		
Ivalonjoki	1.30	1.11	470	7
Mean	1.23	1.08	465	9
Standard deviation	0.10	0.05		
Number of values	76	76	20	20

Appendix 4. Parameter values from calibration of the temperature index model for all sub-basins in operational watershed models: degree-day constant (Eqs. 24 and 29) and retention capacity (Eqs. 25 and 31).

Basin	TM	KMIN	KMAX	KC	CMAX	CMIN	CC
Säkylän Pyhäjärvi							
— Yläneenjoki	−0.3	1.3	2.6	0.033	0.09	0.02	0.030
— Pyhäjoki	−0.3	1.3	2.6	0.033	0.09	0.02	0.030
Loimijoki	0.7	3.5	4.5	0.005	0.20	0.05	0.015
Ylä-Karvianjoki							
— -Nummijoki	2.1	1.0	3.3	0.049	0.35	0.04	0.018
— Karvianjärvi	0.1	1.1	6.0	0.033	0.22	0.04	0.005
— Suomijärvi	0.3	1.1	5.2	0.041	0.28	0.04	0.019
— Vahokoski	0.1	0.8	5.8	0.075	0.29	0.04	0.016
— Vatajankoski	0.3	1.4	10.7	0.047	0.38	0.04	0.009
Kyrönjoki							
— Pitkämö	0.6	1.4	6.5	0.027	0.10	0.10	0.002
— Ala-Jalasjoki	0.5	1.2	8.0	0.046	0.09	0.09	0.008
— Hirvijoki	0.5	1.0	7.4	0.077	0.13	0.04	0.014
— Mustajoki	0.6	1.0	5.6	0.077	0.21	0.04	0.020
— Ala-Kauhajoki	0.2	1.4	8.0	0.032	0.10	0.10	0.002
— Ikkelänjoki	0.4	1.4	3.6	0.022	0.09	0.09	0.001
— Hyypänjoki	0.8	1.7	3.9	0.024	0.08	0.08	0.059
— Päntäneenjoki	0.7	2.0	3.2	0.033	0.22	0.04	0.018
— Kainastonjoki	0.8	1.6	5.2	0.023	0.09	0.09	0.002
Lapuanjoki							
— Kuorasjärvi	−0.2	1.1	4.0	0.036	0.08	0.03	0.011
— Hirvijärvi	−0.3	1.1	4.0	0.037	0.08	0.01	0.030
— Kuortane	−0.2	1.1	3.8	0.038	0.08	0.01	0.030
— Pappilankari	−0.2	1.1	3.9	0.038	0.09	0.01	0.020
Ähtävänjoki							
— Alajärvi	−0.3	1.1	3.2	0.037	0.15	0.04	0.010
— Lappajärvi	−0.1	1.1	3.2	0.037	0.07	0.06	0.010
— Evijärvi	0.1	1.1	3.7	0.032	0.15	0.08	0.008
Perhonjoki							
— Venetjärvi	−0.2	1.1	5.8	0.037	0.28	0.04	0.023
— Tunkkari	−0.2	1.1	4.7	0.032	0.35	0.04	0.022
— Ullavanjoki	0.4	1.8	6.9	0.031	0.22	0.08	0.094
— Köyhänjoki	0.1	1.2	14.0	0.090	0.08	0.04	0.004
— Vissavesi	0.1	1.4	5.2	0.042	0.11	0.04	0.007
— Pelo	−0.3	1.2	8.1	0.110	0.45	0.04	0.011
Kalajoki							
— Reis-Vuohtojärvi	0.0	1.3	4.3	0.036	0.10	0.03	0.007
— Hautaperä	0.0	1.1	4.2	0.032	0.15	0.03	0.008
— Settijärvi	0.1	1.2	3.6	0.027	0.15	0.04	0.008
— Haapajärvi	0.1	1.2	3.4	0.029	0.15	0.05	0.005
— Pidisjärvi	0.0	1.2	3.8	0.027	0.14	0.05	0.005
— Niskakoski	0.2	1.2	4.2	0.027	0.14	0.05	0.005
Tujuoja	0.4	1.0	3.8	0.042	0.20	0.01	0.031
Siikajoki							
— Iso-Lamujärvi	0.6	1.7	3.8	0.030	0.06	0.02	0.063
— Kortteinen	0.3	1.4	5.4	0.037	0.10	0.02	0.035
— Lamujoki	0.3	1.2	4.6	0.043	0.10	0.02	0.065
— Uljua	0.1	1.2	4.0	0.046	0.08	0.02	0.016
— Harjunniva	0.3	1.3	6.0	0.039	0.13	0.03	0.018
Iisalmen reitti							
— Salahminjärvi	0.2	1.4	4.2	0.024	0.11	0.06	0.028
— Iisalmen reitti	0.5	1.3	6.5	0.036	0.10	0.05	0.022

Appendix 4. Continued.

Basin	TM	KMIN	KMAX	KC	CMAX	CMIN	CC
Nilsiän reitti							
— Laakajärvi	1.4	2.2	4.7	0.044	0.11	0.04	0.003
— Kiltuanjärvi	0.4	1.1	4.2	0.060	0.12	0.06	0.003
— Sälevä	0.3	1.2	3.3	0.026	0.21	0.04	0.001
— Ala-Tiilikanjoki	0.5	1.2	4.5	0.029	0.15	0.04	0.006
— Ylä-Tiilikanjoki	0.6	0.8	5.3	0.063	0.08	0.07	0.007
— Keyritynjoki	0.8	0.9	4.0	0.072	0.12	0.04	0.009
— Luostanjoki	0.3	0.8	4.9	0.073	0.10	0.04	0.004
— Syväri	1.2	1.2	4.4	0.062	0.12	0.06	0.003
— Vuotjärvi	0.5	0.8	5.5	0.074	0.10	0.04	0.004
Kuivajoki							
— Ala-Kuivajoki	0.3	1.3	5.8	0.036	0.35	0.11	0.020
— Hamarinjoki	−0.0	0.8	9.2	0.057	0.19	0.08	0.035
— Kivijoki	−0.2	1.5	3.4	0.065	0.30	0.11	0.039
Hyrynsalmen reitti							
— Hossa	0.2	1.0	8.4	0.046	0.21	0.04	0.004
— Ämmäkoski	0.3	1.4	6.7	0.046	0.21	0.04	0.040
— Aittokoski	0.3	1.3	6.1	0.018	0.21	0.05	0.004
— Seitenoikea	0.2	2.5	3.2	0.059	0.11	0.08	0.001
— Koirakoski	0.5	1.1	3.0	0.054	0.21	0.04	0.007
— Iso-Pyhäntä	0.4	1.2	4.6	0.024	0.21	0.04	0.036
— Uvajärvi	0.6	1.4	3.4	0.055	0.21	0.09	0.001
— Leppikoski	1.6	1.6	3.7	0.031	0.13	0.04	0.007
— Alanteenjärvi	0.3	1.4	6.3	0.012	0.21	0.04	0.006
Kemijoki							
— Kummaniva	−0.5	1.3	2.7	0.031	0.30	0.02	0.009
— Ylä-Kemijoki	−0.3	0.9	4.2	0.021	0.13	0.12	0.008
Ounasjoki							
— Köngäs	0.4	1.3	2.7	0.061	0.12	0.08	0.032
— Kaukonen	−0.4	1.2	3.1	0.029	0.19	0.13	0.021
— Marraskoski	−0.3	1.1	3.0	0.020	0.20	0.13	0.010
Raudanjoki	−0.3	1.0	2.8	0.036	0.29	0.05	0.030
Tornionjoki							
— Karesuvanto	0.5	2.7	2.9	0.025	0.20	0.04	0.044
— Muonio	1.2	2.5	2.9	0.089	0.20	0.04	0.038
— Kallio	1.1	3.0	3.5	0.089	0.18	0.04	0.077
— Pello	0.6	3.0	3.0	—	0.14	0.03	0.007
Ivalonjoki	1.5	1.1	3.0	0.033	0.10	0.04	0.001
Mean	.31	1.4	4.7	0.043	0.17	0.05	0.018
Standard deviation	.49	.52	1.9	0.020	0.084	0.028	0.019
Number of values	76	76	76	75	76	76	76

Appendix 5. Parameter values from calibration of the temperature index model for all sub-basins: depression storage (Eqs. 32 and 33), refreezing (Eq. 28), evaporation from snow (ESC) and melt due to ground heat (GM).

Basin	SVM	CSVM	SC	TF	FM	e	ESC	GM
Säkylän Pyhäjärvi								
— Yläneenjoki	10	—	0.10	−1.2	3.7	1.0	0.20	—
— Pyhäjoki	5	—	0.25	−1.2	3.7	1.0	0.20	—
Loimijoki	—	0.21	0.46	−4.6	2.1	1.0	0.06	—
Ylä-Karvianjoki								
— Nummijoki	—	0.62	0.17	−1.1	0.9	0.01	0.00	0.15
— Karvianjärvi	—	0.53	0.13	−1.3	0.3	0.06	0.00	0.03
— Suomijärvi	—	0.90	0.25	−1.1	0.5	0.06	0.00	0.01
— Vahokoski	—	0.90	0.23	−1.7	0.3	.001	0.00	0.00
— Vatajankoski	—	0.64	0.01	−0.5	0.1	.001	0.00	0.00
Kyrönjoki								
— Pitkämö	—	0.74	0.03	−0.8	0.7	.001	0.08	0.08
— Ala-Jalasjoki	—	0.80	0.07	−0.8	0.7	.001	0.09	0.04
— Hirvijoki	—	0.34	0.18	−0.8	0.1	.001	0.14	0.00
— Mustajoki	—	0.54	0.14	−0.8	0.1	.001	0.15	0.00
— Ala-Kauhajoki	—	0.45	0.89	−0.8	0.8	0.05	0.07	0.06
— Ikkelänjoki	—	0.92	0.11	−1.5	0.9	0.01	0.10	0.09
— Hyypänjoki	—	0.89	0.13	−1.0	0.5	.001	0.03	0.03
— Päntäneenjoki	—	0.80	0.10	−1.0	.06	.001	0.04	0.02
— Kainastonjoki	—	0.05	0.18	−0.9	0.6	.001	0.07	0.08
Lapuanjoki								
— Kuorasjärvi	35	—	0.08	−1.1	3.4	1.0	0.20	—
— Hirvijärvi	33	—	0.08	−1.1	3.0	1.0	0.20	—
— Kuortane	33	—	0.07	−1.3	3.2	1.0	0.20	—
— Pappilankari	28	—	0.09	−1.6	3.4	1.0	0.20	—
Ähtävänjoki								
— Alajärvi	40	—	0.10	−1.2	1.7	1.0	0.20	—
— Lappajärvi	40	—	0.09	−1.3	3.0	1.0	0.20	—
— Evijärvi	35	—	0.05	0.0	0.9	1.0	0.20	—
Perhonjoki								
— Venetjärvi	—	0.14	0.60	−2.2	1.7	0.10	0.00	0.000
— Tunkkari	—	0.60	0.07	−2.9	1.0	0.12	0.08	0.000
— Ullavanjoki	—	0.74	0.05	−2.8	0.2	0.10	0.00	0.000
— Köyhänjoki	—	0.95	0.24	−1.7	0.6	.001	0.00	0.000
— Vissavesi	—	0.54	0.09	−1.3	0.5	.002	0.02	0.095
— Pelo	—	0.74	0.23	−1.1	0.4	.001	0.06	0.000
Kalajoki								
— Reis-Vuohtojärvi	18	—	0.05	−0.2	0.9	1.00	0.20	—
— Hautaperä	15	—	0.22	−0.2	0.7	1.0	0.20	—
— Settijärvi	28	—	0.17	−0.3	0.7	1.0	0.10	—
— Haapajärvi	28	—	0.17	−0.3	0.7	1.0	0.10	—
— Pidisjärvi	30	—	0.25	−0.3	0.7	1.0	0.20	—
— Niskakoski	30	—	0.25	−0.3	0.7	1.0	0.20	—
Tujuoja	28	—	0.10	−0.6	0.5	1.0	0.14	—
Siikajoki								
— Iso-Lamujärvi	—	0.40	0.02	−0.1	4.4	0.69	0.09	0.00
— Kortteinen	—	0.53	0.14	−1.6	0.2	0.08	0.07	0.15
— Lamujoki	—	0.52	0.08	−3.1	0.4	0.62	0.07	0.05
— Uljua	20	—	0.12	−0.6	3.0	1.0	0.20	—
— Harjunniva	—	0.70	0.02	−1.6	0.4	0.05	0.07	0.01
Iisalmen reitti								
— Salahminjärvi	—	0.26	0.02	−3.1	1.0	0.71	0.00	0.04
— Iisalmen reitti	—	0.31	0.05	−2.8	2.8	0.01	0.00	0.31

Appendix 5. Continued.

Basin	SVM	CSVM	SC	TF	FM	e	ESC	GM
Nilsiän reitti								
— Laakajärvi	—	0.59	0.08	−3.3	2.7	.001	0.12	0.02
— Kiltuanjärvi	—	0.36	.001	−0.7	0.1	.002	0.00	.0001
— Sälevä	—	0.10	0.84	−0.8	0.1	.001	0.13	.0001
— Ala-Tiilikanjoki	—	0.80	0.26	−3.7	4.0	.001	0.00	.0001
— Ylä-Tiilikanjoki	—	0.30	0.14	−5.0	.02	0.44	0.00	.0020
— Keyritynjoki	—	0.77	0.36	−0.4	.38	.001	0.00	0.044
— Luostanjoki	—	0.15	0.05	−1.6	1.9	.003	0.14	0.11
— Syväri	—	0.54	0.23	−3.4	.19	.008	0.00	0.028
— Vuotjärvi	—	0.84	0.86	−1.3	.08	.002	0.00	.0001
Kuivajoki								
— Ala-Kuivajoki	—	0.58	0.11	−0.5	0.9	.025	0.15	0.16
— Hamarinjoki	—	0.87	0.02	−0.9	1.1	.001	0.11	0.05
— Kivijoki	—	0.79	0.04	−1.0	0.3	.001	0.02	0.02
Hyrynsalmen reitti								
— Hossa	—	1.00	0.22	−3.6	2.1	.001	0.00	0.06
— Ämmäkoski	—	0.83	0.04	−3.2	1.3	.001	0.00	0.10
— Aittokoski	—	0.70	0.28	−3.0	4.7	.001	0.10	.0001
— Seitenoikea	—	0.33	0.38	−2.8	3.3	.002	0.10	.0001
— Koirakoski	—	0.92	0.29	−3.1	2.1	.001	0.11	0.09
— Iso-Pyhäntä	—	0.35	0.19	−4.3	3.0	.001	0.00	0.04
— Uvajärvi	—	0.22	0.46	−4.2	2.7	0.56	0.07	0.12
— Leppikoski	—	0.10	0.81	−4.3	4.9	.001	0.13	.0004
— Alanteenjärvi	—	0.63	0.24	−3.0	4.9	.001	0.13	.0001
Kemijoki								
— Kummaniva	5	—	0.10	−1.5	1.3	1.0	0.10	—
— Ylä-Kemijoki	9	—	0.06	−3.0	0.5	1.0	0.10	—
Ounasjoki								
— Köngäs	—	0.30	0.05	−1.6	0.4	0.59	0.00	0.00
— Kaukonen	—	0.32	0.08	−2.1	1.0	0.50	0.05	0.01
— Marraskoski	—	0.10	0.05	−1.4	1.8	0.53	0.08	0.10
Raudanjoki	—	0.27	0.001	−1.8	4.0	0.10	0.27	0.00
Tornionjoki								
— Karesuvanto	—	0.60	0.10	−1.4	0.2	0.44	0.00	0.00
— Muonio	—	0.32	0.001	−1.2	0.3	0.23	0.01	0.15
— Kallio	—	0.20	0.006	−1.3	0.4	0.24	0.01	0.13
— Pello	—	0.57	0.007	−0.5	0.1	0.04	0.00	0.07
Ivalonjoki	20	—	0.70	−2.0	3.5	1.0	0.10	—
Mean	24	0.54	0.18	−1.7	1.5	0.36	.085	.047
St. deviation	11	0.27	0.21	1.2	1.4	0.44	.076	.062
Number of values	20	56	76	76	76	76	76	52

Appendix 6. Parameter values from calibration of the temperature index model for sub-basins: depletion of the snow covered area (Eqs. 35 — 38).

Basin	LS	exs	LS2	exs2	AMIN
Loimijoki	0.55	0.42A	—	—	0.10
Ylä-Karvianjoki					
— Nummijoki	—	—	0.82	0.83B	0.09
— Karvianjärvi	—	—	0.80	1.2 A	0.07
— Suomijärvi	—	—	0.50	5.9 A	0.22
— Vahokoski	—	—	0.68	0.92B	0.07
— Vatajankoski	—	—	0.82	0.83B	0.09
Kyrönjoki					
— Pitkämö	—	—	0.88	0.47B	0.28
— Ala-Jalasjoki	—	—	0.85	0.56B	0.29
— Hirvijoki	—	—	0.86	0.23B	0.30
— Mustajoki	—	—	0.89	0.16B	0.27
— Ala-Kauhajoki	—	—	0.88	0.50B	0.30
— Ikkelänjoki	—	—	0.91	0.57B	0.28
— Hyypänjoki	—	—	0.86	0.77B	0.13
— Päntäneenjoki	—	—	0.82	0.14B	0.19
— Kainastonjoki	—	—	0.91	0.59B	0.30
Perhonjoki					
— Venetjärvi	—	—	0.71	0.77B	0.04
— Tunkkari	—	—	0.61	1.3 A	0.04
— Ullavanjoki	—	—	0.52	2.8 A	0.16
— Köyhänjoki	—	—	0.42	1.5 A	0.18
— Vissavesi	—	—	0.90	1.1 A	0.09
— Pelo	—	—	0.50	4.2 A	0.08
Tujuoja	0.46	0.59A	—	—	0.10
Siikajoki					
— Iso-Lamujärvi	—	—	0.69	0.81B	0.25
— Kortteinen	—	—	0.80	1.2 A	0.10
— Lamujoki	—	—	0.68	1.4 A	0.19
— Harjunniva	—	—	0.59	0.55B	0.20
Iisalmen reitti					
— Salahminjärvi	—	—	0.57	1.8 A	0.10
— Iisalmen reitti	—	—	0.70	1.8 A	0.10
Nilsiän reitti					
— Laakajärvi	—	—	0.50	1.7 A	0.08
— Kiltuanjärvi	—	—	0.91	0.86B	0.09
— Sälevä	—	—	0.52	2.8 A	0.13
— Ala-Tiilikanjoki	—	—	0.52	2.9 A	0.09
— Ylä-Tiilikanjoki	—	—	0.59	1.7 A	0.12
— Keyritynjoki	—	—	0.50	2.8 A	0.10
— Luostanjoki	—	—	0.67	1.6 A	0.09
— Syväri	—	—	0.64	3.0 A	0.20
— Vuotjärvi	—	—	0.63	2.7 A	0.13
Kuivajoki					
— Ala-Kuivajoki	—	—	0.66	0.50B	0.08
— Hamarinjoki	—	—	0.34	0.10B	0.10
— Kivijoki	—	—	0.89	0.59B	0.22
Hyrynsalmen reitti					
— Hossa	—	—	0.84	1.2 A	0.08
— Ämmäkoski	—	—	0.85	1.0 A	0.08
— Aittokoski	—	—	0.50	0.94B	0.08
— Seitenoikea	—	—	0.71	0.40B	0.08
— Koirakoski	—	—	0.50	1.1 A	0.08
— Iso-Pyhäntä	—	—	0.86	0.91B	0.08
— Uvajärvi	—	—	0.50	0.77B	0.28
— Leppikoski	—	—	0.51	0.86B	0.09
— Alanteenjärvi	—	—	0.50	0.87B	0.08
Kemijoki					
— Kummaniva	0.50	0.90A	—	—	0.10
— Ylä-Kemijoki	0.49	0.92A	—	—	0.10

Appendix 6. Continued.

Basin	LS	exs	LS2	exs2	AMIN
Ounasjoki					
— Köngäs	—	—	0.64	0.66B	0.01
— Kaukonen	—	—	0.44	1.4 A	0.07
— Marraskoski	—	—	0.60	1.2 A	0.10
Raudanjoki	—	—	0.75	1.2 A	0.05
Tornionjoki					
— Karesuvanto	—	—	0.61	1.0	0.07
— Muonio	—	—	0.55	0.64B	0.04
— Kallio	—	—	0.62	0.70B	0.05
— Pello	—	—	0.60	0.40B	0.07
Ivalonjoki	0.90	1.0	—	—	0.10
Mean	0.58	0.77A	0.67	1.26A	0.13
St. deviation	0.18	0.25	0.16	1.06	0.08
Number of values	5	5	55	55	59

Appendix 7. Parameter values for degree-day snowmelt model separately for open and forested areas.

Basin	Open areas				Forested areas			
	TM	KMIN	KMAX	KC	TM	KMIN	KMAX	KC
Loimijoki	0.9	4.9	9.0	0.021	0.9	3.0	3.9	0.015
Ylä-Karvianjoki								
— Nummijoki	0.1	1.0	4.2	0.055	0.2	1.0	2.9	0.045
— Karvianjärvi	−0.1	1.1	7.5	0.053	−0.1	1.1	5.2	0.021
— Suomijärvi	0.3	1.1	5.2	0.064	0.3	1.1	5.2	0.025
— Vahokoski	−0.1	0.8	8.6	0.075	0.2	0.8	4.6	0.075
— Vatajankoski	−0.3	1.4	12.7	0.047	0.5	1.4	10.0	0.047
Kyrönjoki								
— Pitkämö	0.1	1.5	9.3	0.029	1.0	1.3	4.6	0.021
— Ala-Jalasjoki	0.3	1.2	13.4	0.056	0.5	1.1	5.7	0.042
— Hirvijoki	0.0	1.4	14.0	0.077	0.7	0.9	5.8	0.077
— Mustajoki	−0.3	1.5	13.4	0.077	0.8	0.9	3.9	0.077
— Ala-Kauhajoki	0.1	1.4	9.2	0.033	0.2	1.4	7.5	0.032
— Ikkelänjoki	0.1	1.4	6.4	0.022	0.5	1.4	2.9	0.029
— Hyypänjoki	0.0	1.7	9.3	0.025	0.9	1.6	2.5	0.023
— Päntäneenjoki	0.0	3.7	6.2	0.057	0.8	1.5	2.4	0.027
— Kainastonjoki	0.3	2.0	9.3	0.023	1.0	1.4	3.4	0.023
Nilsiän reitti								
— Laakajärvi	1.1	3.0	5.7	0.068	1.6	1.7	4.2	0.032
— Kiltuanjärvi	0.2	1.4	4.7	0.069	0.5	0.8	3.8	0.053
— Sälevä	0.3	1.2	12.7	0.074	0.3	1.1	6.7	0.019
— Ala-Tiilikanj.	0.1	2.0	6.4	0.023	1.2	1.3	2.5	0.022
— Ylä-Tiilikanj.	0.4	0.9	4.7	0.056	0.5	0.8	4.7	0.055
— Keyritynjoki	0.7	1.0	6.8	0.074	0.9	0.9	2.7	0.070
— Luostanjoki	0.0	0.8	8.1	0.068	0.5	0.8	3.2	0.068
— Syväri	1.2	1.3	4.7	0.063	1.2	1.2	4.4	0.062
— Vuotjärvi	0.3	1.0	13.0	0.086	0.5	6.8	2.8	0.070
Kuivajoki								
— Ala-Kuivajoki	0.2	1.3	8.7	0.065	0.4	1.3	8.7	0.015
— Hamarinjoki	0.0	0.9	11.6	0.057	0.0	0.7	7.5	0.057
— Kivijoki	−0.2	1.5	4.6	0.043	−0.2	1.5	4.5	0.029
Hyrynsalmen r.								
— Hossa	0.0	1.0	11.0	0.043	0.2	1.0	7.6	0.043
— Ämmäkoski	0.0	3.6	7.1	0.090	0.4	0.9	6.7	0.038
— Aittokoski	0.1	1.3	6.1	0.018	0.4	1.3	6.1	0.018
— Seitenoikea	0.9	2.5	3.5	0.076	1.3	2.5	3.1	0.052
— Koirakoski	0.0	2.3	3.6	0.088	0.6	1.0	3.0	0.050
— Iso-Pyhäntä	0.2	1.2	6.2	0.049	0.4	1.2	4.0	0.015
— Uvajärvi	0.4	2.9	5.3	0.094	0.6	0.8	2.7	0.040
— Leppikoski	0.0	2.2	6.0	0.089	1.7	1.5	3.5	0.026
— Alanteenjärvi	0.2	1.4	8.8	0.017	0.4	1.4	5.4	0.011
Mean	0.2	1.7	7.8	0.056	0.6	1.4	4.7	0.040
St. deviation	0.35	0.9	3.1	0.023	0.44	1.0	1.9	0.020
Number of values	36	36	36	36	36	36	36	36

Appendix 8. The values of parameter PKM of Eq. 37 from calibrations of different sub-basins.

Basin	PKM (mm $°C^{-1}$ mm^{-1} d^{-1})
Loimijoki	0.10
Ylä-Karvianjoki	
— Nummijoki	0.0003
— Karvianjärvi	0.0003
— Suomijärvi	0.09
— Vahokoski	0.08
— Vatajankoski	0.0001
Kyrönjoki	
— Pitkämö	0.0001
— Ala-Jalasjoki	0.0001
— Hirvijoki	0.0001
— Mustajoki	0.0000
— Ala-Kauhajoki	0.0001
— Ikkelänjoki	0.0002
— Hyypänjoki	0.018
— Päntäneenjoki	0.019
— Kainastonjoki	0.0001
Perhonjoki	
— Venetjärvi	0.046
— Tunkkari	0.001
— Ullavanjoki	0.15
— Köyhänjoki	0.0000
— Vissavesi	0.0002
— Pelo	0.0001
Tujuoja	0.000
Siikajoki	
— Iso-Lamujärvi	0.23
— Kortteinen	0.12
— Lamujoki	0.20
— Harjunniva	0.14
Iisalmen reitti	
— Salahminjärvi	0.013
— Iisalmen reitti	0.0001
Nilsiän reitti	
— Laakajärvi	0.28
— Kiltuanjärvi	0.0001
— Sälevä	0.0001
— Ala-Tiilikanjoki	0.0002
— Ylä-Tiilikanjoki	0.0001
— Keyritynjoki	0.0001
— Luostanjoki	0.0002
— Syväri	0.024
— Vuotjärvi	0.0001
Kuivajoki	
— Ala-Kuivanjoki	0.022
— Hamarinjoki	0.42
— Kivijoki	0.013
Hyrynsalmen reitti	
— Hossa	0.30
— Ämmäkoski	0.31
— Aittokoski	0.30
— Seitenoikea	0.20
— Koirakoski	0.12
— Iso-Pyhäntä	0.27
— Uvajärvi	0.079
— Leppikoski	0.35
— Alanteenjärvi	0.27
Ounasjoki	
— Köngäs	0.15
— Kaukonen	0.15
— Marraskoski	0.10
Raudanjoki	0.19
Tornionjoki	
— Karesuvanto	0.19
— Muonio	0.001
— Kallio	0.001
— Pello	0.30
Mean	0.092
Standard deviation	0.117
Number of values	57

Appendix 9. The parameters from calibration of the basic temperature index model from Table 7 (Chapter 6.5) with different energy balance components (Eqs. 37, 44 — 48) at Tujuoja.

Model	RKM	TR J	LH J	TR2 J	eal	EKM	UKM	PKM
Basic+RS2	—	—	92	0.0	2E-5	—	—	—
Basic+RS	.00043	0.5	—	—	—	—	—	—
Basic+RLAT	—	—	—	—	—	.046	—	—
Basic+RSEN	—	—	—	—	—	—	12E-4	—
Basic+RS2+RLAT	—	—	200	0.0	6E-6	1.1	—	—
Basic+RS+RLAT	.00043	0.5	—	—	—	.12	—	—
Basic+RS+RSEN	.00043	0.5	—	—	—	—	.014	—
Basic+RSEN+RLAT	—	—	—	—	—	.051	.034	—
Basic+RS+RSEN+RLAT	.00041	0.5	—	—	—	.034	.38	—
Ba+RS+RSEN+RLAT+RP	.00045	0.5	—	—	—	.42	.048	.12
Basic+RSEN+RLAT+RP	—	—	—	—	—	.044	.010	.049
Basic+RS+RP	—	—	—	—	—	—	—	—
Mean	.00043	0.5	—	—	—	.26	.081	.085
Standard deviation	1.4E-5	0.0	—	—	—	.40	.15	.050
Number of values	5	5	—	—	—	7	6	2

Appendix 10. The parameters from calibration of the basic temperature index model (Eqs. 24 and 29) from Table 7 (Chapter 6.5) with different energy balance components at Tujuoja.

Model	TM	KMIN	KC	KMAX
Basic+RS2	0.58	0.90	0.047	2.8
Basic+RS	0.71	0.98	0.049	3.5
Basic+RLAT	0.60	1.10	0.040	2.4
Basic+RSEN	0.45	1.00	0.051	4.4
Basic+RS2+RLAT	1.30	1.20	0.028	4.0
Basic+RS+RLAT	0.74	0.97	0.051	3.4
Basic+RS+RSEN	0.79	0.98	0.049	3.5
Basic+RSEN+RLAT	0.60	1.00	0.051	4.6
Basic+RS+RSEN+RLAT	1.20	1.10	0.056	4.0
Ba+RS+RSEN+RLAT+RP	0.79	0.32	0.057	4.0
Basic+RSEN+RLAT+RP	0.59	1.10	0.041	4.5
Basic+RS+RP	—	—	—	—
Mean	0.76	0.97	0.047	3.7
Standard deviation	0.26	0.23	8.2E-3	0.70
Number of values	11	11	11	11

Appendix 11. The parameters from calibration of the basic temperature index model from Table 7 (Chapter 6.1) with different energy balance components (Eqs. 37, 44 — 48) at the Loimijoki basin.

Model	RKM	TR J	LH J	TR2 J	eal	EKM	UKM	PKM
Basic+RS2	—	—	17	0.1	0.2	—	—	—
Basic+RS	.0013	57	—	—	—	—	—	—
Basic+RLAT	—	—	—	—	—	.89	—	—
Basic+RSEN	—	—	—	—	—	—	.16	—
Basic+RS2+RLAT	—	—	—	—	—	—	—	—
Basic+RS+RLAT	.0024	540	—	—	—	1.6	—	—
Basic+RS+RSEN	.0022	1090	—	—	—	—	.081	—
Basic+RSEN+RLAT	—	—	—	—	—	.89	.35	—
Basic+RS+RSEN+RLAT	.0022	300	—	—	—	1.4	.13	—
Ba+RS+RSEN+RLAT+RP	.0074	15	—	—	—	1.6	.17	1.E-4
Basic+RSEN+RLAT+RP	—	—	—	—	—	1.8	.18	.0093
Basic+RS+RP	.0020	310	—	—	—	—	—	.11
Mean	.0029	390	—	—	—	1.4	.18	.040
Standard deviation	.0022	390	—	—	—	.39	.091	.061
Number of values	6	6	—	—	—	6	6	3

Appendix 12. The parameters from calibration of the basic temperature index model (Eqs. 24 and 29) from Table 7 (Chapter 6.1) with different energy balance components at the Loimijoki basin.

Model	TM	KMIN	KC	KMAX
Basic+RS2	0.85	3.1	0.059	3.5
Basic+RS	0.92	3.1	0.010	4.7
Basic+RLAT	0.81	2.6	0.042	5.6
Basic+RSEN	0.92	4.3	0.058	4.4
Basic+RS2+RLAT	—	—	—	—
Basic+RS+RLAT	1.80	2.5	0.066	5.7
Basic+RS+RSEN	0.86	4.0	0.030	4.3
Basic+RSEN+RLAT	1.00	2.6	0.046	5.2
Basic+RS+RSEN+RLAT	0.92	4.3	0.058	4.4
Ba+RS+RSEN+RLAT+RP	1.30	4.4	0.078	4.4
Basic+RSEN+RLAT+RP	1.30	5.8	0.013	6.6
Basic+RS+RP	1.60	5.8	0.028	5.8
Mean	1.20	3.8	0.042	5.1
Standard deviation	0.39	1.2	0.022	0.93
Number of values	11	11	11	11

Appendix 13. The parameter values of snowmelt simulation with diurnal temperature difference (Eqs. 58 — 60, 24 and 29), Chapter 6.6.

Model	Parameters									
version	KST	TM_{mean}	KST2	TM_{max}	KLT	TM_{min}	TM	KMIN	KC	KMAX
Tujuoja										
Basic+RST	.095	−2.1	—	—	—	—	.92	.87	.055	2.6
Basic+RST2	—	—	.15	0.0	—	—	.57	1.0	.029	5.7
Loimijoki										
Basic+RST2	—	—	.088	.04	—	—	1.0	5.3	—	5.3
Basic+RLT	—	—	—	—	−0.13	.95	.85	3.9	.053	5.3

Appendix 14. Verification results for the Loimijoki basin (1970—1976) simulated by the best temperature index model, Chapter 6.8. The water equivalent of snow is simulated separately for open (——) and forested areas (- - -). Observed water equivalent:(o), simulated discharge:(- - -).

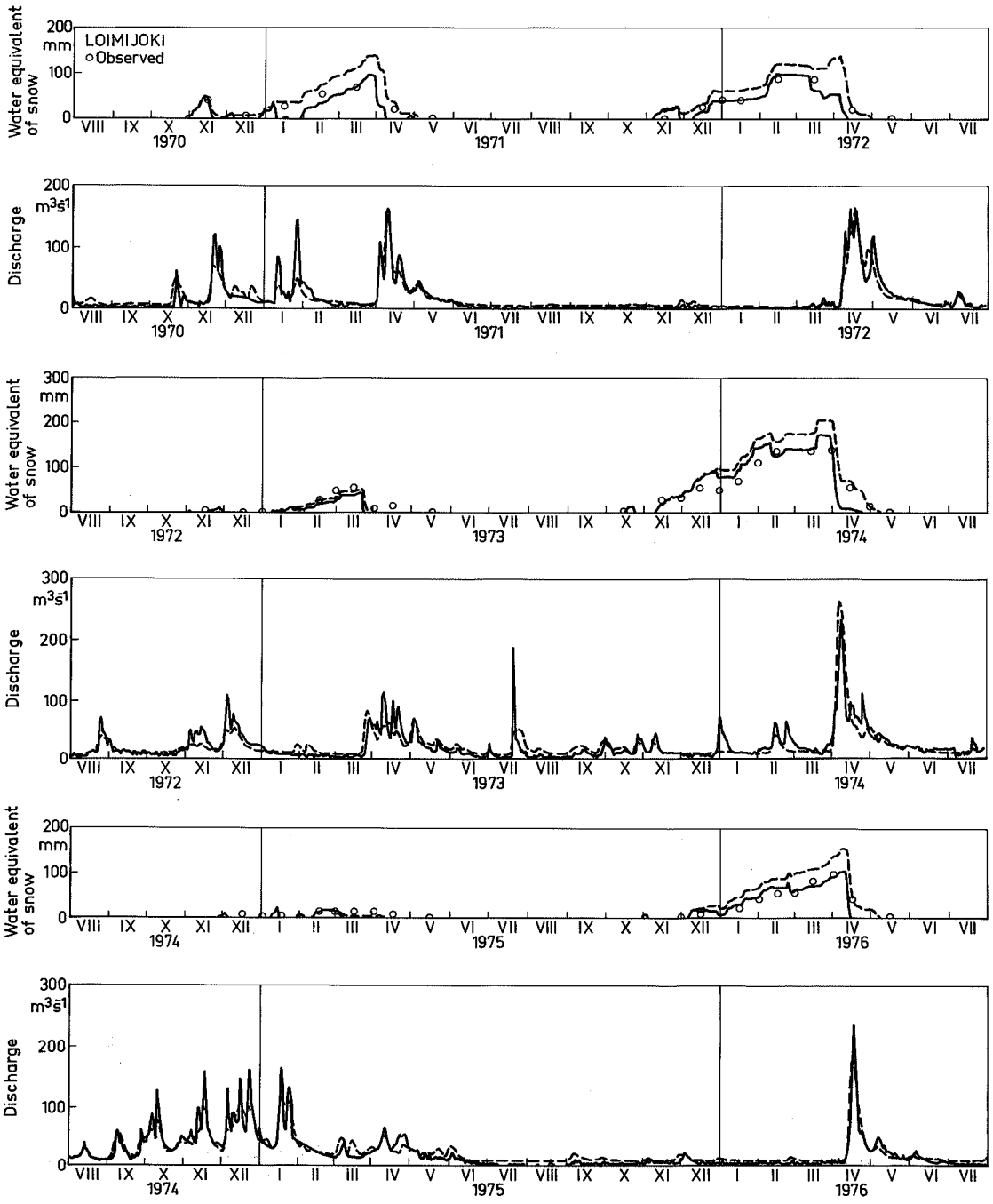

Appendix 15. Verification results for the Tujuoja basin (1970—1976) simulated by the best temperature index model, Chapter 6.8. The observed water equivalent of snow is marked by (o) and simulated runoff by (- - -).

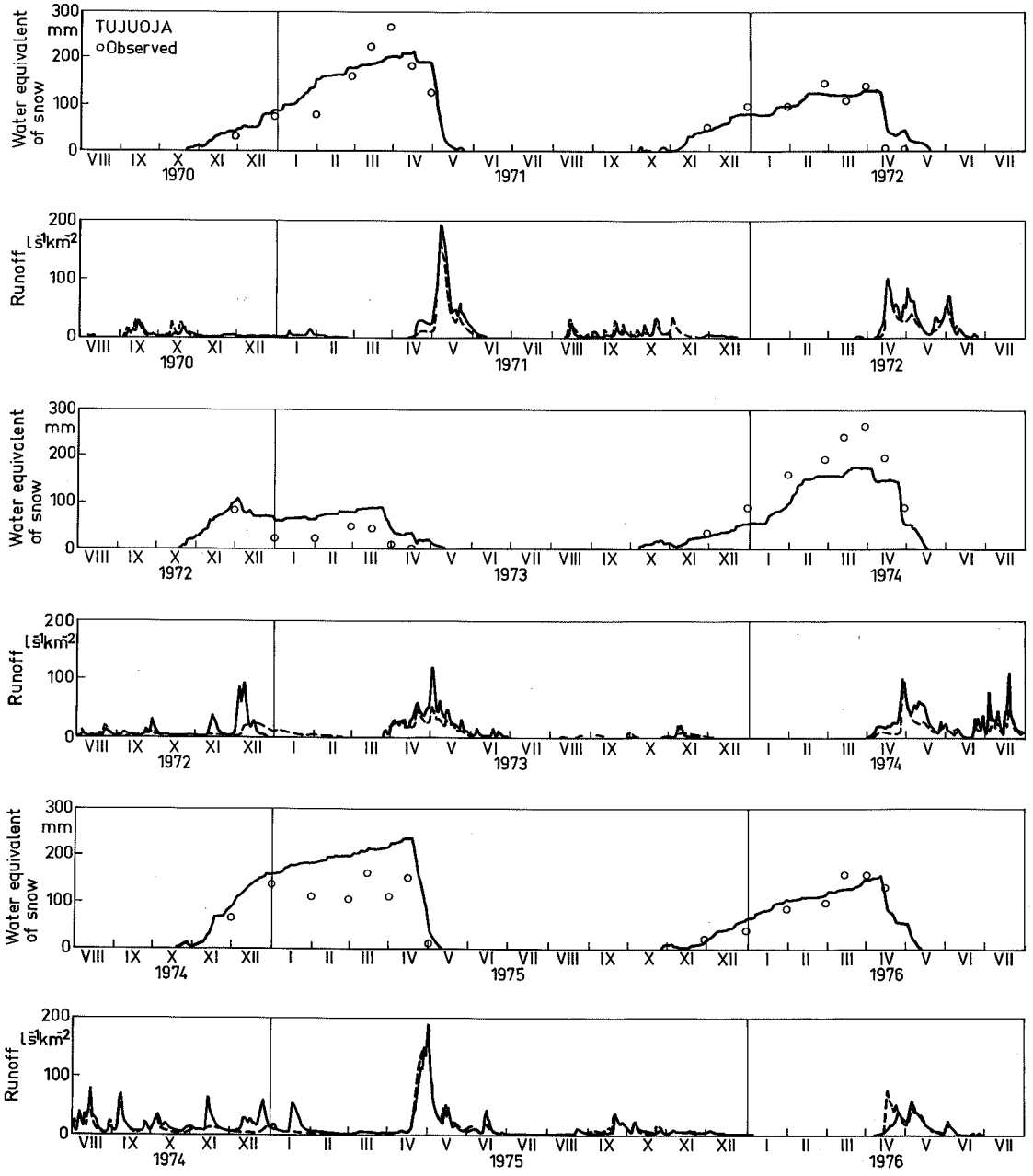

Appendix 16. Loimijoki basin: Simulation of water equivalent and discharge (- - -) by the watershed model with the snowmelt energy balance model during the verification period of 1970—1976. Observed water equivalent (o) and observed discharge (—).

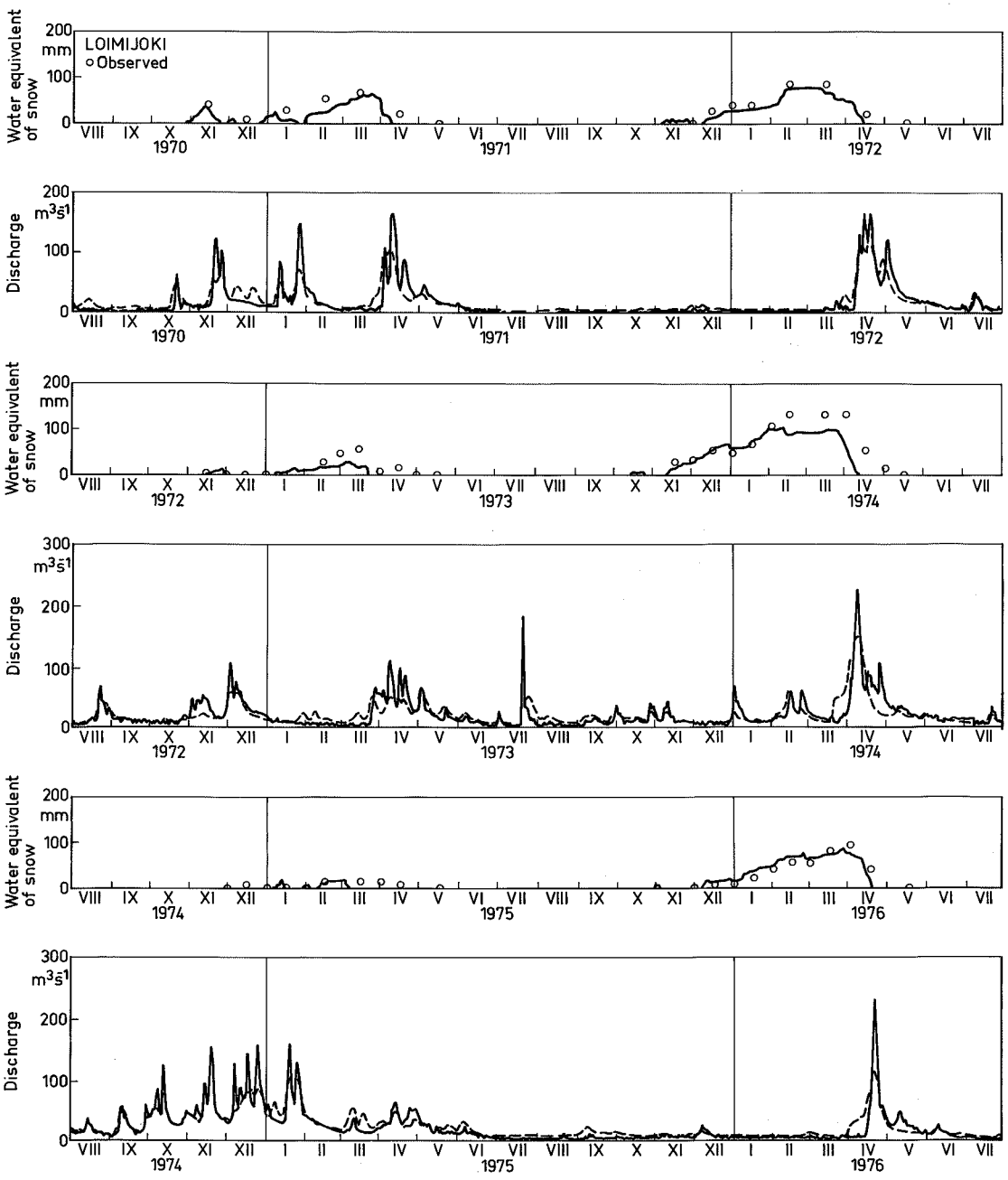

Appendix 17. Loimijoki basin: Simulation of water equivalent and discharge (- - -) by the watershed model with the snowmelt energy balance model and the physical snow cover model during the verification period of 1970—1976. Observed water equivalent (o) and observed discharge (—).

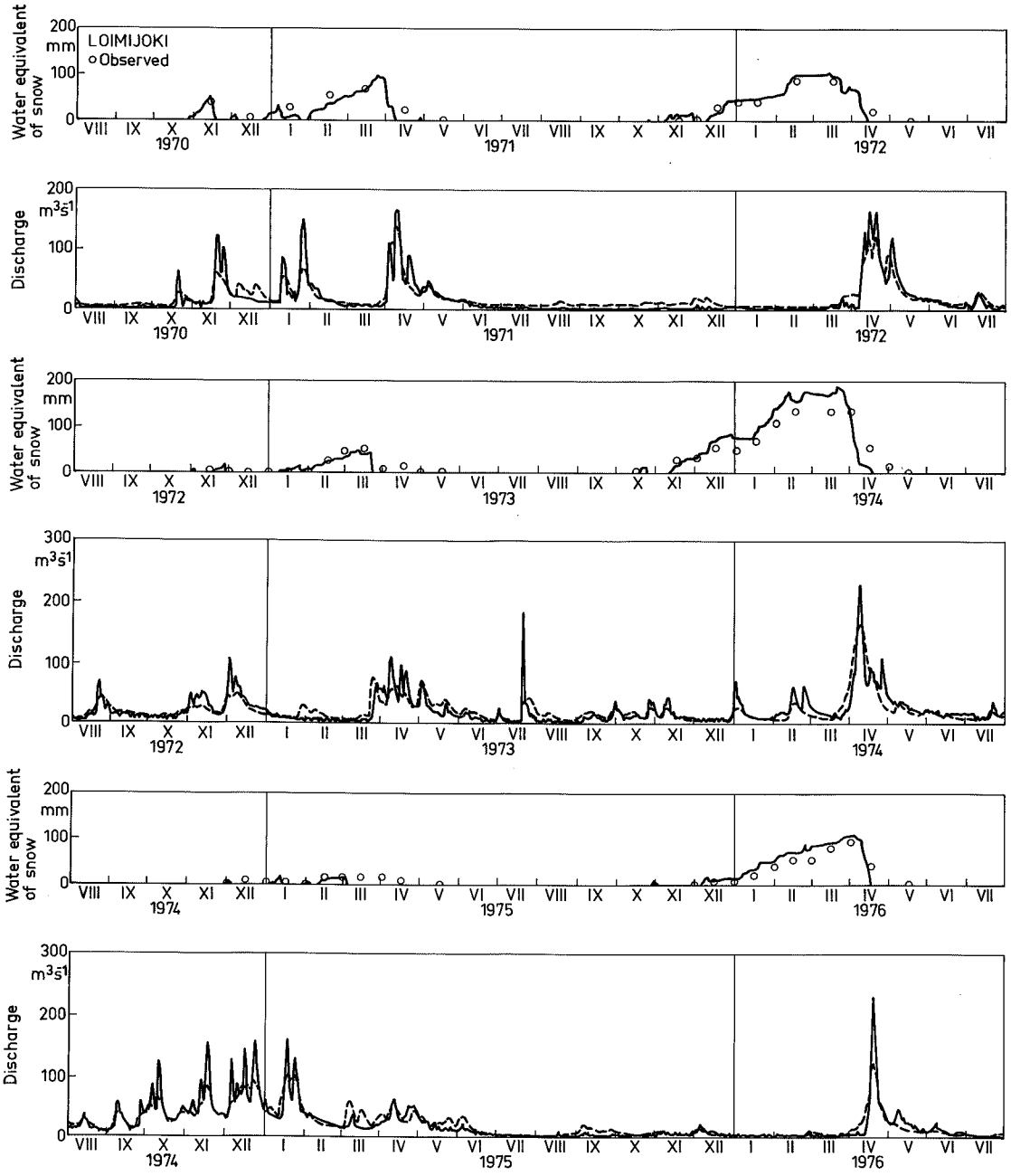

Appendix 18. The Tujuoja basin: Simulation of water equivalent and runoff (- - -) by the watershed model with the snowmelt energy balance model and the physical snow cover model during the verification period of 1970—1976. Observed water equivalent (o) and observed runoff (——).